Seismic Performance Evaluation of the Base Isolation Systems

Mohammad Reza Bagerzadeh Karimi

Submitted to the
Institute of Graduate Studies and Research
in partial fulfillment of the requirements for the degree of

Doctor of Philosophy
in
Civil Engineering

Eastern Mediterranean University
January 2020
Gazimağusa, North Cyprus

Approval of the Institute of Graduate Studies and Research

Prof. Dr. Ali Hakan Ulusoy
Director

I certify that this thesis satisfies all the requirements as a thesis for the degree of Doctor of Philosophy in Civil Engineering.

Prof. Dr. Umut Türker
Chair, Department of Civil Engineering

We certify that we have read this thesis and that in our opinion it is fully adequate in scope and quality as a thesis for the degree of Doctor of Philosophy in Civil Engineering.

Assoc. Prof. Dr. Mehmet Cemal Geneş
Supervisor

Examining Committee

1. Prof. Dr. Uğurhan Akyüz
2. Assoc. Prof. Dr. Mürüde Çelikağ
3. Assoc. Prof. Dr. Mehmet Cemal Geneş
4. Assoc. Prof. Dr. Giray Özay
5. Assoc. Prof. Dr. Rifat Reşatoğlu

ABSTRACT

As Seismic isolation is one of the remedies for providing earthquake-resistant features for structural components, non-structural components, and contents of the building systems, its performance may become counter-productive under the effect of near-field ground motions, in which case an increased structural response might result due to resonance. For this reason, one of the greatest challenges of researchers is to understand the behavior of base isolation systems and base-isolated buildings under the conditions of different ground motions. The specific objective of this study is to evaluate the seismic response of multi-story base-isolated buildings with lead core rubber bearings (LCRBs) and buildings that are not isolated when subjected to different types of ground motions with different components.

To this end, the vulnurablity of the base-isoated buildings and the isolation system against near-field pulse period ground motions as a result of resonance are being evaluated and shows that base-isolated builindgs and base isolation system are period dependent. Then, in this direction, the response of a high-rise and a low-rise building, which are isolated with Lead Core Rubber Bearing (LCRB) subjected to near-field pulse period ground motions are investigated. Since the fundamental natural period of a structure is not affected by fluid viscous dampers (FVD), FVD was implemented together with LCRB forming a kind of Fluid Viscous Damper-Base Isolation System (FVD-BIS).Therefore, several ground motions have been generated synthetically with a specific pulse period, and have been used in the analyses, which is set close to the fundamental period of the base-isolated high-rise building to facilitate resonance. However, some investigations have suggested that FVD can improve the performance of the base-isolated buildings, but the impact of FVD-BIS on the base-

isolated high-rise and low-rise buildings at the time of resonance is not clear yet. The results of this study have been illustrated that the intensity of the resonance phenomenon can be sharply mitigated in the base-isolated high-rise building using FVD-BIS.

Keywords: Lead core rubber bearing, Fluid viscous damper-base isolation system, Resonance phenomenon, Pulse-like ground motions, Probabilistic evaluation

ÖZ

Sismik yalıtım, yapısal bileşenler, yapısal olmayan bileşenler ve bina sistemlerinin içindeki ekipmanlar için depreme dayanıklı özellikler sağlamak üzere etkili çözümlerden biri olmasına rağmen, yakın-alan yer hareketlerinin etkisi altında rezonans nedeniyle beklenenin tersine artmış bir yapısal tepki ve dolayısı ile performansta ters verim kazandırabilmektedir. Bu nedenle, araştırmacıların en büyük zorluklarından biri, taban yalıtım sistemlerinin ve taban yalıtımlı binaların farklı yer hareketleri koşulları altında davranışını anlamaktır. Bu çalışmanın temel amacı, temelden yalıtılmış çok katlı binaların, Kurşun Çekirdekli Kauçuk Mesnetli (KÇKM) ve farklı bileşenli farklı yer hareketlerine maruz kaldıklarındaki tepkileri, yalıtılmamış binaların sismik tepkileri ile karşılaştırmak ve değerlendirmektir.

Bu amaçla, temel izolasyonlu binaların ve izolasyon sistemlerinin rezonans sonucu yakın alan darbe periyodu yer hareketlerine karşı zayıflığı değerlendirilmiş ve elde edilen sonuçlar, temeli izole binaların ve temel izolasyon sistemlerinin davranışı süreye bağlı olduğu gösterilmiştir. Daha sonra, bu doğrultuda yakın-alan darbe periyotlu yer hareketlerine maruz kalan KÇKM ile izole edilmiş çok katlı ve az katlı iki binanın tepkisi araştırılmıştır. Bir yapının doğal titreşim periyodunun Akışkan Viskoz Sönümleyicilerinden (AVS) etkilenmemesi nedeniyle, Akışkan Viskoz Sönümleyici ve Kurşun Çekirdekli Kauçuk Mesnet birlikte kullanılarak bir tür Akışkan Viskoz Sönümleyici-Temel Yalıtım Sistemi (AVS-TYS) oluşturularak uygulanmıştır. Bu nedenle, rezonansı kolaylaştırmak için, ele alınan temel yalıtımlı çok katlı binanın hakim titreşim periyoduna yakın olarak belirlenen belirli bir darbe periyodu ile sentetik olarak birkaç yer hareketi üretilmiş ve analizlerde kullanılmıştır. Bununla birlikte, bazı araştırmalar AVS'nin taban yalıtımlı binaların performansını

iyileştirebileceğini öne sürmüştür. Ancak, AVS-TYS'nin rezonans sırasındaki taban yalıtımlı çok katlı ve az katlı binalara olan etkisi henüz belli değildir. Bu çalışmanın sonuçları, rezonans davranışı şiddetinin, AVS-TYS kullanılarak temel-yalıtımlı çok katlı binalarda belirgin bir şekilde hafifletilebileceğini göstermiştir.

Anahtar Kelimeler: Kurşun Çekirdekli Kauçuk Mesnet, Akışkan Viskoz Sönümleyici-Temel Yalıtım Sistemi, Rezonans, Darbe-şeklinde yer hareketleri, Olasılıksal değerlendirme

Oh my lord, Let my entry be by the gate of truth and honour, and likewise my exit by the gate of truth and honour.

To my love Negin

For her advice, her patience, and her faith, because she always understood

ACKNOWLEDGMENT

First and foremost, praises and thanks to God, the Almighty, for his showers of blessings throughout my research work to complete the research successfully.

I would like to express my sincere gratitude to my supervisor, Assoc. Prof. Dr. Mehmet Cemal Geneş for his enduring patience, invaluable advice, kindly guidance and encouragement throughout this research effort. His warm communications due to their enthusiasm and cheerful heart are greatly appreciated.

Besides my advisor, I would like to thank Assoc. Prof. Dr. Mürüde Çelikağ, Assoc. Prof. Dr. Rifat Reşatoğlu and Prof. Dr. Polat Gulkan for their encouragement and insightful comments.

I also wish to express my deep gratitude to my mother for her continuous prayers and encouragement to my beloved wife, Negin for her special deep feeling and moral support.

In particular, I would like to sincerely dedicate this thesis to the memory of my father.

TABLE OF CONTENTS

LIST OF TABLES

LIST OF FIGURES

LIST OF SYMBOLS

$\ddot{u}_b$	Relative acceleration of the base slab
$\ddot{u}_g$	Longitudinal earthquake acceleration
a_0	Proportional coefficients
b_0	Proportional coefficients
c_d	Damping coefficient of viscous damper
c_{eff}	Effective Damping of the isolator
f_0	Normalized yield strength
F_b	Restoring force
f_y	Yield strength of the isolator
k_{eff}	Effective stiffness
k_i	Pre-yielding stiffness of the bearing
k_p	Post-yielding stiffness of the bearing
m_b	Mass of the base slab
m_t	Total mass
T_b	Isolator period
T_p	Pulse period
T_{sBI}	Fundamental period of the base-isolated building
T_{sFB}	Fundamental period of the conventional building
u_y	Yield displacement of the isolator
α_1	Post to pre-yielding stiffness ratio
ξ_d	Damping ratio of a viscous damper
ξ_{eff}	Effective damping ratio of an isolator

ξ_i	Structural damping ratio at mode i
ξ_j	Structural damping ratio at mode j
ω_b	Isolator frequency
ω_d	Damped natural frequency
ω_i	Structural modal frequencies at mode i
ω_j	Structural modal frequencies at mode j
C	Damping matrix
g	Gravitational acceleration
K	Stiffness matrix
M	Mass matrix
m	Mass of each floor
N	Number of stories
Q	Force at which the isolator hysteresis loop intercepts the vertical axis
u	Displacement vector
W	Overall weight of the building
z	Component of hysteretic displacement which is non-dimension

LIST OF ABBREVIATIONS

BIB	Base isolated building
BIS	Base isolation system
Du	Duration of the ground motions
FBB	Fixed base building
FD	Fault distance (km)
FVD	Fluid viscous damper
GMs	Ground motions
LCRB	Lead core rubber bearing
LRB	Laminated rubber bearing (without lead)
NPLGM	Non-pulse-like ground motions
PF	Probability of failure
PGA	Peak ground acceleration
PGD	Peak ground displacement
PGR	Peak ground response
PGV	Peak ground velocity
PHA	Peak horizontal acceleration
PLGM	Pulse like ground motions
PRF	Peak response of floor
PSD	Power spectral density
PVA	Peak vertical acceleration
RACC	Roof acceleration
RDIS	Roof displacement

Chapter 1

INTRODUCTION

1.1 Background and Basic Concepts

Failure of structures caused by the overall lateral drift resulting from the large earthquakes is a well-documented hazard. In an effort to achieve safer structures, research has been focused on developing auxiliary components relating to the seismic design of structures that limit the number of damages of a structure which can experience during earthquakes. These systems have been introduced where there is a prevalence of strong ground motions and considered to be essential or retrofit projects that are cost-prohibitive for alternative solutions.

Oscillation control is a set of technical means to minimize seismic damages on structural and non-structural components. Structural response to the ground motion remains the overriding challenge of dissipating large amounts of energy over a short period of time. Adding of control devices to the conventional structural system can achieve means of energy dissipation that isolate damage from or significantly reduces damage to primary structural elements. These control systems can be classified in Table 1.

Table 1: Structural seismic resistant systems [1]

“Passive control”	“Seismic isolation”	“Sliding or rolling mechanism”	“Slide plate bearing”
			“Sliding layers”
			“Roller bearing”
			“Others”
		“Flexible elements”	“Multi-layered elastomeric bearing”
			“Flexible pile bearing”
			“Others”
	“Energy dissipation”	“Hysteretic type”	“Steel”
			“Lead”
			“Others”
		“Friction type”	
		“Fluid type”	“Hydraulic type”
			“Viscous type”
			“Others”
		“Viscoelastic type”	
	“Active mass effect”	“Mass and spring type”	
		“Pendulum type”	
		“Vibration of liquid”	
		“Others”	
	“Others”		
“Semi active control”	“Damping control”	“Variable damping system”	“Hydraulic type”
			“Others”
	“Stiffness control”	“Variable stiffness system”	“Brace type”
			“Others”
	Others		
“Active and hybrid control”	“Additional mass effect”	“Active mass damper”	
		“Hybrid mass damper”	
		“Others”	
	“Force control”	“Active tendon”	
		“Others”	
	“Others”		

Over the past few years, passive control is considerably used as a system to approach for controlling earthquake vibration. These systems have been widely used because of their simplicity and low cost and easy to install and maintain rather than the active control system.

In the last three decades, base isolation systems (using passive control) have been widely implemented, and also several studies have been conducted in the last several decades in this direction. The seismic isolation method is now commonly used in many places in the world. Typically, a seismic protection device is put at the basis of a building. The isolation device partly represents and effectively absorbs some of the

earthquake entry energy by means of its functionality before this energy can be passed to the building.

1.1.1 Different Type of Seismic Isolation Systems

Several base isolation systems for seismic safety of buildings have been constructed and introduced around the world. In this section, a brief explanation of the mechanical properties, numerical and fundamental modeling is given for a limited number of different base isolation systems. Followings are given three samples for the most commonly used base isolation systems:

1.1.1.1 Natural Rubber Bearings (NRB)

Natural Rubber Bearings (namely Laminated Rubber Bearing (LRB)) were widely used to protect the buildings against earthquakes in Japan. This type of isolation system comprises many natural rubber layers and thin steel sheets and two thick endplates (illustrated in Figure 1a). The rubber is vulcanized under the heat and pressure to the steel shims within a mold. Steel shims in the bearings provide the high vertical stiffness, which has no effects on the lateral stiffness and has low shear modulus. The behavior of the material is almost linear (Figure 1b) in this type of the bearings (shear strain 100%), the damping ranges between 2% and 3%. Moreover, the advantages and disadvantages have been illustrated in Table 2.

Table 2: The advantages and disadvantages of LRB

Advantages	Disadvantages
- Simple to manufacture - Easy to model - Response not strongly sensitive to the rate of loading, history of loading, temperature, and aging.	- Need supplemental damping system

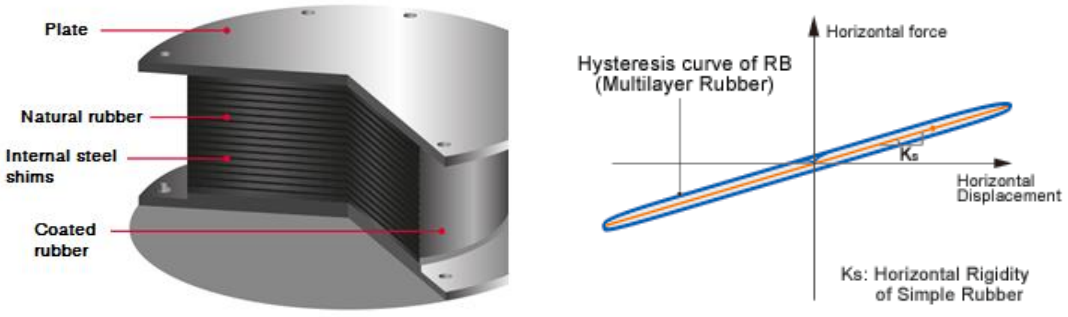

(a) (b)

Figure 1: a) Natural Rubber Bearing (Laminated Rubber Bearing (LRB)); b) Linear behavior of the Natural Rubber Bearing (K_s is the lateral stiffness) [2]

1.1.1.2 Lead Core Rubber Bearing (LCRB)

The Lead Core Rubber Bearing (LCRB) was invented in New Zealand in 1975 [3; 4], and it has been widely used in New Zealand, the United States, and Japan. Lead Core Rubber Barings are similar to Natural Rubber Bearing but contain lead plug which is inserted into the holes through the rubber and steel shims in the base isolation system (details are presented in Figure 2a). The steel sheet in the system makes the lead plug to deform in shear. The lead plug deforms in flow stress of about 10 Mpa and provides the base isolation system with a bilinear behavior (Figure 2b).

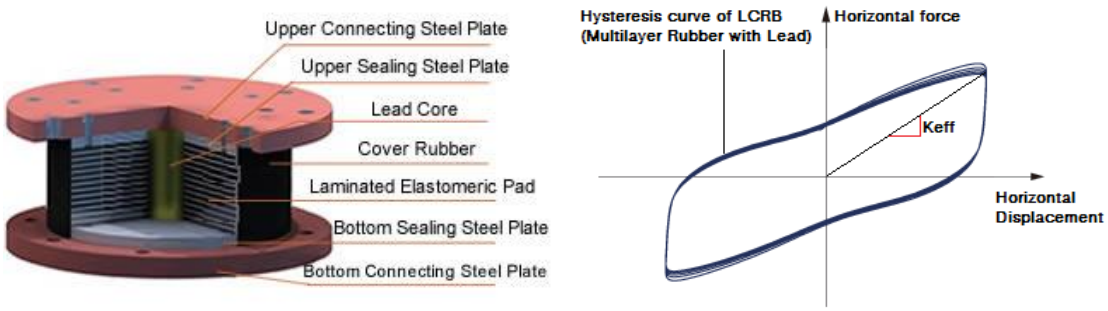

(a) (b)

Figure 2: a) Lead Core Rubber Bearing (LCRB); b) bilinear behavior of Lead Core Rubber Bearing (K_{eff} is the lateral effective stiffness) [5; 6]

1.1.1.3 Friction Pendulum System (FPS)

The friction pendulum system (FPS) is a system of frictional isolation that combines a sliding action with geometry restoring forces. FPS bearing provides a spherical surface and is the most common seismic isolation system used within the U.S. Figure 3 represents the details of FPS. As can be seen from this figure, the sliding surface shows the concave shape of the FPS. The concave surface with the radius of R defines the geometry of the spherical sliding surface. The spherical surface is made when the circle is rotated above a vertical axis. A part of that surface forms the bearing's sliding surface (Figure 4).

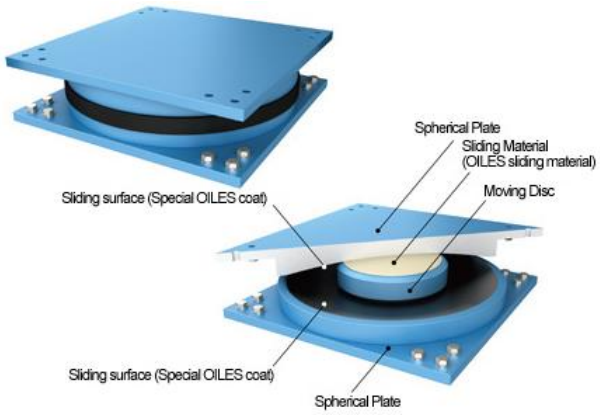

Figure 3: Spherical Sliding Bearing: Friction Pendulum System (FPS)[7]

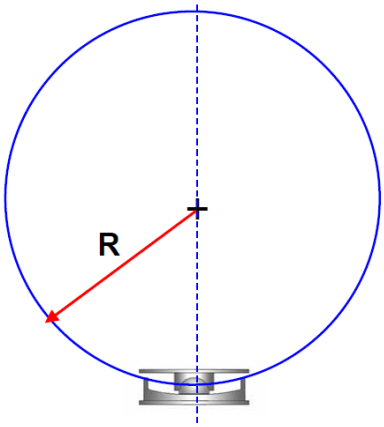

Figure 4: Radius of curvature of Friction Pendulum System[7]

1.1.2 Period Shift, Damping and Flexibility

Dominant periods of the typical ground motions are almost between 0.1 s and 1 s, as illustrated in Figure 5, and the maximum severity of the ground motions often lie between 0.2 s and 0.6 s. The buildings, whose fundamental period lies between the range of 0.1 s and 1 s, are vulnerable against those earthquakes because they may resonate. The most important specification of the base isolation system is by increasing the flexibility of the buildings, fundamental period of the buildings increases. Since the period is increased beyond that of the ground motions, resonance, or close-to-resonance is avoided, and the response of seismic acceleration is decreased [8].

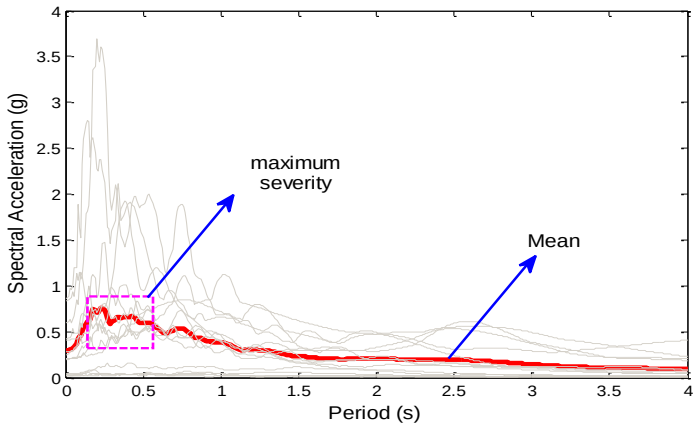

Figure 5: Response spectral for a range of earthquakes and their median

Basically, the base isolation system's main aim is to decrease the seismic forces exerted on the superstructure of a building. This decrease in seismic forces is partially obtained by decreasing the spectral accelerations of the superstructure. This acceleration is decreased as period shifts (fundamental period of the isolated building increased), and damping increased as the energy dissipated by base isolation systems. Period shifts and increased damping are both illustrated in Figure 6. On the other hand, as the period increases, the displacement of the base isolation system

(structure) also increases (see Figure 7). Figure 7 briefly shows the main and strategy of using the base isolation systems.

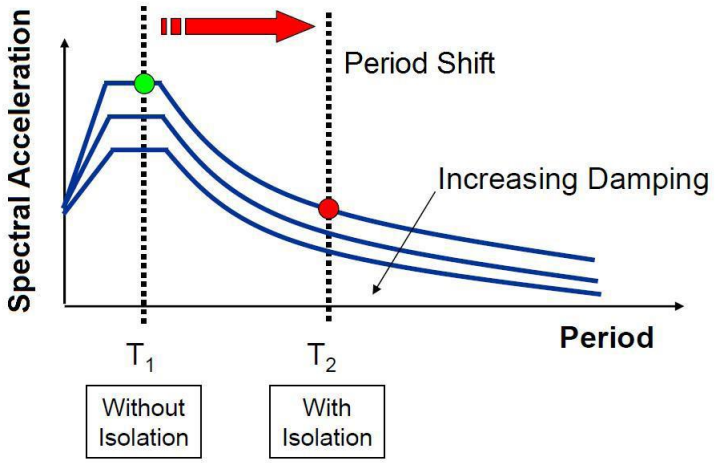

Figure 6: Period shift when the base isolation system is used [9]

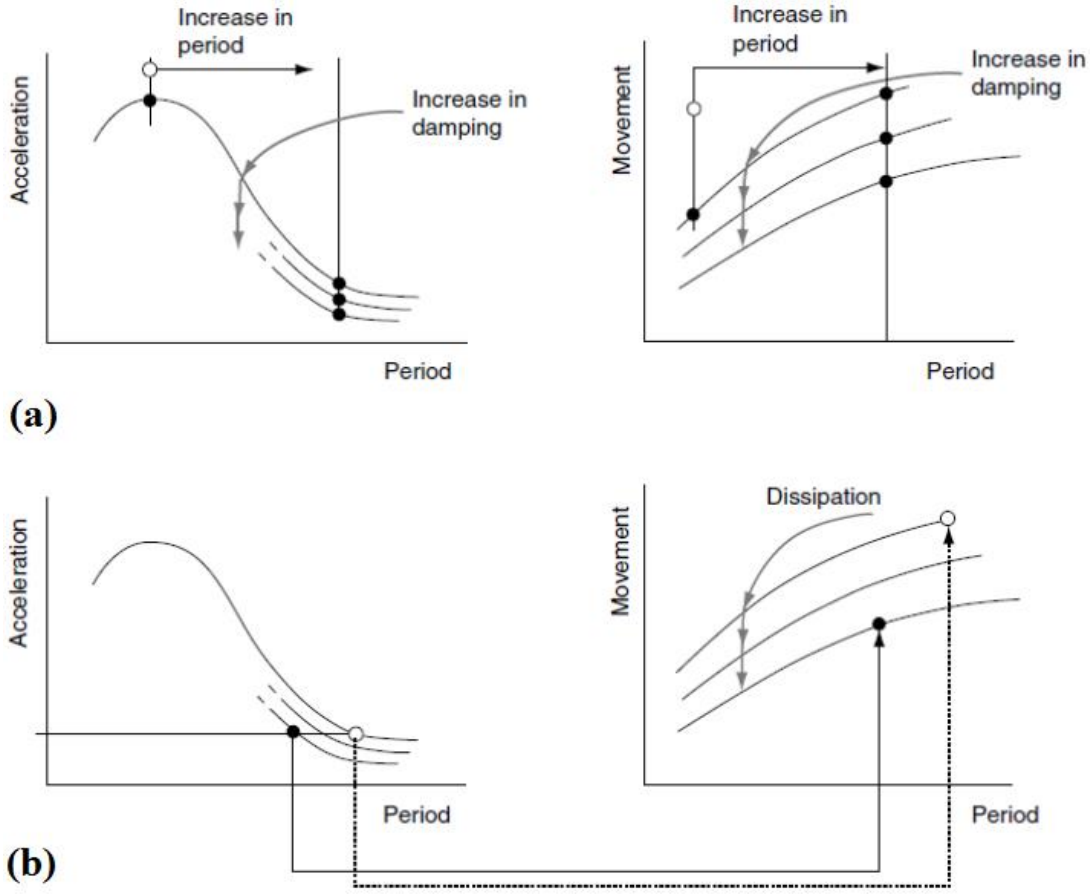

Figure 7: The aim and strategy of using the base isolation system: a) increasing period; b) limitation of the force and damping [10]

According to Eq. (1), an effective period of the base isolation system can be calculated [11]. In this equation, it can be seen that the period and stiffness of the system is inversely correlated. Briefly, as the lateral stiffness of the structure decreases (flexibility increases), the period of the structure increases.

$$T = 2\pi\sqrt{\frac{M}{K}} \qquad \downarrow K \Longrightarrow T \uparrow \tag{1}$$

Where:

T: effective period

K: effective stiffness

M: total mass

Damping of the base isolation system is developed by partially limiting the movements of the bearings via energy dissipating. In the case of Lead Core Rubber Bearing (LCRB), which is the type of isolation system used in this investigation, the restoring force of this type of isolation system causes energy dissipation. In the next section, the restoring force of this type of bearing will be discussed in more detail. The amount of energy dissipated by this type of isolation system can be calculated by calculating the area under the force-deformation curve of the isolation bearing. The force-deformation behavior of the bearing is modeled as non-linear hysteresis behavior which is illustrated by bi-linear model (Figure 8), and for this type of isolation system elastic stiffness for each cycle of loading is obtained from experimental force-deformation behavior which can be mathematically derived as [12; 11]:

$$k_{eff} = \frac{F^{+} - F^{-}}{\Delta^{+} - \Delta^{-}} \tag{2}$$

Moreover, effective viscous damping of the isolator can be calculated for each cycle of the loop as:

$$\beta_{eff} = \frac{2}{\pi}\left(\frac{E_{loop}}{k_{eff}(|\Delta^+| - |\Delta^-|)^2}\right) \quad (3)$$

E_{loop} (EDC: Energy Dissipated Per-cycle) is the area under the curve which is equal to the amount of damping. The definition of a loop is the isolator movements to the maximum displacement then back to the minimum displacement, which forms a loop. As it is clear in Eq. (3), effective viscous damping (β_{eff}) is based on E_{loop} and effective stiffness (k_{eff}) of the isolation system.

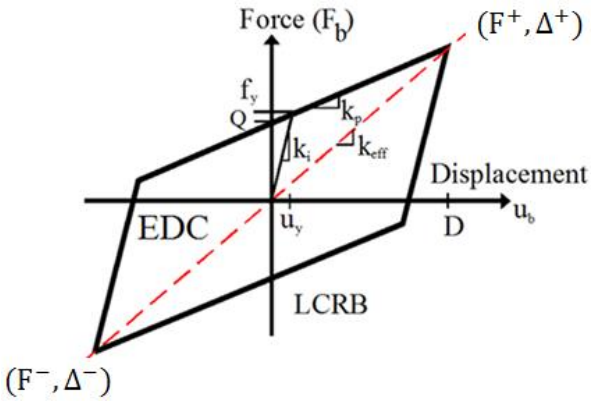

Figure 8: Bi-linear hysteresis model of LCRB

By reducing the responses, the building remains in the elastic region, or close to the elastic region according to the design level event. At the same time, decreases in acceleration and drift requirements obtained by seismic isolation devices make it one of the most helpful strategies to obtain greater efficiency despite severe and rare earthquake events. Several isolated systems have been suggested, applied, and researched since the creation of the base isolation technique, particularly concentrating on their ability to bear vertical stresses and resist large lateral deformations. However, rarely investigations have been carried out to study the behavior of the base isolation system under the ground motions with different components.

Since its behavior is uncertain due to the effect of near-field earthquakes, mainly when it is used for different types of building varied in height, an excessive structural response could be obtained because of the resonance phenomenon.

1.2 Significance of This Research

In recent years, several practical systems have been developed and executed worldwide to achieve seismic isolation and various energy dissipation devices. Since there is limited scientific understanding on the behavior of the most practical isolator, LCRB, and base-isolated buildings, one of the greatest challenges faced by researchers is understanding the behavior of the base isolation system and base-isolated buildings under the conditions of different ground motions (PGA/PGV and T_p) by considering the effectiveness of the ground motion's components and inherent mechanical properties of the designed base-isolated buildings. One of the significant focuses of this research will be on this challenging subject.

Moreover, the performance of the base-isolated buildings is also questionable under the effect of pulse-like ground motions, in which case an increased structural response might be obtained due to resonance. After an extensive literature survey performed during this research, it has been found that no considerable research has been done on the resonance phenomenon, which can be highly mitigated by using a passive control system, which is more economical than active or semi-active control systems. Another significant focus of this research will also be on this problem.

1.3 Objective of the Research

The main objective of this research is to get a better understanding of the behavior of the base-isolated buildings (5-, 10-, 15-, 20-, 25, 30- and 35-story) and one of the most practical base isolation systems (LCRB) subjected to the most credible excitations. In this study, the effect of the ground motion's components and

mechanical properties of the base-isolated buildings and the base isolation system considering the key responses of the seismically isolated buildings have been assessed and highlighted the type of the ground motions that can be used appropriately to evaluate the behavior of the long period base-isolated buildings.

In addition, however, the seismic isolation is one of the methods which provides earthquake-resistant for structural components, non-structural components, and contents of the buildings. Its' performance is questionable under the effect of the pulse-like ground motions, in which case an increased structural response might be obtained due to resonance. Since the base isolators and base-isolated buildings are period dependent and the pulse periods of ground motions are usually between 2 and 13 seconds, the responses of the buildings will be highly amplified when the fundamental period of the base-isolated building is close to the dominant period of the ground motions, especially in the base-isolated high-rise buildings.

Thus, the second objective of this research is to evaluate the resonance phenomenon (vulnerability) of the base-isolated high-rise building, which will be, firstly, subjected to syntactically generated ground motions due to a parametric study, and then, to different natural near-field pulse period ground motions.

Finally, as the fundamental natural period of a structure is not affected by fluid viscous damper (FVD), the final objective of this study is to add FVD to LCRB system, which forms a model of Fluid Viscous Damper-Base Isolation System (FVD-BIS). Then, the seismic responses of the base-isolated buildings (5- and 20-story), which will be compared with those of the base-isolated buildings without additional damping subjected to different pulse period earthquake motions, were investigated at the particular instant of time when resonance occurs. However, some investigations have suggested that FVD can improve the performance of the base-

isolated buildings, but the impact of FVD-BIS on the base-isolated buildings at the time of resonance is not clear yet. The results of this study provide some clarification in this direction.

1.4 Research Plan

The aim of this study was fulfilled through the following five-task study plans:

1. The governing equation of motion of base-isolated building and base isolation system has been developed and modeled in MATLAB, and then the validity of the program was confirmed by comparing the results obtained from [13] and [14].

2. However, by the existence of the various historical ground motions, they may not be sufficient to undertake parametric studies. In this direction, near-field earthquakes have been created synthetically according to the method proposed by He and Agrawal [15] and validated with the synthetically generated ground motions in [16].

3. Natural ground motions are selected randomly from PEER strong ground motion database center and categorized into three different ratios in terms of PGA/PGV, and seven different types of base-isolated buildings (different in height) have been considered. In order to evaluate the behavior of the base-isolated buildings, a two-factor factorial design (the first factor is the ratio of PGA/PGV and the second factor is the height of the base-isolated buildings) was conducted using Minitab software (version 2017).

4. In order to investigate the resonance phenomenon in base isolation system and base-isolated high-/low-rise building, first, ground motion is generated synthetically with specific pulse period (T_P) at different fault distances and equalized to the fundamental period of the base-isolated high-rise building (T_{sBI}), which is the main condition that needs to be set to show the resonance phenomenon. Then, the

compound system has been modeled using the base isolation system and fluid-viscous damper (FVD) to show the percentage reduction of the intensity of the ground motions induced to the base-isolated building at the time of resonance.

5. Pulse-like ground motions have been selected from PEER strong ground motion database with different pulse periods and have been set in order (pulse period of the natural ground motions found to be between 0.5 s and 14 s). Then the characteristic behavior of the ground motions and the responses of the base-isolated high-rise building (20-story base-isolated building) and low-rise building (5-story base-isolated building) subjected to the above-mentioned ground motions have been studied.

1.5 Organization of Thesis Proposal

To evaluate the behavior of the base isolation system and base-isolated buildings subjected to the different ground motions with different components following steps have been organized:

Chapter 2 gave some information about the previous studies and a brief background of the subject area.

Chapter 3 represents the methodology and the limitations that are considered during analysis for base-isolated buildings and characteristic behavior of the base isolation system (LCRB) and the mechanical properties of this system have been discussed. Then in Chapter 4, the validity of the written code in MATLAB has been evaluated and compared with Ref. [13] and [14].

Chapter 5 discussed different components of the ground motions which were selected from PEER strong ground motions data base. In this chapter, the intensity of the selected ground motions with regards to their components has been evaluated and illustrated in figures.

In Chapter 6, behavior of the base-isolated buildings and base isolation system subjected to various earthquakes with different components had been assessed for seven different base-isolated buildings in height (5 to 35-story building).

In chapter 7, in order to investigate the effectiveness of Fluid Viscous Damper (FVD) combined with base isolation system against the resonance phenomenon and due to the importance of the Pulse-Like Ground Motions (PLGMs) for the highest intensity, PLGMs have been selected to carry out the parametric investigation. Then, the vulnerability of the base isolation system and base-isolated buildings for both low-rise (5-story) and high-rise (20-story) base-isolated buildings had been discussed. Therefore, by implementing the FVD-BIS (Fluid Viscous Damper-Base Isolation System), the effectiveness of this system had been investigated at the critical instant of time (at the time of resonance) subjected to different type of pulse-like ground motions.

Finally, in Chapter 8, conclusions achieved from this study were given.

Chapter 2

LITERATURE REVIEW AND BACKGROUND

2.1 Introduction

Severe earthquakes frequently result in loss of lives and societal disruption because of the collapse of buildings due to the absence of appropriate design of earthquake-resistant systems. To prevent the loss of lives, the methodology of the earthquake-resistant design should be based on the ductile behavior of the structures where it should be mobilized during severe earthquakes. Over the past few years, passive control has been frequently used as a system for mitigating earthquake vibration. These systems are widely used because of their simplicity and low cost along with easy installation and maintenance compared to the active control systems.

Seismic isolation is a methodology to design structures against earthquakes. By uncoupling the building from the imposed ground motion effects, the earthquake excitation will result in lower forces to the building than the conventional building without an isolator.

In a base-isolated building, the building is physically separated from the ground. When an earthquake occurs, the period shifts and causes a reduction in the acceleration of the floor and inter-story drift on the superstructure, which can be compared with a building that is not isolated. As the responses are reduced, it allows the building to remain in the elastic, or close to the elastic region according to the design level event. Simultaneously, reductions in acceleration and drift demands, which are gained by seismic isolation systems, make it one of the most useful tactics

to achieve better performance following strong and infrequent earthquake events. Since the development of the base isolation method, several isolation devices have been suggested, implemented, and studied, especially focusing on their capacity to carry vertical loads and withstand large horizontal deformations.

As a result, a better performance level of the building can be achieved using base isolators. However, as the isolators are period dependent (e.g., generally base isolation system period is between 2 s and 5 s), it makes them vulnerable under long-period earthquakes, thereby necessitating resistant structural system components to be designed by taking this into account. Moreover, the base isolation systems and base-isolated buildings are highly affected by ground motion characteristics and may behave differently for different seismic events.

2.2 Review of Seismic Isolation History

Although the idea of seismic isolation goes back over 100 years, it has only been executed for the last three centuries in the United States. The first seismic isolation record is submitted as a U.S. patent (1870) in San Francisco for a two rolling ball bearing, which is known as “Earthquake-proof building” [17; 18]. The mentioned bearing in 1870, is similar to the modern Friction Pendulum bearings [18; 19]. After one hundred and fifteen years (1985), the Justice Center in Rancho Cucamonga, California and the Foothill Communities Law were the first base-isolated buildings built in the U.S. [11]. They were both built on 98 high-damped natural rubber bearings. Naiem and Kelly have an in-depth historical view and chronology of seismic isolation [11]. Since 1980s, constructing seismically isolated buildings dramatically increased both in China and Japan. Seismic isolation has also been used to protect the nonstructural buildings such as offshore platforms, liquefied natural

gas (LNG) tanks, and bridges [20]. However, as the focus of this article is on seismic isolation of buildings, these systems are not discussed further.

A variety of latest and old publications have given extensive assessments of multiple elements of seismic isolation technology development, theories, and implementation. They were outstanding thorough early assessments. The most practical work is still based on a sequence of deterministic inelastic dynamic time-history analyses [21; 22].

Kelly [23] presented a historical view from the rudimentary origins of earthquake isolation technologies, accompanied by a thorough chronology of research and development efforts. Besides, Buckle and Mayes [24] included a historical debate and an extensive catalog of initial applications that paved the way for acceptance and wider implementation. Taylor et al. [25] provided a study of elastomer used in seismic isolation bearings, focusing on their long-term behavior. A study in the mid-1990s presented data on several subtopics, including hypothesis, tests, and implementation of friction bearings, hybrid testing, development, and practice in many countries [26]. Since the quantity of seismic isolation information in the last 10-15 years has increased dramatically, the efforts to complete an evaluation have declined. However, there have been several concentrated studies. In addition to analytic, experimental, and parametrical studies, Kunde and Jangid [27] have prepared extensive research and application of seismic isolation on bridges. Symans et al. [28] evaluated the design and implementation of wood framework structure seismic isolating and damping technologies which are extremely difficult to identify due to the comparatively lightweight and flexibility of the framing system. The latest primer, developed by the American Society of Civil Engineers (ASCE) [29], addresses the United States-specific requirements for the hypothesis, technology,

evaluation, design, and testing. Eventually, a partnership between global professionals working as portion of the International Council for Research and Innovation in Building and Construction (CIB) Task Group 44, provided a document assessing equipment, design codes and current state of the practice of seismic isolation between countries that have made progress with the implementation of seismic isolation technology [1].

A vast majority of research has been done to present the effectiveness of seismic isolation that provides the building to behave linearly elastic during the horizontal ground motions, and due to the lack of space, It was impossible to state all previous studies in this investigation.

2.3 Background

Several interesting studies have been conducted on base-isolated structures and base isolation systems under different seismic activities [30; 31; 32; 33; 34; 35; 36]. The performance limits of seismically protected structures with a broad variety of distinct isolation periods and isolation damping properties are reported at variable fault distances in the near-field region, which are subject to "practical" maximum base displacement and top floor acceleration [16].

It has been found that isolator displacement decreases significantly by variation of the mechanical property of the base isolation systems such as increasing yielding strength around the particular yield strength. This implies that increasing the bearing yield strength can reduce the bearing displacement without significantly affecting the superstructure acceleration [37].

Alhan et al. [16] noted the performance limit of base-isolated buildings subjected to various near-field ground motions with different velocity pulse periods. Although the isolation system may be effective under far-field ground motions, it is still

complicated for near-field ground motions. It was also illustrated that the proportion of the base isolation period to the pulse period of ground motions (T_b/T_p) considerably affects the displacement of the base and the acceleration of the story for long and short pulse periods, respectively. In addition, this was found for small ratios of the base isolation system period to pulse period and for shorter fault distances.

Deringöl et al. [38] studied the effectiveness of the isolation period and ratio of isolation strength to the weight in terms of the roof displacement, absolute acceleration, inter-storey drifts, force-deformation behavior and base shear for 5 and 10-story base-isolated buildings. They observed that by reducing the yielding strength to weight ratio and isolation period, it causes to reduce the absolute acceleration, relative displacement, base shear and inter-story drift ratio for 5-story base-isolated building. And also they concluded that beside mechanical properties of the isolation system characteristics behavior of the ground motions and number of story had significant effect on the responses of the base-isolated buildings.

Matsagar et al. [12] illustrated that the responses of multi-story base-isolated buildings affected by different characteristic parameters of the isolator. The shape of the force-deformation behavior of the isolator, which affects the responses of the base-isolated structure, is investigated under the main varied parameters, such as the yield displacement of the isolator, flexibility of the superstructure, time period of the isolator and number of stories of the base-isolated structure. It was found that the form of the hysteresis loop of the isolation system considerably affects the responses of the base-isolated buildings.

In addition, Samali et al. [39] carried out a case study with an experimental setup on a shake table. In their research, a mass modeled with eccentricity above the base isolation system was considered. Therein, the dynamic behavior of a five-story

bench-mark building with mass eccentricity under four different earthquake scenarios was investigated. Moreover, it was demonstrated that the related base isolation system behaves ineffectively under some kinds of earthquakes.

Jangid [37] assessed the behavior of the LCRB system for multi-story buildings subject to near-fault ground motions. In his study, the response of the system under six different ground motions was evaluated, and variations in top-floor absolute accelerations and bearing displacements of the multi-story base-isolated building were examined and illustrated. As a result, the yield strength (f_y) of the LCRB was found to be between 10% and 15% of the building weight under different ground motions.

Mavronicola [40] studied two special cases of isolated building responses during seismic activities. First, the nonlinear behavior of the lead rubber bearing and, second, a base-isolated building with an adjacent structure were investigated when subjected to very strong earthquakes. The relative displacements of the isolator were underestimated, and the peak floor accelerations were overestimated by the bilinear model.

Chimamphant et al.[41] proposed 3-, 9- and 20-story base-isolated and fixed-base buildings (MDOF shear-beam models), and the effects of such essential structural parameters, such as the isolator stiffness, the damping ratio of the isolator and the number of stories, on the responses of the base-isolated buildings were studied parametrically. It was discovered that the return period might be very sensitive to short buildings and less sensitive to tall buildings. Moreover, they also found that longer isolation period has low drift ratios and less acceleration. In contrast, higher damping ratios of isolation increase the acceleration and drift ratios. And compared with fixed-base building, base isolation systems are efficient even for tall buildings.

Takewaki et al. [42] investigated the strength of the base-isolated tall buildings with the code defined for ground motions. They considered two kinds of base isolation systems, namely, linear or natural rubber bearings and friction-type bearings. In their assessment, the inverse problem was generated for the targeted drift of the base-isolated building to specify the required amount of additional viscous damping. As the height of the base-isolated building increases, the damping ratio decreases. Moreover, it was concluded that high-rise buildings that are base-isolated have low resistance against ground motions than base-isolated low-rise buildings.

Jalai et al. [43] studied the performance of the multi-story base-isolated buildings with lead core rubber bearing considering the superstructure mechanical properties such as stiffness, damping and mass. They observed that the mass has positive effect on the energy dissipation through the base isolation system and they found that by increasing the mass, the isolation performance increases for the mid-rise base-isolated buildings, while the variation of the superstructure mass does not significantly affect the performance of the low-rise base-isolated buildings.

Besides, in previous studies, it was reported that the seismic responses of the base-isolated buildings could be increased if the pulse period of the earthquakes is equal to the fundamental period of the base-isolated building or base isolation system [35; 44; 45; 46]. As such, different types of active or semi-active control systems are used to overcome this problem, which is not economical and needs sustained maintenance.

Addressing the problem mentioned above, several studies have been carried out to study the vulnerability of a base-isolated building and investigate the reduction of the responses of the building under some design earthquakes using passive and active control systems [16; 47; 48].

In other studies, to enhance the sustainability of the base isolator, Yang et al. [49] investigated the benefit of a new type of isolator called magneto-rheological-elastomer (MRE) under severe earthquakes. The Fuzzy Logic method was used in their semi-active control system to control the magnitude of the electromagnetic field based on the real-time responses of the floors of a building. They concluded that the lateral stiffness of this kind of system would increase by about 18 times. Further, increasing the frequency of the isolator helps it keep the structural frequency far from the resonance and reduce the oscillation in the structure.

Politopoulos et al. [50] studied the vulnerability of the base-isolated building and conventional building. They found that the base-isolated buildings are more sensitive when subjected to some ground motions and the probability of damage will be the same for both types of buildings, although the isolated buildings are designed according to FEMA 368[51] and show less damage than a conventional building.

Hall et al. [52] tested the effect of the near-field earthquake on the flexibility of structures. In their studies, they generated ground motions with the magnitude of M_w = 7.0, causing responses to be further enhanced in tall fixed-base buildings. They concluded that a typical base-isolated building in Southern California would impact the perimeter wall (barriers) and other components if it is located within the region of the near-field earthquakes. This damage to the building as well as its contents and cause the facilities to remain un-functional after the earthquake.

Jangid et al. [53] studied the behavior of the base isolation system for near-fault motions. They observed that increasing the bearing damping may decrease the bearing displacement to some extent while raising the acceleration in the superstructure.

Moreover, hybrid control systems of base isolation systems with other additional damping devices or a combination of passive control systems parallel with active control systems are also investigated to study the behavior of the seismically base-isolated buildings. In this direction, Lyan-Ywan Lu et al. [54] numerically investigated a different type of semi-active damper with the conventional base isolation system. They found that this kind of system is capable of reducing the acceleration responses of the base-isolated building subjected to the ground motions with a long period compared to the conventional one.

Yunfeng et al. [55] assessed the behavior of a combination of base isolators and semi-active control systems called Tuned Interaction (TI) damper for a 5-story base-isolated building. They found that this kind of system is highly capable of reducing the inter-story drifts and accelerations at low levels under near-field earthquakes. They also suggested that the additional viscous base damper would be more useful for the behavior of the base-isolated buildings at the displacement of the base and acceleration at each floor level under earthquakes for a long period.

Regards to the effectiveness of the viscous damper, Elif et al. [56] evaluated the effects of the isolation system on the capacity of the viscous damper of the base-isolated adjacent buildings. They found that changing the mechanical properties of the base isolation system causes a considerable effect on the behavior of the adjacent buildings, which is a result of the isolator period that shifts the fundamental period of the superstructure. They also stated that as the number of story increases (multi-story building), the flexibility of the base-isolated building considerably affects the relative displacement between the base and top floors. In this case, the viscous damper was successful in mitigating the pounding for multi-story base-isolated adjacent buildings.

Alhamaydeh M. H. et al. [57] presented about implementing of the multi regression model to isolation systems including the combination of the natural rubber bearing and viscous fluid damper subjected to near field earthquake ground motions for a 5-story building. They compare the total maximum displacement, maximum damper force and top floor acceleration ratio of the base-isolated building to the fixed-base building. As a result, total maximum displacement, as well as the base shear, was the most important criteria of the key performance according to the multi regression analysis model.

Providakis et al. [58] studied the influence of the lead-rubber bearing together with viscous damper for base-isolated building subjected to near field ground motions. They investigated the effect of the isolation damping on the bearing and the superstructure drift. They concluded that providing supplemental damping devices such as viscous damping to the bearing will increase the drift when subjected to near field ground motions.

Wolff E.D. et al. [59] evaluated the effectiveness of viscous damping equipment on the base-isolated buildings. They found that when damping is required to reduce the displacement of the isolator linear viscous damping causes the least damaging effect on the base-isolated building. They also added, to predict floor response spectra and the peak floor acceleration may cause errors that should be considered as designing subsidiary devices.

Chapter 3

METHODOLOGY

3.1 Typical Step for Model Analysis

In this investigation, the lumped-mass stick model, previously introduced by Kelly [11; 60], has been used to represent a multi-degree of freedom structure (Figure 9). The modeling and time history analyses of the seismically isolated buildings have been implemented in the program originally developed in MATLAB. In this study, the response quantities of interest are the absolute acceleration and relative displacement for the base-isolated buildings.

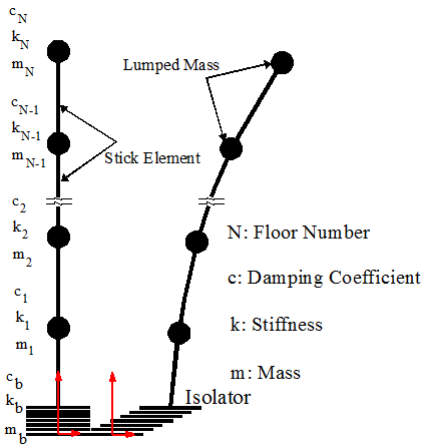

Figure 9: Lumped-mass stick model

3.1.1 Limitations

During analysis, the following assumptions are made for the structural systems:

- Throughout the time-history analyses, the superstructure is assumed to remain linear-elastic (design of element cross-sections have not been made)

- Each floor is considered to be rigid in its own plane
- The model is subjected to only one horizontal component of the ground motions
- Lumped mass is assumed to exist at each floor level
- The force-deformation behavior of the LCRB is considered to be bilinear, and it is modeled by using Wen's equation [61]
- Overturning of the base isolation system does not occur during the sliding
- Torsion does not occur during shaking due to the symmetric plane of the buildings

An idealized model of a multi-story structure is illustrated in Figure 10. This illustrates and idealizes the model of the base-isolated building (Figure 10a), idealization of LCRB system (Figure 10b), Bilinear force-deformation hysteresis of LCRB (Figure 10c) and fixed base building (Figure 10d).

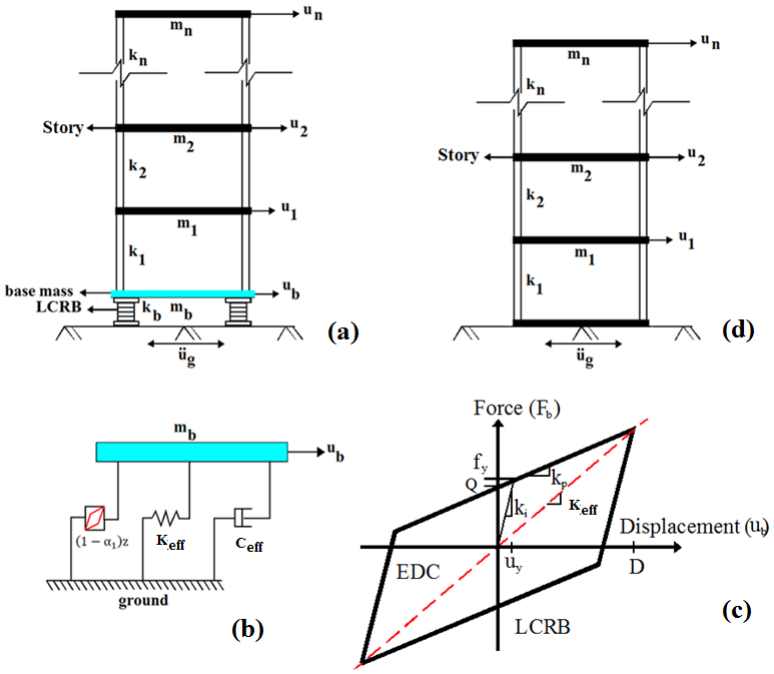

Figure 10: Idealized model of a multi-story structure: a) Base-isolated building (BIB); b) Idealization of the LCRB isolator; c) Bilinear force-deformation hysteresis of LCRB; and d) Fixed-base building (FBB)

3.1.2 Governing Equations of Motion

The governing equation of motion has been generated by considering the equilibrium of forces at each degree of freedom for the models in Figure 9 and Figure 10.

3.1.2.1 Fixed-Base Building

The equation of motion is as follows for a fixed base building, [11; 62]:

$$\mathrm{M\ddot{u} + C\dot{u} + Ku = -Mr\ddot{u}_g} \quad (4)$$

Where, M is a diagonal mass matrix and specified by each floors' mass, which is kept constant (i.e., m_i = m for i = 1, 2, 3…, N-1 for top floor m/2), C is damping matrix, and K denotes the stiffness matrix of the superstructure ($n \times n$); u is the relative displacement vector ($n \times 1$) with respect to the ground, and a dot denotes derivative with respect to time; r shows an influence vector ($n \times 1$) with unit in the earthquake direction and $\ddot{u}_g$ reflects the acceleration of an earthquake exerted to the base of the building. The structural damping matrix (C) can be calculated using the Rayleigh method, which is the proportion of the mass and stiffness as follows:

$$\mathrm{C} = a_0\mathrm{M} + b_0\mathrm{K} \quad (5)$$

Where, $a_0 = \xi_i \frac{2\omega_i\omega_j}{\omega_i+\omega_j}$ and $b_0 = \xi_i \frac{2}{\omega_i+\omega_j}$ are damping proportional coefficients; ω_i and ω_j represent structural modal frequencies, and ξ_i and ξ_j show structural damping ratios for modes i and j, respectively.

3.1.2.2 Base-Isolated Building

The governing equation of motion for a base-isolated building including m_b is [11]:

$$\mathrm{M\ddot{u} + C\dot{u} + Ku = -Mr(\ddot{u}_g + \ddot{u}_b)} \quad (6)$$

Where, $\ddot{u}_b$ is the acceleration of the base slab relative to the ground. Hence, the equation of motion related to the base slab is as follows [11]:

$$m_b\ddot{u}_b+c_b\dot{u}_b + F_b - k_1u_1 - c_1\dot{u}_1 = -m_b\ddot{u}_g \quad (7)$$

Where, F_b is known as restoring force generated in the isolator system (Figure 11); c_b reflects the damping coefficient of the isolator; k_1 is the stiffness, and c_1 is the damping coefficient of the first floor; u_1 denotes the displacement and $\dot{u}_1$ is the velocity of the first floor. Finally, m_b is the mass of the base slab.

For hybrid control devices (implementing FVD-BIS), the governing equation of motion given in Eq. (6) for the building will be changed to:

$$M\ddot{u} + C\dot{u} + Ku + F_d = -Mr(\ddot{u}_g + \ddot{u}_b) \quad (8)$$

Where, F_d is the damping force of the viscous damper.

Since the damping matrix is not explicitly known, equivalent viscous damping was modeled differently for the base-isolated building (non-classical damping). Generally, the damping matrix is created for conventional buildings using the Rayleigh method, which is mass and stiffness proportional (mentioned above in Eq. (5)). Instead, for seismically isolated buildings, a more appropriate stiffness-proportional damping model was adopted, according to Ryan and Polanco [63] and Pant et al. [64] by associating the damping ratio of 2% and first mode frequency as follows:

$$C = b_0K \quad (9)$$

Where, $b_0 = \xi_i \frac{2}{\omega_i}$ is the damping proportional coefficient.

3.1.3 Numerical Modeling of Lead Core Rubber Bearing (LCRB)

LCRB systems are commonly recognized as N-Z isolator systems. LCRB systems are laminated rubber bearing (LRB) systems, But, in order to enhance the energy dissipating ability and initial hardness against small shakes, a lead-core system is placed in the center [65; 66]. This system essentially behaves as a hysteretic damping

device. The hysteretic behavior of the LCRB is generally represented by non-linear characteristics (Figure 11).

For the present investigation, the Bouc Wen model [61] has been applied to determine the hysteretic behavior of the LCRB, as displayed schematically in Figure 11. Further, with regards to the governing equation, implementation of the restoring force for the isolation bearing is considered as [61]:

$$F_b = \alpha_1 k_i u_b + (1 - \alpha_1) f_y z \quad (10)$$

In Eq. (10), f_y is the isolator's yielding strength where the pre-stiffness is changed to post-stiffness; Q represents the characteristic strength, u_y denotes the yielding displacement (Figure 11); α_1 shows post- to pre-yielding stiffness ratio; and k_i is the pre-yielding stiffness of the LCRB, typically at a displacement less than 25.4 mm (see Figure 11). The ratio between the post- to pre-yielding stiffness ($\alpha_1 = \frac{k_p}{k_i}$) is α_1 and u_b denotes the base slab relative displacement with respect to the ground. The value of k_i is dominated by the size of the lead core and is important for controlling the service load response. k_p is the post-yielding stiffness of the LCRB and is a function of the modulus, total height, and area of the rubber. z is the component of the hysteretic displacement, which is non-dimensional and satisfies the following differential equation which can be written as [61]:

$$\dot{z} = u_y{}^{-1}(A\dot{u}_b - \beta|\dot{u}_b||z|^{n-1}z - \gamma\dot{u}_b|z|^n) \quad (11)$$

Where u_y is the yield displacement, γ, β, A, and *n* represent the parameters of Eq. (11). Note that the system parameters are selected in a way that the responses, which are predicted from the model, closely match the experimental results. In Eq. (11), n is an integer, which is constant and controls the changes from elastic to the plastic response. In this investigation, the other parameters of the LCRB are kept constant (e.g., $\gamma = \beta = 0.5$, $A = 1$, and n = 2) [61].

3.1.4 Bi-linear Behavior of the Lead Core Rubber Bearing (LCRB)

The LCRB isolation system is determined by the effective period of an isolator, (T_b), target displacement, (D), and gravity design load (Dead Load and Live Load).

Concerning the bearing displacements, it has been reported that rubber bearings' maximum design displacements are typically within the range of 40–55 cm in Japan. Also, the ultimate displacement usually varies from 55 to 80 cm. The isolators that can withstand large lateral displacements can be obtained through a large diameter (130 – 150 cm) depending on the material property [60].

EDC is the energy dissipated at each cycle of the hysteresis loop, which can be obtained by calculating the area under the hysteresis loop. It is a value that measures the damping of the isolator (Figure 11).

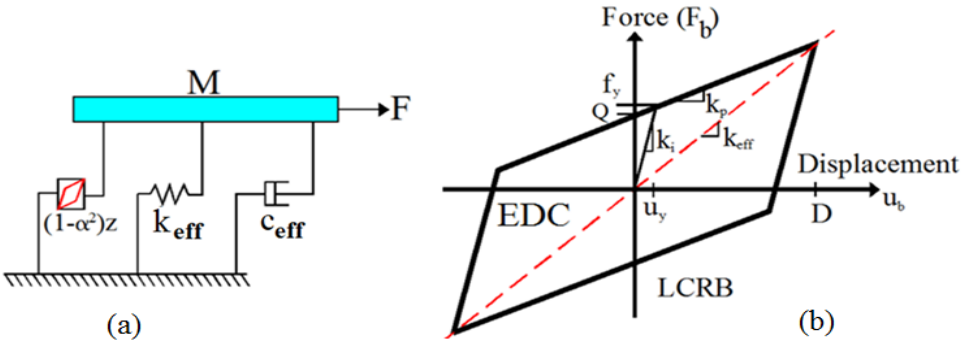

Figure 11: A) Idealization of the LCRB system B) Hysteretic model of the LCRB (bilinear behavior)

Eq. (12) and (13) are used to calculate the effective stiffness and effective damping coefficient of the base isolation system, respectively.

$$k_{eff} = \frac{m_t}{\left(\frac{T_b}{2\pi}\right)^2} \tag{12}$$

$$c_{eff} = 2m_t\omega_b\xi_{eff} \tag{13}$$

Where, m_t represents the overall mass of the superstructure and $\omega_b = \frac{2\pi}{T_b}$ shows the isolator frequency, where the basement mass (m_b) is defined in Eq. (14):

$$m_t = m_b + \sum_{i=1}^{N} m_i \quad (14)$$

3.1.5 Solution Procedures for the Equations of Motion

In the present study, the solutions of equations have been conducted using the Runge-Kutta method, which is known as an implicit and explicit iterative method [67]. The solutions of Eq. (6), Eq. (7) and Eq. (8) are performed using the Runge-Kutta method by solver ode45 in MATLAB. ode45 is based on the Runge-Kutta (4,5) formula, which is mostly used as a first attempt to solve the problem [68]. The function is utilized for the time integration procedure at an equal time interval of Δt.

For a conventionally fixed-base structure, the equation of motion is given by Eq. (4). By placing the structural model on a base isolation system (Figure 9), which consists of a base mass (m_b), stiffness (k_b) and damping (c_b), Eq. (4) changes to Eq. (6).

The equation of motion for the building combined with a base raft (with isolator) can be written as:

$$r^T M(\ddot{u} + r\ddot{u}_b + r\ddot{u}_g) + m_b(\ddot{u}_b + \ddot{u}_g) + c_b\dot{u}_b + k_b u_b = 0 \quad (15)$$

which can also be shown in the following form:

$$r^T M\ddot{u} + (m_t)\ddot{u}_b + c_b\dot{u}_b + k_b u_b = -(m_t)\ddot{u}_g \quad (16)$$

Eq. (16) identifies $r^T M$ as the overall mass of the superstructure; therefore, $m_t = m + m_b$ is the overall mass carried by the isolator. The matrix form of this equation is:

$$\mathbf{M}^*\ddot{u}^* + \mathbf{C}^*\dot{u}^* + \mathbf{K}^* u^* = -\mathbf{M}^* r^* \ddot{u}_g \quad (17)$$

Where

$$\mathbf{M}^* = \begin{bmatrix} m + m_b & r^T M \\ Mr & M \end{bmatrix},\ \mathbf{C}^* = \begin{bmatrix} c_b & 0 \\ 0 & C \end{bmatrix},\ \mathbf{K}^* = \begin{bmatrix} k_b & 0 \\ 0 & K \end{bmatrix},\ r^* = \begin{bmatrix} 1 \\ 0 \end{bmatrix},\ u^* = \begin{bmatrix} u_b \\ u \end{bmatrix}, m = \sum_{i=1}^{N} m_i$$

3.2 Flowchart to Perform Investigation

Following chart briefly illustrate the procedure to implement the research:

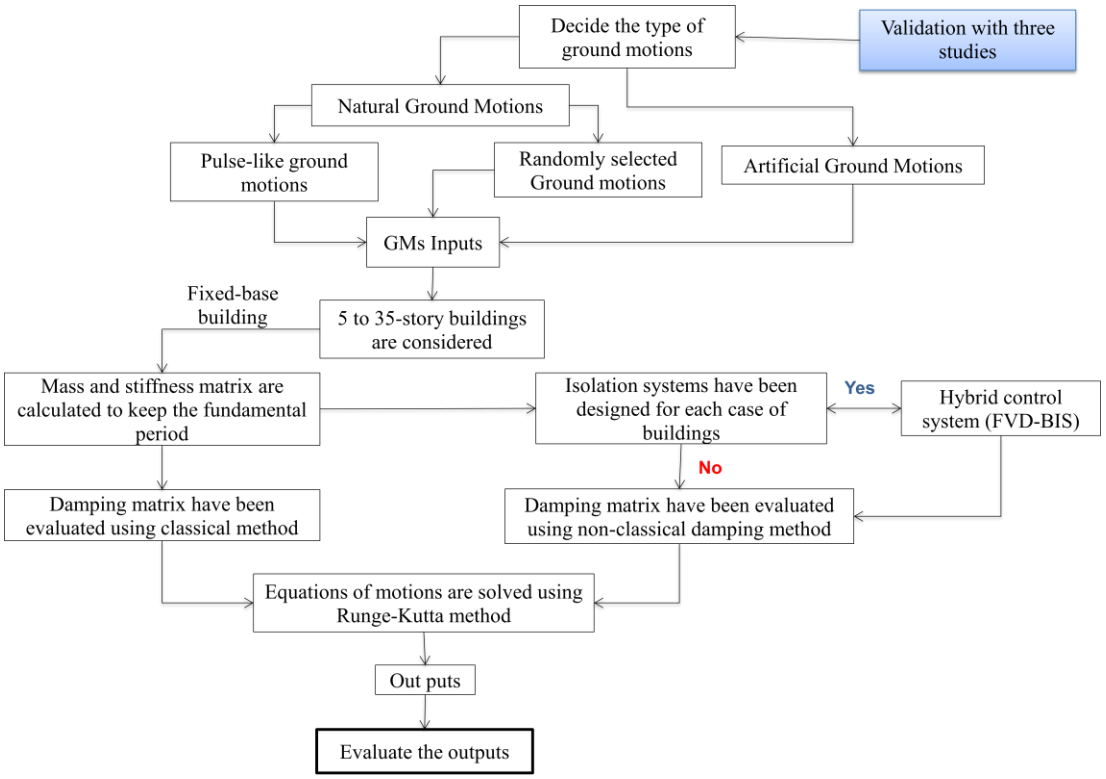

Figure 12: Schematic chart to implement the research

Chapter 4

PROGRAM VALIDATION

The validity of the program was confirmed by comparing the results obtained from the following studies:

Chao Xu et al. [13] studied a three-story base-isolated building. The floor stiffness, floor mass, floor viscous damping coefficient, and parameters of the bilinear model of the isolation system are illustrated in Figure 13. In their investigation, the behavior of the base isolation system is considered to be a bilinear hysteresis model, and the superstructure is considered to be linear-elastic during the numerical analysis. The output result of their investigation is illustrated in Figure 14b.

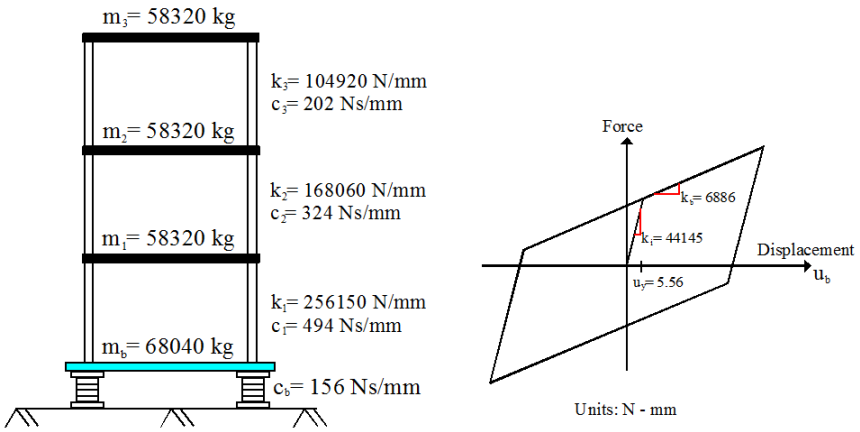

Figure 13: Model parameters of the 3-story base-isolated building [13](the stiffness is in N/mm, damping coefficient is in Ns/mm, and mass is in tons)

Moreover, Jeevan A. Kulkarni et al. [14] investigated a five-story base-isolated building with one degree of freedom at each floor. In their study, the behavior of the

force-deformation of the laminated rubber bearing (LRB) is considered to be equivalent linear, and the LCRB or NZ is considered to be bilinear. Finally, the results related to the top floor acceleration, and the base displacements are shown in Table 3 (mid column of Table 3 related to Ref [14]).

In the aforementioned studies, numerical analysis was implemented using Newmark's step-by-step method of integration.

Based on the above studies, for the purpose of verification, parameters were extracted from previous studies (data illustrated both in Figure 13 [13] and Table 3 [14]) and then implemented into the program, which is written in MATLAB, for modeling. In the present study, the solutions of equations are performed using the Runge-Kutta method, which is known as an implicit and explicit iterative method. The similarity between the results illustrated in Figure 14 and Table 3 confirms the validity of the program.

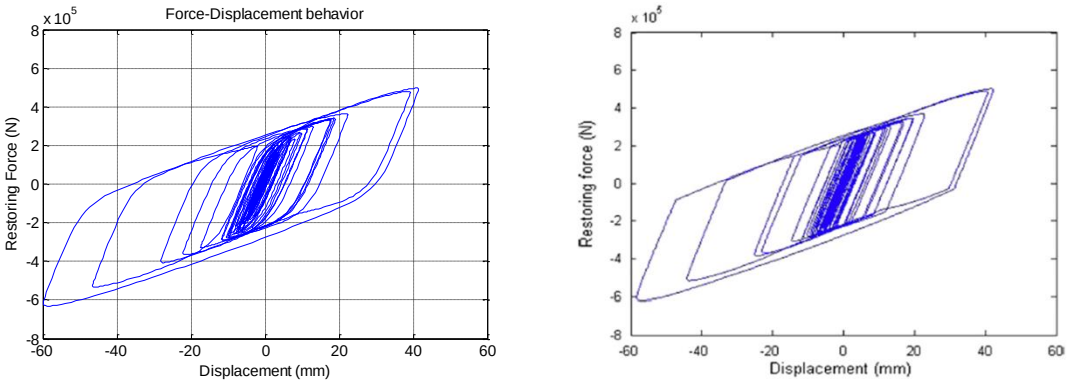

a) Validated b) Results given in Ref [13]

Figure 14: LCRB numerical analysis model validation with the results of [13]

Table 3: Numerical analysis model validation with the results given in Ref [14]

Acc.: Acceleration Dis.: Displacement Abs.: Absolute

	Numerical analysis				Results in [14]				Difference in percent (%)			
	Top Floor Abs Acc. (g)		Base Dis. (cm)		Top Floor Abs Acc. (g)		Base Dis. (cm)		Acc. ratio	Acc. ratio	Dis. ratio	Dis. ratio
Ts	LRB	LCRB	LRB	LCRB	LRB	LCRB	LRB	LCRB	LRB	LCRB	LRB	LCRB
0.4	0.358	0.3714	31.59	28.2	0.358	0.376	31.5	29.3	0.06	2.02	0.93	3.75
0.5	0.432	0.426	30.91	27.9	0.427	0.4239	30.57	28.7	1.13	0.72	1.01	2.787
0.6	0.476	0.4224	29.86	27.31	0.473	0.4508	29	28	0.48	2.88	1.91	2.46
0.7	0.5	0.513	28.66	27.33	0.493	0.526	28	27.5	1.35	2.60	1.27	0.61
0.8	0.455	0.487	28.11	27.29	0.448	0.483	27.9	27.2	1.43	1.29	2.22	0.47

Chapter 5

CONCEPT OF GROUND MOTION PARAMETERS

5.1 Introduction

Despite the fact that previous studies have been conducted different types of ground motions (GMs) in order to study the behavior of the seismically isolated buildings and the building with no base isolation systems, the behavior of the structures subjected to different types of ground motions are still unknown. For the above reason, in this section concept of ground motion parameters is briefly discussed. In this direction, different kinds of ground motions with different components have been selected from PEER strong ground motion database center and categorized them into two different groups, *Pulse-Like ground motions (PLGM)* and *Non-Pulse-Like ground motions (NPLGM).*

In order to describe an earthquake, there are three significant aspects which are as follows:

1. Amplitude
2. Frequency Content
3. Duration

5.2 Amplitude Parameters

Peak Acceleration:

It is often called “Peak Ground Acceleration” (PGA) or A_{max}. And also called Peak Horizontal Acceleration (PHA) or Peak Vertical Acceleration (PVA) to distinguish differences between horizontal and vertical accelerations. This is the most

widely-used amplitude parameter, which is governed by *high-frequency* ground motions.

Peak Velocity:

It is often called "Peak Ground Velocity" (PGV), V_{max}, or Peak Horizontal Velocity (PHV), which is also governed by *intermediate-frequency* ground motions. It is often used instead of PGA if dealing with longer-period structures (e.g., tall buildings, bridges, etc.)

Peak Displacement:

It is often called "Peak Ground Displacement" (PGD). It isn't as widely used because it governed by *low-frequency* ground motions. It is appropriate for design on very high period structures such as long bridges, very tall buildings, or water tanks.

Other less-used parameters are also mentioned as follows:

- Effective acceleration
- Effective design acceleration
- Sustained maximum acceleration or velocity

5.2.1 Principle Problem with Relying on Amplitude Alone

Amplitude parameters of ground motions are popular because they are easy to obtain and easy to understand. For that reason, many engineers liked to use them in different design applications. For instance, to calculate the horizontal force applying to a building during an earthquake, generally, one may multiply the mass of the building to the peak amplitude of the ground motions acceleration to obtain the largest force applied to the building.

Figure 15 illustrates acceleration plots from two different earthquakes shown on the same scale. The scale of time and acceleration is the same for both earthquakes. There are very similar peak accelerations, demonstrating the limitations of using

peak amplitude as the sole measure of strong ground motions. The earthquake on the left (Figure 15a) illustrates the very high-frequency ground motion which has a huge peak. And the ground motion on the right (Figure 15b) has approximately the same peak, but in fact, it has a very slight smaller amplitude than the peak acceleration of the ground motion on the left. Between these two ground motions, to design application, one may automatically select the ground motion on the left (Figure 15a) which has the highest peak acceleration. But the ground motion on the right (Figure 15b) generally has much more energy associated with it. So, if the structure hit by the ground motion on the right, it would be more likely damaged than the structure hit by the ground motion on the left. By relying on the amplitude parameters alone, we often miss the effect of the frequency and duration of the ground motion. [69]

(a) (b)

Figure 15: Accelerograms from a) the N29W Melendy Ranch record of the 1972 Stone Canyon (M=4.6) earthquake, b) the longitudinal record from the 1967 Koyna (M=6.5) earthquake [69]

5.3 Frequency Content Parameters

Frequency content describes how the amplitude of ground motion is distributed across a broad range of frequencies (periods). The most common set of frequency content parameters involves the use of a spectrum.

5.3.1 Fourier Spectrum

A Fourier series shows how the amplitude of the time history is distributed with respect to the frequency (period). [69]

$$x(t) = A_0 + A_1 \sin(\omega_1 t + \phi_1) + A_2 \sin(\omega_2 t + \phi_2) \ldots + A_n \sin(\omega_n t + \phi_n) \quad (18)$$

Where A is Fourier amplitude, ω is the Circular frequency of the "sin wave," and ϕ is the phase shift.

5.4 Non-Pulse-Like and Pulse-Like Ground Motions

Table 4 and Table 5 illustrate the ground motions with their specifications selected from PEER strong ground motion database center.

Table 4: Pulse-like ground motions (PLGMs)

EQ No.	RSN*	EQ Name	Year	Mag.	Tp (s)	Duration (s)	PGA (cm/s^2)	PGV (cm/s)	PGD (cm)	PGA/PGV (1/s)
1	1050	NORTHR_PAC175	1994	6.69	0.588	19.98	407.89	44.29	5.01	9.21
2	1052	NORTHR_PKC360	1994	6.69	0.728	39.98	424.60	51.38	7.21	8.26
3	566	GREECE_K-KAL-NS	1986	5.4	0.789	15.20	158.31	12.79	1.31	12.38
4	568	SANSALV_GIC180	1986	5.8	0.805	9.02	412.84	62.29	13.09	6.63
5	1004	NORTHR_SPV360	1994	6.69	0.931	47.80	914.30	76.27	17.67	11.99
6	1106	KOBE_KJM090	1995	6.9	1.092	149.98	617.69	76.11	18.31	8.12
7	569	SANSALV_NGI180	1986	5.8	1.127	20.27	396.29	56.38	19.64	7.03
8	148	COYOTELK_G03140	1979	5.74	1.155	26.85	251.50	29.58	6.34	8.50
9	150	COYOTELK_G06230	1979	5.74	1.232	27.10	413.77	44.35	12.44	9.33
10	459	MORGAN_G06090	1984	6.19	1.232	30.00	286.71	36.49	5.95	7.86
11	1054	NORTHR_PAR--T	1994	6.69	1.232	22.12	296.56	54.03	11.07	5.49
12	1063	NORTHR_RRS228	1994	6.69	1.246	19.94	857.45	148.00	41.88	5.79
13	149	COYOTELK_G04360	1979	5.74	1.351	27.22	246.89	31.84	5.24	7.76
14	1044	NORTHR_NWH360	1994	6.69	1.372	39.98	579.19	96.59	34.33	6.00
15	147	COYOTELK_G02140	1979	5.74	1.463	26.87	250.69	31.93	5.72	7.85
16	1120	KOBE_TAK000	1995	6.9	1.554	40.99	605.97	120.68	39.94	5.02
17	3548	LOMAP_LEX090	1989	6.93	1.568	81.94	403.65	95.78	30.29	4.21
18	1013	NORTHR_LDM334	1994	6.69	1.617	26.57	318.03	47.38	24.57	6.71
19	77	SFERN_PUL164	1971	6.61	1.638	41.74	1195.88	114.47	39.02	10.45
20	764	LOMAP_GOF160	1989	6.93	1.638	40.00	279.85	43.39	9.86	6.45
21	285	ITALY_A-BAG270	1980	6.9	1.713	36.87	186.14	34.71	13.75	5.36
22	766	LOMAP_G02090	1989	6.93	1.729	40.00	316.59	40.37	18.46	7.84
23	722	SUPER.B_B-KRN360	1987	6.54	2.128	21.99	136.36	29.61	7.93	4.61
24	159	IMPVALL.H_H-AGR273	1979	6.53	2.338	28.44	187.71	41.68	11.60	4.50
25	723	SUPER.B_B-PTS225	1987	6.54	2.394	22.34	423.61	134.29	46.17	3.15
26	1086	NORTHR_SYL360	1994	6.69	2.436	39.98	827.33	129.37	32.12	6.40
27	2734	CHICHI.04_CHY074N	1999	6.2	2.436	130.05	334.74	43.50	16.18	7.70
28	1182	CHICHI_CHY006-W	1999	7.62	2.570	150.00	348.30	60.25	23.50	5.78
29	767	LOMAP_G03090	1989	6.93	2.639	40.00	361.23	45.43	24.11	7.95
30	1114	KOBE_PRI000	1995	6.9	2.828	41.99	341.25	90.67	39.31	3.76
31	1045	NORTHR_WPI046	1994	6.69	2.982	24.99	411.41	118.18	42.53	3.48

Table 4 (Cont.)

32	1084	NORTHR_SCS052	1994	6.69	2.982	43.87	611.16	116.25	39.44	5.26
33	982	NORTHR_JEN292	1994	6.69	3.157	28.60	605.36	97.36	23.44	6.22
34	2114	DENALI_PS10-047	2002	7.9	3.157	92.10	326.28	115.72	53.44	2.82
35	292	ITALY_A-STU270	1980	6.9	3.272	39.35	314.43	71.96	29.33	4.37
36	171	IMPVALL.H_H-EMO270	1979	6.53	3.423	40.00	291.93	92.61	34.50	3.15
37	1085	NORTHR_SCE011	1994	6.69	3.528	54.70	836.50	120.97	34.03	6.91
38	983	NORTHR_JGB022	1994	6.69	3.535	28.65	560.35	76.13	41.90	7.36
39	181	IMPVALL.H_H-E06230	1979	6.53	3.773	39.10	440.51	113.55	72.89	3.88
40	180	IMPVALL.H_H-E05230	1979	6.53	4.13	39.40	375.87	96.90	75.22	3.88
41	182	IMPVALL.H_H-E07230	1979	6.53	4.375	36.87	460.17	113.14	46.94	4.07
42	316	WESMORL_PTS225	1981	5.9	4.389	41.70	227.67	55.58	37.10	4.10
43	161	IMPVALL.H_H-BRA225	1979	6.53	4.396	37.90	159.52	36.61	25.68	4.36
44	170	IMPVALL.H_H-ECC092	1979	6.53	4.417	40.00	230.95	73.39	48.01	3.15
45	178	IMPVALL.H_H-E03230	1979	6.53	4.501	39.65	218.29	43.29	25.53	5.04
46	173	IMPVALL.H_H-E10050	1979	6.53	4.515	37.07	169.85	50.69	35.39	3.35
47	802	LOMAP_STG090	1989	6.93	4.571	40.00	320.03	45.97	33.33	6.96
48	1511	CHICHI_TCU076-E	1999	7.62	4.732	90.00	337.94	51.84	33.27	6.52
49	179	IMPVALL.H_H-E04230	1979	6.53	4.788	39.10	363.39	80.41	74.27	4.52
50	185	IMPVALL.H_H-HVP315	1979	6.53	4.823	37.90	217.24	51.46	35.83	4.22
51	1176	KOCAELI_YPT060	1999	7.51	4.949	35.00	222.45	69.72	62.33	3.19
52	1510	CHICHI_TCU075-E	1999	7.62	4.998	90.00	325.67	109.56	96.61	2.97
53	879	LANDERS_LCN345	1992	7.28	5.124	48.12	773.77	28.11	25.54	27.53
54	1476	CHICHI_TCU029-N	1999	7.62	5.285	90.00	194.59	51.87	37.66	3.75
55	1244	CHICHI_CHY101-E	1999	7.62	5.341	90.00	333.20	65.00	34.94	5.13
56	1165	KOCAELI_IZT090	1999	7.51	5.369	30.00	225.80	38.29	24.29	5.90
57	1480	CHICHI_TCU036-N	1999	7.62	5.383	90.00	122.35	47.54	51.83	2.57
58	803	LOMAP_WVC270	1989	6.93	5.649	40.00	324.94	64.91	37.85	5.01
59	1503	CHICHI_TCU065-N	1999	7.62	5.74	90.00	564.54	92.13	50.20	6.13
60	1477	CHICHI_TCU031-N	1999	7.62	5.929	90.00	122.18	46.98	28.12	2.60
61	1161	KOCAELI_GBZ000	1999	7.51	5.992	28.00	255.80	44.63	41.16	5.73
62	143	TABAS_TAB-T1	1978	7.35	6.188	32.98	845.38	123.40	93.61	6.85
63	184	IMPVALL.H_H-EDA270	1979	6.53	6.265	39.00	345.92	75.58	57.15	4.58
64	1483	CHICHI_TCU040-N	1999	7.62	6.433	90.00	122.28	47.32	55.40	2.58
65	1501	CHICHI_TCU063-N	1999	7.62	6.552	90.00	130.07	82.83	52.69	1.57
66	1193	CHICHI_CHY024-N	1999	7.62	6.65	90.00	162.34	43.53	29.83	3.73
67	1531	CHICHI_TCU104-N	1999	7.62	7.189	90.00	86.98	47.49	45.19	1.83
68	900	LANDERS_YER360	1992	7.28	7.504	43.98	148.87	29.09	23.15	5.12
69	1498	CHICHI_TCU059-E	1999	7.62	7.784	90.00	157.11	51.38	46.99	3.06
70	1486	CHICHI_TCU046-N	1999	7.62	8.043	85.00	116.78	26.28	23.38	4.44
71	1515	CHICHI_TCU082-E	1999	7.62	8.099	90.00	221.03	54.92	95.08	4.02
72	1475	CHICHI_TCU026-E	1999	7.62	8.372	90.00	116.21	37.87	44.31	3.07
73	1502	CHICHI_TCU064-N	1999	7.62	8.456	90.00	113.54	55.31	59.16	2.05
74	1530	CHICHI_TCU103-E	1999	7.62	8.687	90.00	126.42	70.25	68.39	1.80
75	8161	SIERRA.MEX_E12360	2010	7.2	8.722	273.00	324.99	72.61	54.65	4.48
76	1479	CHICHI_TCU034-N	1999	7.62	8.869	90.00	103.43	24.27	22.07	4.26
77	1550	CHICHI_TCU136-N	1999	7.62	8.881	90.00	170.87	51.47	44.14	3.32
78	1496	CHICHI_TCU056-N	1999	7.62	8.939	90.00	140.38	39.56	47.67	3.55
79	1478	CHICHI_TCU033-E	1999	7.62	8.974	90.00	154.54	41.55	49.39	3.72
80	1548	CHICHI_TCU128-N	1999	7.62	9.023	90.00	163.57	62.65	52.29	2.61
81	838	LANDERS_BRS090	1992	7.28	9.128	39.98	132.88	25.04	17.47	5.31
82	1482	CHICHI_TCU039-N	1999	7.62	9.331	90.00	136.03	56.58	51.40	2.40
83	1485	CHICHI_TCU045-E	1999	7.62	9.338	90.00	464.09	50.08	39.30	9.27
84	1481	CHICHI_TCU038-E	1999	7.62	9.576	90.00	142.07	56.77	44.81	2.50
85	1529	CHICHI_TCU102-N	1999	7.62	9.632	90.00	168.46	66.43	50.71	2.54
86	8164	DUZCE_487-NS	1999	7.14	10.05	55.02	297.60	38.95	20.10	7.64

Table 4 (Cont.)

87	1489	CHICHI_TCU049-E	1999	7.62	10.22	90.00	273.44	53.55	74.26	5.11
88	1528	CHICHI_TCU101-E	1999	7.62	10.31	49.00	207.89	76.81	73.48	2.71
89	1491	CHICHI_TCU051-E	1999	7.62	10.38	90.00	157.16	53.84	73.89	2.92
90	1519	CHICHI_TCU087-N	1999	7.62	10.39	90.00	111.66	40.48	34.07	2.76
91	1492	CHICHI_TCU052-E	1999	7.62	11.95	90.00	350.76	151.21	210.4	2.32
92	1505	CHICHI_TCU068-E	1999	7.62	12.28	90.00	501.96	249.59	297.1	2.01
93	1487	CHICHI_TCU047-E	1999	7.62	12.31	90.00	292.18	41.98	39.71	6.96
94	1493	CHICHI_TCU053-N	1999	7.62	13.11	90.00	132.03	46.32	49.42	2.85

*RSN: Record Serial Number from PEER strong ground motions database-PEER center

Table 5: Non-Pulse-like ground motions (NPLGMs)

EQ No.	RSN*	EQ Name	Year	Mag.	Duration (s)	PGA (cm/s^2)	PGV (cm/s)	PGD (cm)	PGA/PGV (1/s)
1	12	KERN.PEL_PEL090	1952	7.36	69.995	41.426	8.627	4.739	4.802
2	13	KERN_PAS180	1952	7.36	77.24	47.068	5.877	1.814	8.009
3	14	KERN_SBA042	1952	7.36	75.44	87.986	11.412	3.428	7.710
4	15	KERN_TAF021	1952	7.36	54.34	155.867	15.230	6.105	10.234
5	137	TABAS_BAJ-L1	1978	7.35	38.98	89.008	7.425	4.887	11.987
6	138	TABAS_BOS-L1	1978	7.35	34.98	103.521	13.303	7.636	7.782
7	139	TABAS_DAY-L1	1978	7.35	20.98	317.736	22.300	15.213	14.248
8	140	TABAS_FER-L1	1978	7.35	39.98	91.330	5.425	2.273	16.834
9	141	TABAS_KSH-L1	1978	7.35	32.98	31.717	9.238	5.523	3.433
10	142	TABAS_SED-L1	1978	7.35	39.98	26.339	3.488	3.124	7.551
11	280	TRINIDAD.B_B-RDL000	1980	7.2	19.695	60.463	7.521	3.992	8.039
12	281	TRINIDAD.B_B-RDE000	1980	7.2	21.995	160.076	9.482	3.722	16.882
13	282	TRINIDAD.B_B-RDW000	1980	7.2	21.995	148.188	8.867	3.599	16.713
14	570	SMART1.45_45C00EW	1986	7.3	55.04	119.970	29.671	9.410	4.043
15	571	SMART1.45_45EO1EW	1986	7.3	54.64	156.924	24.712	7.981	6.350
16	572	SMART1.45_45EO2EW	1986	7.3	32.99	133.181	14.429	6.727	9.230
17	573	SMART1.45_45I01EW	1986	7.3	46.89	130.013	30.925	8.919	4.204
18	574	SMART1.45_45I07EW	1986	7.3	56.34	116.257	23.422	10.073	4.964
19	575	SMART1.45_45M01EW	1986	7.3	37.94	117.078	28.363	10.586	4.128
20	576	SMART1.45_45M07EW	1986	7.3	53.44	152.315	26.883	9.106	5.666
21	577	SMART1.45_45O01EW	1986	7.3	72.94	122.774	22.372	10.343	5.488
22	578	SMART1.45_45O02EW	1986	7.3	52.29	156.985	19.725	9.816	7.959
23	579	SMART1.45_45O04EW	1986	7.3	50.24	124.192	32.176	8.620	3.860
24	580	SMART1.45_45O06EW	1986	7.3	48.54	168.225	23.705	6.606	7.097
25	581	SMART1.45_45O07EW	1986	7.3	47.49	151.056	19.617	8.367	7.700
26	582	SMART1.45_45O08EW	1986	7.3	60.59	138.938	24.647	8.544	5.637
27	583	SMART1.45_45O10EW	1986	7.3	58.19	145.037	24.621	10.334	5.891
28	584	SMART1.45_45O12EW	1986	7.3	49.74	137.301	25.225	9.129	5.443
29	825	CAPEMEND_CPM000	1992	7.01	29.98	1465.19	122.33	32.614	11.977
30	826	CAPEMEND_EUR000	1992	7.01	43.98	151.115	20.235	5.820	7.468
31	827	CAPEMEND_FOR000	1992	7.01	43.98	114.545	29.055	19.705	3.942
32	830	CAPEMEND_SHL000	1992	7.01	35.98	224.168	6.922	0.389	32.383
33	832	LANDERS_ABY000	1992	7.28	49.98	112.787	18.206	10.512	6.195
34	833	LANDERS_WBA000	1992	7.28	50.595	50.736	16.554	14.441	3.065
35	834	LANDERS_ARC172	1992	7.28	46.095	27.980	10.449	14.936	2.678
36	835	LANDERS_CAM009	1992	7.28	59.07	47.311	8.520	4.225	5.553
37	836	LANDERS_BAK050	1992	7.28	49.98	105.624	9.258	6.545	11.409
38	837	LANDERS_NHO180	1992	7.28	34.27	34.832	13.035	11.130	2.672
39	839	LANDERS_JAB220	1992	7.28	48.395	36.155	8.515	13.779	4.246
40	840	LANDERS_TUJ262	1992	7.28	51.07	25.392	4.481	5.507	5.666
41	841	LANDERS_BFS000	1992	7.28	39.98	116.674	12.696	8.896	9.190

Table 5 (Cont.)

42	842	LANDERS_FLO020	1992	7.28	58.595	41.773	12.360	11.365	3.380
43	843	LANDERS_BPK090	1992	7.28	35.145	47.554	12.625	10.325	3.767
44	844	LANDERS_BUE250	1992	7.28	54.62	55.034	6.679	2.099	8.240
45	845	LANDERS_VIR200	1992	7.28	46.57	17.684	3.034	0.775	5.830
46	846	LANDERS_DEV000	1992	7.28	59.32	28.979	11.881	13.070	2.439
47	847	LANDERS_CAS000	1992	7.28	46.27	62.724	17.456	27.998	3.593
48	848	LANDERS_CLW-LN	1992	7.28	27.9981	278.292	27.615	18.204	10.077
49	849	LANDERS_BAD000	1992	7.28	55.82	66.789	16.557	13.776	4.034
50	850	LANDERS_DSP000	1992	7.28	49.98	167.975	19.456	8.155	8.634
51	851	LANDERS_DWN000	1992	7.28	69.98	50.530	18.395	23.632	2.747
52	852	LANDERS_MEL090	1992	7.28	36.97	29.074	4.471	2.314	6.503
53	853	LANDERS_FAI095	1992	7.28	39.395	41.380	12.404	8.028	3.336
54	854	LANDERS_FEA000	1992	7.28	43.98	50.015	6.915	3.495	7.233
55	855	LANDERS_FTI000	1992	7.28	39.98	111.414	9.535	3.441	11.684
56	856	LANDERS_EUC022	1992	7.28	52.42	69.181	19.207	11.525	3.602
57	857	LANDERS_GLP177	1992	7.28	56.695	41.198	4.899	1.206	8.409
58	858	LANDERS_OAK080	1992	7.28	56.745	39.051	6.579	4.536	5.935
59	859	LANDERS_COM140	1992	7.28	62.595	45.900	12.540	9.545	3.660
60	860	LANDERS_H05000	1992	7.28	55.98	79.849	5.546	1.331	14.399
61	861	LANDERS_WAI200	1992	7.28	42.02	50.753	11.156	10.486	4.549
62	862	LANDERS_IND000	1992	7.28	59.98	101.927	9.588	4.977	10.631
63	863	LANDERS_ING000	1992	7.28	69.98	41.835	15.631	18.861	2.676
64	864	LANDERS_JOS000	1992	7.28	43.98	268.386	27.021	7.708	9.932
65	865	LANDERS_116000	1992	7.28	69.98	41.511	14.100	17.928	2.944
66	866	LANDERS_VER090	1992	7.28	48.095	34.897	8.643	9.924	4.038
67	867	LANDERS_FLE144	1992	7.28	60.77	42.845	8.516	7.498	5.031
68	868	LANDERS_FIG058	1992	7.28	47.395	27.161	3.656	0.864	7.430
69	869	LANDERS_WST000	1992	7.28	39.67	36.626	11.822	16.613	3.098
70	870	LANDERS_OBR000	1992	7.28	69.98	41.740	15.608	15.681	2.674
71	871	LANDERS_GR2090	1992	7.28	42.695	33.404	9.552	13.634	3.497
72	872	LANDERS_W15090	1992	7.28	57.445	25.463	7.282	5.607	3.497
73	873	LANDERS_W70000	1992	7.28	47.945	62.154	16.888	18.836	3.680
74	874	LANDERS_OR2010	1992	7.28	52.645	50.398	17.121	23.258	2.944
75	875	LANDERS_NYA090	1992	7.28	51.27	24.890	3.744	3.048	6.649
76	876	LANDERS_BRC000	1992	7.28	43.295	37.384	12.472	13.754	2.997
77	877	LANDERS_RIM015	1992	7.28	51.395	33.352	11.593	9.312	2.877
78	878	LANDERS_DEL000	1992	7.28	50.97	58.472	20.057	22.058	2.915
79	880	LANDERS_MCF000	1992	7.28	99.82	123.805	6.802	2.123	18.201
80	881	LANDERS_MVH045	1992	7.28	56.07	218.810	29.944	5.010	7.307
81	882	LANDERS_FHS000	1992	7.28	99.82	133.428	11.158	4.629	11.958
82	883	LANDERS_STC090	1992	7.28	56.32	34.837	12.571	8.286	2.771
83	884	LANDERS_PSA000	1992	7.28	59.98	74.185	10.770	6.978	6.888
84	885	LANDERS_PMN000	1992	7.28	54.98	65.564	12.828	6.912	5.111
85	886	LANDERS_PLC000	1992	7.28	64.98	45.632	1.989	0.409	22.946
86	887	LANDERS_RIV180	1992	7.28	49.98	41.828	2.994	1.736	13.972
87	888	LANDERS_HOS090	1992	7.28	119.99	76.344	19.818	10.494	3.852
88	889	LANDERS_GRN180	1992	7.28	46.045	48.780	14.368	15.413	3.395
89	890	LANDERS_EJS030	1992	7.28	57.095	59.269	10.799	11.755	5.488
90	891	LANDERS_SIL000	1992	7.28	54.98	48.914	3.765	1.933	12.991
91	892	LANDERS_RO3000	1992	7.28	59.82	36.431	15.166	17.253	2.402
92	893	LANDERS_SUL230	1992	7.28	43.545	24.883	3.870	3.007	6.430
93	894	LANDERS_GLE170	1992	7.28	63.92	33.164	13.415	20.232	2.472
94	895	LANDERS_TAR000	1992	7.28	60.08	64.578	8.326	4.225	7.756

*RSN: Record Serial Number from PEER strong ground motions database-PEER center

To be fair for the comparison of the responses of the structures, however, PLGM and NPLGM should be somewhat comparable. Still, a comparable set of PLGM and NPLGM is challenging for what they constitute.

To illustrate the effectiveness of the selected ground motions ANOVA method (Analysis of Variance) has been implemented by using Minitab (version 17) software [70]. Figure 16 clearly illustrates that the intensity of PLGM for three different components, e.g., PGA, PGV and PGD, are more significant than the NPLGM (Units: PGA (cm/s^2), PGV (cm/s) and PGD (cm)).

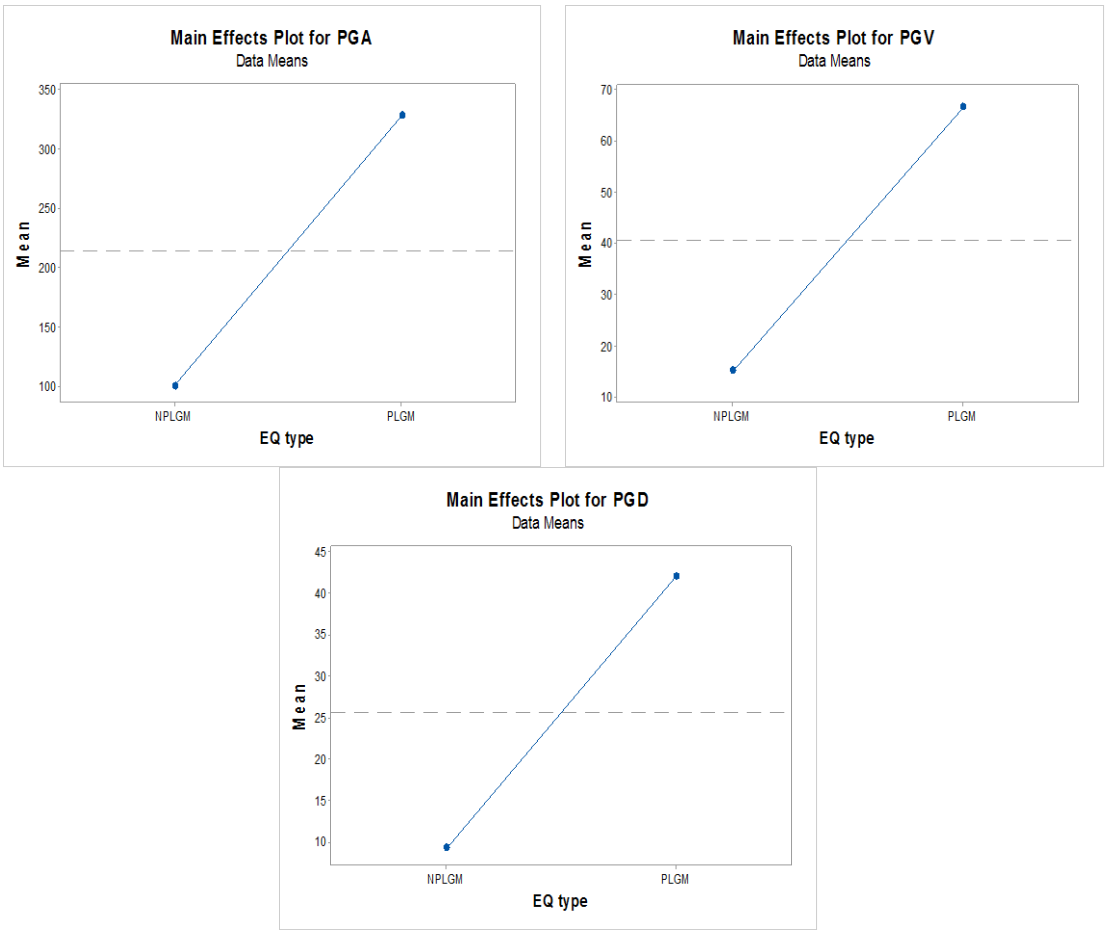

Figure 16: Main effects plot of Peak Ground responses for both PLGM and NPLGM

Moreover, Figure 17 represents the interaction plot between the PLGM and NPLGM vs. PGA/PGV ratio. As it can be seen in Figure 17, for two cases of

earthquakes record, PGA is in the lowest level for when the PGA/PGV ratio is less than 10 (1/s) while it is in the highest level for two other cases (10<PGA/PGV<20 and PGA/PGV>20). PGV for the cases when 10<PGA/PGV<20 and PGA/PGV<10 is at the highest level, in contrast to the case when PGA/PGV>20, PGV is in the lowest level. In addition, Peak Ground Displacement is more significant (in the highest level) for the case when the ratio of PGA/PGV is less than 10 (1/s). As it was mentioned above PLGMs have the highest intensity when compared with NPLGMs.

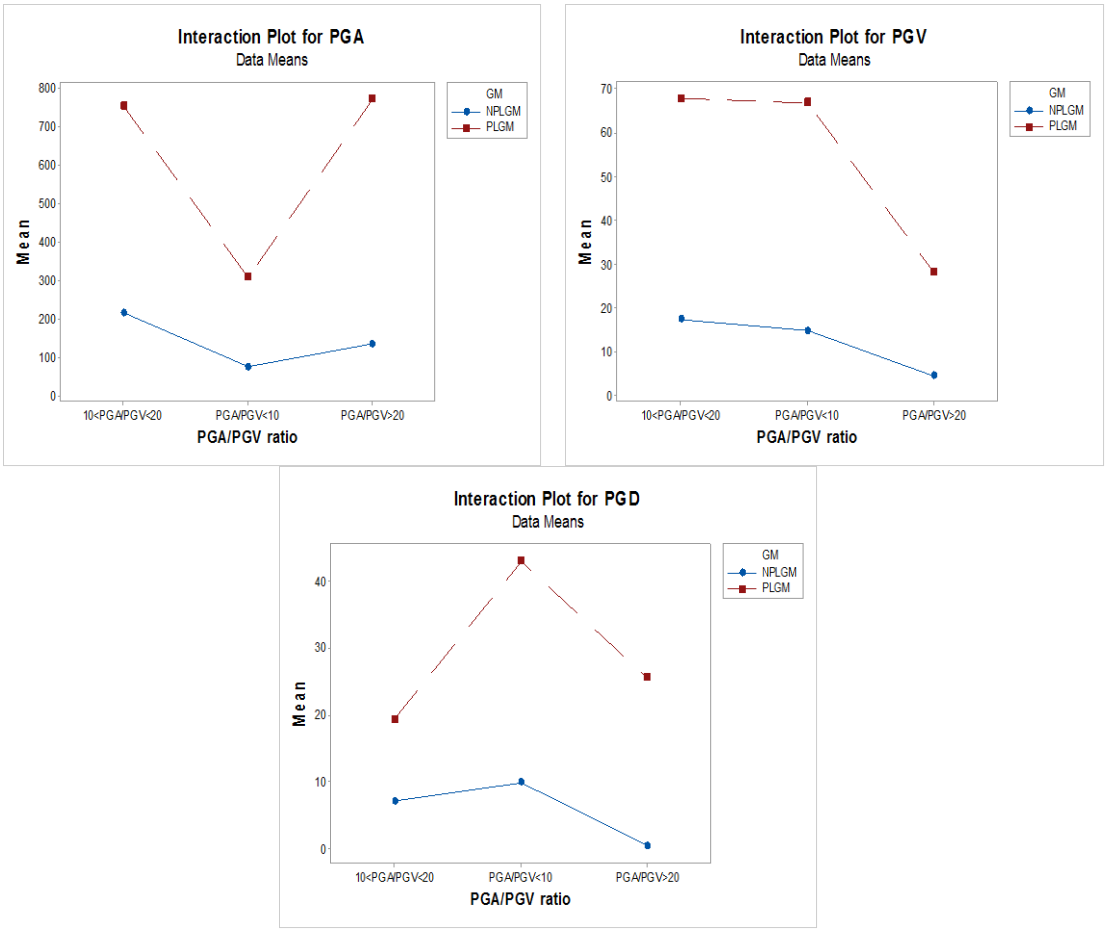

Figure 17: Interaction plot between the PLGM and NPLGM versus PGA/PGV (1/s) ratio.

In addition, the intensity of the selected ground motions is also illustrated for each interval duration (Du) of the ground motions, which are divided into three different groups whose Du<30 s, 30 s<Du<60 s and Du>60 s (Figure 18). It can also be seen

that the intensity of the PLGM is more than the NPLGM for all groups with different duration of ground motions (Figure 18). It is observed that the PGA for the PLGM, whose duration is between 30 s and 60 s is more significant than the two other groups of ground motions whose duration is less than 30 s and more than 60 s. But for NPLGM, when the ground motions duration is less than 30 s the intensity of the ground motions is more significant. Peak Ground Velocity of PLGM is approximately close between the groups of the ground motions (differences are negligible and there is no significant effect and also the same for NPLGM). Considering PGD, it can be seen that PGD for NPLGM for each group of ground motions remains constant, but for PLGM the most significant effect of the ground motions can be observed that when the duration of the ground motions is bigger than 60 s and the lowest when the duration is less than 30 s.

According to Figure 19, it can be clearly observed that the ratio of PGA/PGV for PLGM is less than the ratio for NPLGM. From above results and Figure 19, it can be concluded that for the lowest ratio of PGA/PGV (less than 10 (1/s)) intensity of the ground motions is significant (in above discussion in Figure 17 and Figure 18 it has been observed that the intensity of the PLGMs are higher than the intensity of the NPLGMs). And, for all PLGMs, the ratio of PGA/PGV is less than 10 (1/s). But for NPLGMs whose durations are between 30 s and 60 s, and bigger than 60 s, the ratio of PGA/PGV is less than 10 (1/s) which implies that the group of the ground motions in this range of durations will be more effective.

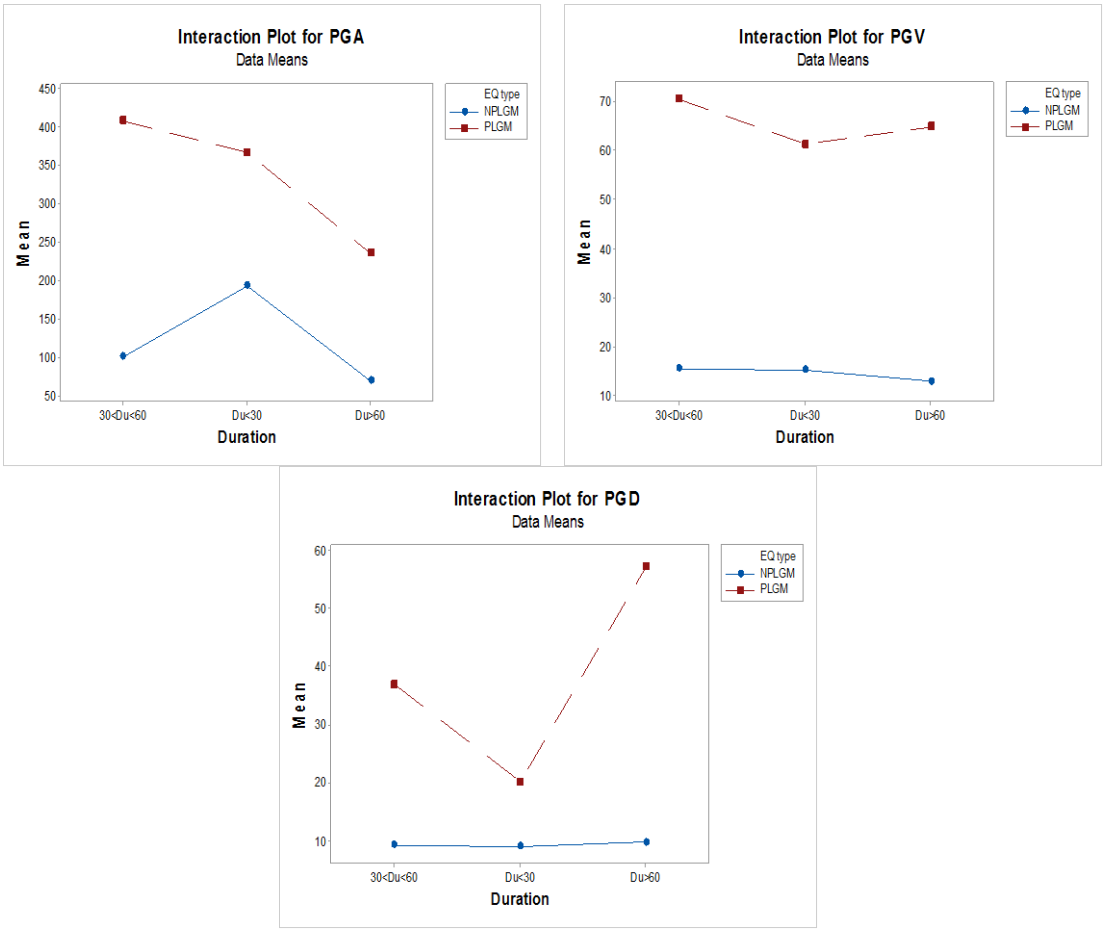

Figure 18: Interaction plot between the PLGM and NPLGM versus the Duration of the ground motions (Du)

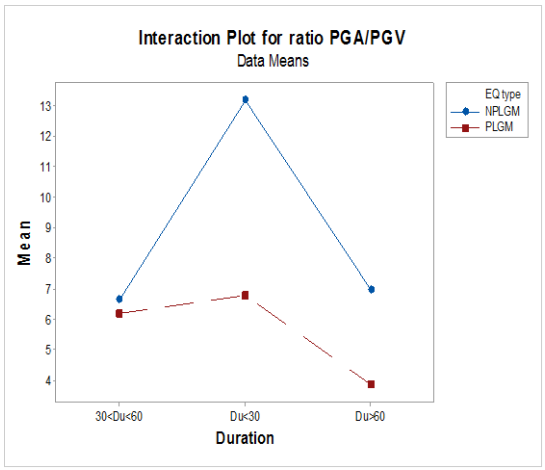

Figure 19: Interaction plot of PGA/PGV ratio versus Duration of the ground motions (Du)

Chapter 6

EVALUATE THE BEHAVIOR OF BASE-ISOLATED BUILDINGS AND BASE ISOLATION SYSTEMS SUBJECTED TO VARIOUS EARTHQUAKES WITH DIFFERENT COMPONENTS

6.1 Introduction

Since there is limited scientific understanding on the behavior of the most practical isolator, LCRB, and base-isolated buildings, one of the greatest challenges faced by researchers is understanding the behavior of the base isolation system and base-isolated buildings under the conditions of different ground motions (PGA/PGV and T_p) by considering the effectiveness of the ground motion's components and the inherited mechanical properties of the designed base-isolated buildings.

For this reason, to better determine the performance of the base isolation system and base-isolated buildings, a set of 45 earthquakes was selected from the Pacific Earthquake Engineering Research (PEER) center database with different PGA-to-PGV ratios. In this investigation, different types of buildings (isolated and nonisolated), with 5, 10, 15, 20, 25, 30, and 35 stories, were considered and assumed that the superstructure remained linear-elastic throughout the time-history analyses. Bearing in mind that both the acceleration and velocity characteristics of an earthquake are very important parameters affecting a building (both in the base-isolated and non-isolated states), these two parameters with their ratios are

considered in this study. The ratios are categorized as $\mathrm{PGA/PGV} < 1, 1 < PGA/PGV < 2$ and $PGA/PGV > 2$. To conduct the numerical analysis, a MATLAB-based code is used to assess the aforementioned parameters. Additionally, a two-factor factorial design is implemented to interpret the results using Minitab software. The results clearly depict the behavior of the LCRB system under the aforementioned earthquakes when used for varied buildings. Finally, the performances of the base isolation system and base-isolated buildings are compared.

6.2 Structural Parameters

The base-isolated buildings are considered symmetrical square buildings consisting of six bays in each direction and have been modeled as a shear-type steel structure mounted on isolation systems with one lateral degree-of-freedom at each floor (Figure 20). The floors are in alignment and equal in height, which is considered to be h = 3 m each. In this study, as the investigated buildings are represented as the residential area - category "A" [71], the live load uniformly distributed in the amount of $1500\ N/\mathrm{m}^2$. According to the Eurocode, the live loads (LLs) are reduced, with a factor of $\psi_{2i} = 0.3$ in a seismic design situation [72]. In addition, uniform surface loads (dead loads or DLs) have been considered to be $2600\ N/\mathrm{m}^2$. By adding the loads (DL+$\psi_{2\mathrm{i}}$LL), the total loads were calculated to be $3053.2\ N/\mathrm{m}^2$.

As the story dimension of the building is 30 m x 30 m (Figure 20d), the mass for each story is calculated to be 2.748×10^5kg. Since the plan of the building is symmetric, frame 4 has been selected as a representative to study the behavior of the buildings. According to the loaded area, the mass calculated for frame 4 is 45798.3 kg.

In this investigation, M is the diagonal mass matrix, which is defined by the mass of each floor for the superstructure and kept constant (i.e., $m_i = m$, $i = 1,2,\ldots,N$). Moreover, the base mass of the isolated building (m_b) is considered to be equal to the floor mass ($m_b = m$). The modal damping ratio of the steel buildings remained unchanged for all modes (ξ_s) and was set at 2%. The stiffness of each story (k) is taken in the proportions of 1, 1.5, 2, 2.5, and 3 (Table 6). The value of k can be computed by providing the required fundamental period of the fixed base buildings as T_s. In this study, the superstructure time period is defined as $T_s = 0.1$ N, where N is the number of stories of the superstructure above the isolation level [41; 42]. The story numbers for the buildings are selected as 5, 10, 15, 20, 25, 30 and 35 (Figure 20a and Figure 20b), thus considering the superstructure periods T_s = 0.5 s; 1.0 s; 1.5 s; 2.0 s; 2.5 s; 3.0 s and 3.5 s, respectively. Table 6 and Table 7 illustrate the properties of the subject buildings and the period of vibration for the first five modes of seismically isolated buildings, respectively.

Table 6: Stiffness proportion and mass properties of the superstructures (steel buildings)

	5-story	10-story	15-story	20-story	25-story	30-story	35-story	Stiffness proportion	m (mass for frame 4) (kg)	ξ_s (%)
Floor level	1	1-2	1-3	1-4	1-5	1-6	1-7	k	45798.3	
	2	3-4	4-6	5-8	6-10	7-12	8-14	$k/1.5$	45798.3	
	3	5-6	7-9	9-12	11-15	12-18	15-21	$k/2$	45798.3	2%
	4	7-8	10-12	13-16	16-20	19-24	22-28	$k/2.5$	45798.3	
	5	9-10	13-15	17-20	21-25	25-30	29-35	$k/3$	45798.3	

Table 7: Period of vibration for each mode of isolated buildings and non-isolated buildings

Mode	Period of Vibration (s)													
	5-story		10-story		15-story		20-story		25-story		30-story		35-story	
	BIB	FBB	BIB	FBB	BIB	FBB	BIB	FBB	BIB	FBB	BIB	FBB	BIB	FBB
1	2.51	0.50	2.64	1.00	2.83	1.50	3.08	2.00	3.40	2.50	3.76	3.00	4.16	3.50
2	0.31	0.18	0.60	0.37	0.82	0.55	1.03	0.73	1.22	0.92	1.39	1.10	1.56	1.28
3	0.16	0.12	0.30	0.22	0.43	0.33	0.56	0.45	0.68	0.56	0.81	0.67	0.92	0.78
4	0.12	0.09	0.20	0.16	0.29	0.24	0.38	0.32	0.47	0.40	0.56	0.48	0.64	0.56
5	0.09	0.07	0.16	0.13	0.22	0.19	0.29	0.25	0.36	0.31	0.43	0.37	0.49	0.43

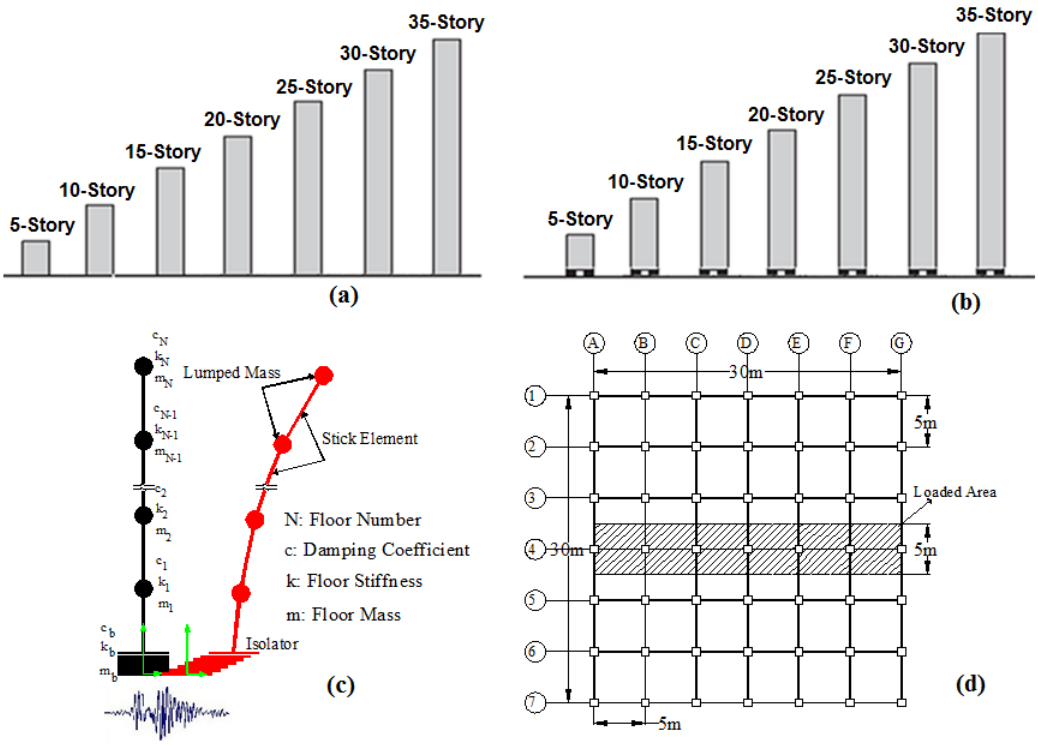

Figure 20: a) Fixed-Base building (FBB); b) Base-isolated building (BIB); c) Lumped-mass stick model; and d) Area plan and selected frame with a loaded area

6.3 Isolator Properties and Earthquake Components

The LCRB system is defined by β_{eff}, T_b and f_0 parameters, which are the damping ratio of the isolation system, the period of the isolator and the normalized yield strength (i.e., $f_0 = \frac{f_y}{W}$), respectively (where $W = m_t g$, W is the weight of the building together with a base raft (m_b) and g is the acceleration due to gravity).

In this study, the behavior of the isolator is taken into account by choosing the acceptable values of the isolator's period adequate to $T_b = 2.5$ s, damping ratio $\beta_{eff} = 5\%$, yielding displacement $u_y = 0.025$ m, and the ratio of post-yielding stiffness to pre-yielding stiffness $\alpha_1 = 0.3$.

Table 8 summarizes the information on the properties of the base isolation system and the base-isolated buildings (BIB) considered in this investigation.

The earthquake motions are selected randomly according to three different ratios, which are shown in Table 9 with their specifications. The top and bearing behavior of the isolated building is the response quantities of interest.

Table 8: Properties of the base isolation system

No. Story	5	10	15	20	25	30	35
T_b (s)	2.5	2.5	2.5	2.5	2.5	2.5	2.5
k_p (N/m)	1.74e6	3.18e6	4.63e6	6.075e6	7.52e6	8.97e6	10.41e6
k_i (N/m)	5.78e6	10.60e6	15.43e6	20.25e6	25.07e6	29.90e6	34.71e6
β_{eff} (%)	5	5	5	5	5	5	5
α_1	0.3	0.3	0.3	0.3	0.3	0.3	0.3
u_y (m)	0.025	0.025	0.025	0.025	0.025	0.025	0.025
$f_0 = \frac{f_y}{W}$	0.05	0.05	0.05	0.05	0.05	0.05	0.05
m_b (base mass) kg	45798.3	45798.3	45798.3	45798.3	45798.3	45798.3	45798.3

Table 9: Ground motions for different cases of **PGA/PGV** (Randomly selected)

RSN	EQ. ID	Earthquake Name	Mag.	Year	Duration time (EQ.)	PGA (g)	PGV (m/s)	PGD (m)	PGA/PGV (g.s/m)
PGA/PGV<1(g.s/m)									
1	25	"TCGH13"	6.63	2004	21	0.590	0.626	0.098	0.945
2	7	"KOBE,Japan"	6.9	1995	50	0.834	0.911	0.211	0.915
3	2	"Imperial Valley-02"	6.95	1940	55	0.280	0.309	0.087	0.905
4	10	"Tabas_ Iran"	7.35	1978	40	0.027	0.034	0.031	0.768
5	29	"Tabas, Iran"	7.35	1978	33	0.861	1.234	0.936	0.698
6	22	"Bam_ Iran"	6.6	2003	33	0.014	0.020	0.013	0.696
7	3	"Imperial Valley-02"	6.95	1940	55	0.210	0.313	0.241	0.670
8	17	"El Mayor_ Mexico"	7.2	2010	130	0.248	0.383	0.482	0.648
9	30	“Northridge-01“	6.69	1994	28	0.426	0.748	0.190	0.569
10	8	"Kocaeli_ Turkey"	7.51	1999	150	0.045	0.081	0.035	0.555
11	23	“Tottori, Japan“	6.61	2000	120	0.018	0.036	0.042	0.511
12	19	"Duzce_ Turkey"	7.14	1999	95	0.017	0.045	0.038	0.373
13	28	"Northridge-01"	6.69	1994	30	0.410	1.114	0.446	0.368
14	14	"Darfield_ New Zealand"	7	2010	140	0.194	0.591	0.491	0.328
15	20	"Darfield_ New Zealand"	7	2010	120	0.209	0.671	0.599	0.311
1(g.s/m)<PGA/PGV<2(g.s/m)									
1	33	"Loma Prieta"	6.93	1989	40	0.416	0.208	0.061	1.997
2	31	"Parkfield"	6.19	1966	30	0.272	0.154	0.031	1.770
3	16	"Ierissos Greece"	6.7	1983	18	0.030	0.017	0.002	1.737
4	15	"Friuli_ Italy 01"	6.5	1976	40	0.069	0.040	0.005	1.717
5	34	"Tottori, Japan"	6.61	2000	300	0.337	0.197	0.064	1.704
6	1	"Imperial Vall-05"	5.4	1955	40	0.050	0.037	0.009	1.361
7	9	"Duzce_ Turkey"	7.14	1999	60	0.734	0.559	0.255	1.312
8	5	"Imperial Vall-06"	6.53	1979	38	0.598	0.467	0.202	1.279
9	21	"Friuli_ Italy 01"	6.5	1976	17	0.029	0.023	0.012	1.252
10	18	"Duzce_ Turkey"	7.14	1999	58	0.806	0.658	0.130	1.223
11	32	"Irpinia, Italy 01"	6.9	1980	25	0.034	0.030	0.005	1.140
12	11	"Bam_ Iran"	6.6	2003	45	0.032	0.028	0.027	1.130
13	35	"Tottori, Japan"	6.61	2000	135	0.131	0.116	0.041	1.125
14	4	"Imperial Vall-03"	5.6	1951	40	0.030	0.027	0.004	1.125
15	27	“Shin-Osaka”	6.9	1995	40	0.233	0.218	0.097	1.069
PGA/PGV>2(g.s/m)									
1	13	"Tottori, Japan"	6.61	2000	300	0.410	0.088	0.025	4.661
2	41	"Westmorland"	5.9	1981	30	0.232	0.054	0.009	4.240
3	37	"San Fernando"	6.61	1971	35	0.169	0.047	0.011	3.571
4	6	"Imperial Vall-07"	5.01	1979	18	0.118	0.036	0.003	3.269
5	38	"Fruili, Italy 03"	5.5	1976	15	0.112	0.038	0.002	2.893
6	40	"Livermore-02"	5.42	1980	40	0.254	0.098	0.005	2.590
7	43	"Nahanni, Canada"	6.76	1985	11	1.107	0.439	0.068	2.522
8	36	"Parkfield"	6.19	1966	25	0.271	0.113	0.038	2.392
9	12	"9173365"	4.26	2001	120	0.010	0.004	0.00044	2.381
10	45	"Tottori, Japan"	6.61	2000	300	0.289	0.124	0.043	2.327
11	26	"Whittier Narrows-01"	5.99	1987	50	0.121	0.052	0.007	2.323
12	39	"Coyote Lake"	5.74	1979	28	0.094	0.042	0.008	2.226
13	24	"Dinar Turkey"	6.4	1995	29	0.065	0.031	0.002	2.101
14	44	"Loma Prieta"	6.93	1989	40	0.460	0.227	0.081	2.022
15	42	"Coalinga-05"	5.77	1983	20	0.405	0.201	0.014	2.012

6.4 Flowchart of the Calculation Procedure

In order to implement the research, the following flowchart of the calculations has been implemented to carry out the research for this chapter:

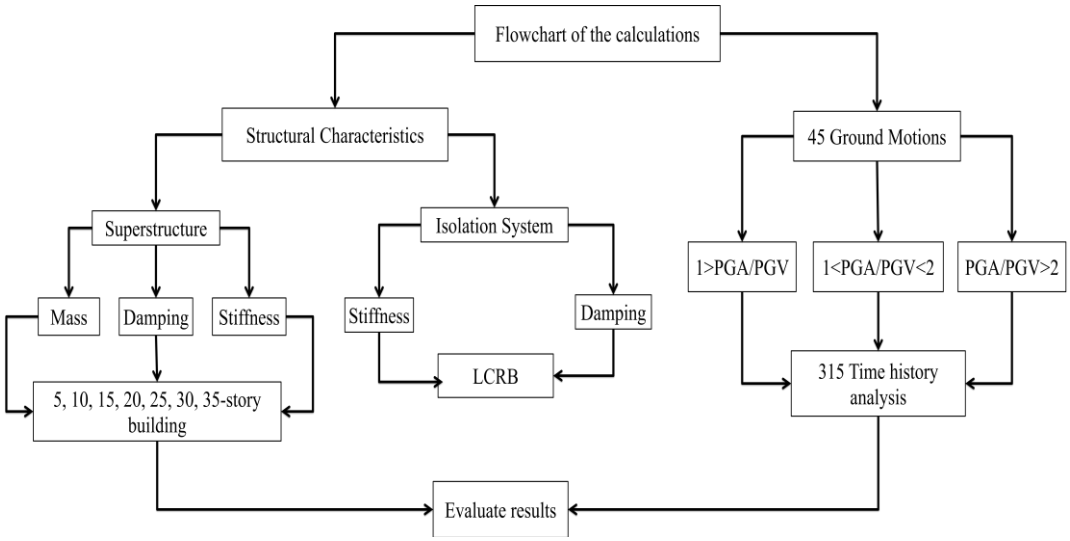

Figure 21: Flowchart of the calculations

6.5 Two-Factor Factorial Design and Probabilistic Evaluation

6.5.1 Two-Factor Factorial Design

In this study, to investigate the effectiveness of the factors of the base-isolated buildings, a two-factor factorial design was conducted using Minitab software (version 2017), considering the factors (ratio of PGA/PGV and number of stories) in Table 10, while all other factors such as T_b, β_{eff}, f_0, α_1 and u_y remained constant (Table 8). In Table 10, y_{abn} (i.e., $y_{111}, y_{112},\ldots$) is the result of the combination of a (ratio of PGA/PGV) and b (number of story) levels for n^{th} ground motion.

For each group of earthquakes (for each ratio of PGA/PGV), 7 different kinds of buildings varying in height (i.e., 5, 10, 15, 20, 25, 30 and 35, as in Figure 20a and Figure 20b) have been considered, and combinations thereof are generated. Thus,

there are 15 ground motions for each base-isolated building in each group of ground motions.

Table 10: Arrangement for two-factor factorial design

Factor		Stories						
	Levels	**5**	**10**	**15**	**20**	**25**	**30**	**35**
Ratio	**1>PGA/PGV**	y_{111}	y_{121}	y_{131}	y_{141}	y_{151}	y_{161}	y_{171}
		y_{112}	y_{122}	y_{132}	y_{142}	y_{152}	y_{162}	y_{172}
		⋮	⋮	⋮	⋮	⋮	⋮	⋮
		y_{11n}	y_{12n}	y_{13n}	y_{14n}	y_{15n}	y_{16n}	y_{17n}
	1<PGA/PGV<2	y_{211}	y_{221}	y_{231}	y_{241}	y_{251}	y_{261}	y_{271}
		y_{212}	y_{222}	y_{232}	y_{242}	y_{252}	y_{262}	y_{272}
		⋮	⋮	⋮	⋮	⋮	⋮	⋮
		y_{21n}	y_{22n}	y_{23n}	y_{24n}	y_{25n}	y_{26n}	y_{27n}
	PGA/PGV>2	y_{311}	y_{321}	y_{331}	y_{341}	y_{351}	y_{361}	y_{371}
		y_{312}	y_{322}	y_{332}	y_{342}	y_{352}	y_{362}	y_{372}
		⋮	⋮	⋮	⋮	⋮	⋮	⋮
		y_{31n}	y_{32n}	y_{33n}	y_{34n}	y_{35n}	y_{36n}	y_{37n}

To evaluate the effectiveness of the subjected factors for each group of the ground motions, 105 analyses have been implemented, which required a total of 315 time history analyses to be carried out. The results are illustrated in the main effect plots for each case of earthquakes (Figure 26 to Figure 29).

6.6 Probabilistic Evaluation

In order to perform probabilistic analysis, the key responses of the base-isolated buildings (the ratio of peak responses of floor to peak ground responses) limitations are considered as follows:

6.6.1 Limit of Responses

The probability of failure (PF) correlated with particular structural parameters, which can be obtained with a function of limitation. In this study, the performance limit is based on the key responses of the peak responses of the floor to the peak

ground responses ratio. The limit state of the responses is formed according to the following function:

$$F(x) = 1 - \left(\frac{PRF}{PGR}\right) \text{ (if } F(x) < 0 \rightarrow \text{fail)} \quad (19)$$

According to the above function (19), if F(x) is smaller than 0, it fails.

6.7 Ground Motion's Parameters

The ratio of PGA/PGV was mentioned as a very important factor affecting the behavior of the isolator. The behavior of the isolator can be reversed under various ground motions even for the same level acceleration of the earthquakes. Figure 22 illustrates the spectral acceleration for each group of earthquakes along with their median, which makes it easy to clarify the difference between the groups of the earthquakes. The acceleration spectra of the selected ground motions in Figure 22 illustrate that as the ratio of PGA/PGV increases, by shifting the period to 2.5 s, their spectral accelerations decrease (at 2.5 s).

Figure 23 reveals that the energy associated with the velocity and displacement spectra for the group of the ground motions where PGA/PGV<1 is much higher than the other group of the ground motions, especially at higher periods.

Moreover, Figure 24 clearly shows that the intensity of the group of the ground motions where PGA/PGV<1is significantly higher than the two other groups of the ground motions where PGA/PGV is between 1 and 2, and more than 2 at the highest intensity when the frequency is about 0.25Hz (Figure 24).

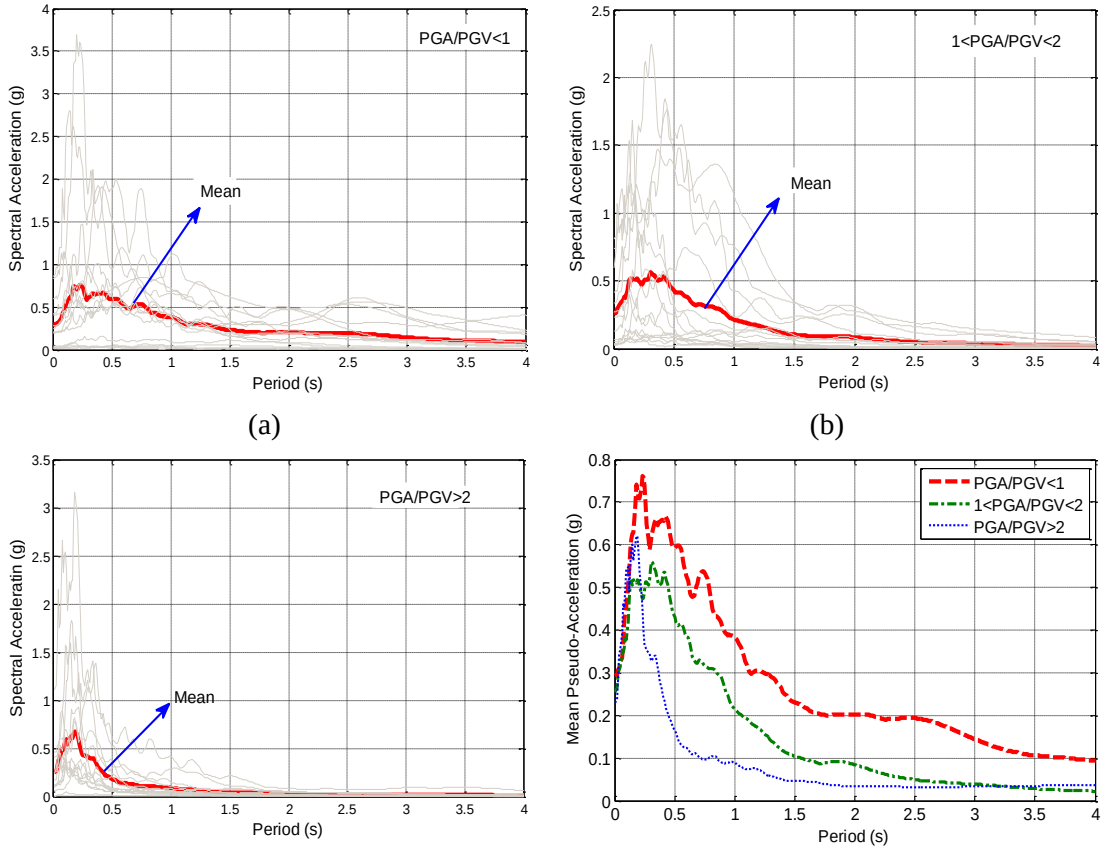

Figure 22: Five percent (5%) damped acceleration spectra of the selected ground motions for three cases; d) Mean of each group (PGA/PGV unit is g.s/m)

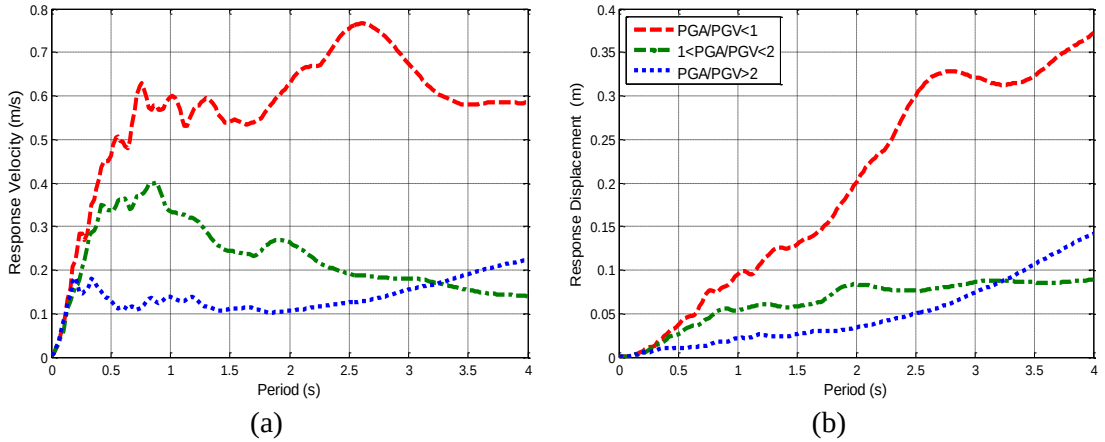

Figure 23: Five percent (5%) damped response spectra of the selected ground motions for three cases; a) Response Velocity, b) Response Displacement

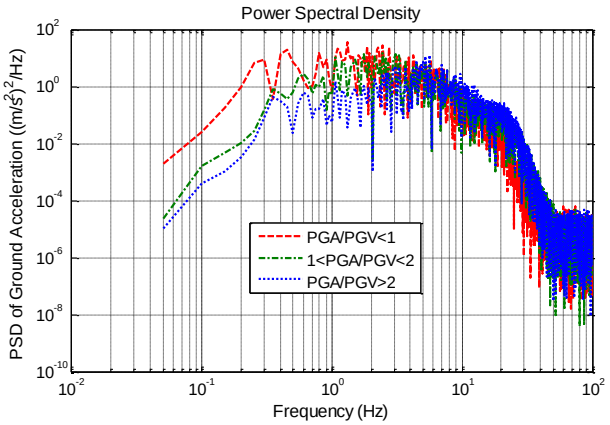

Figure 24: Power Spectral Density (PSD) for each mean group of three different ground motions (PGA/PGV unit is g.s/m)

6.8 Flowchart of the Procedure

Figure 25 briefly illustrates the procedure of the study in this section:

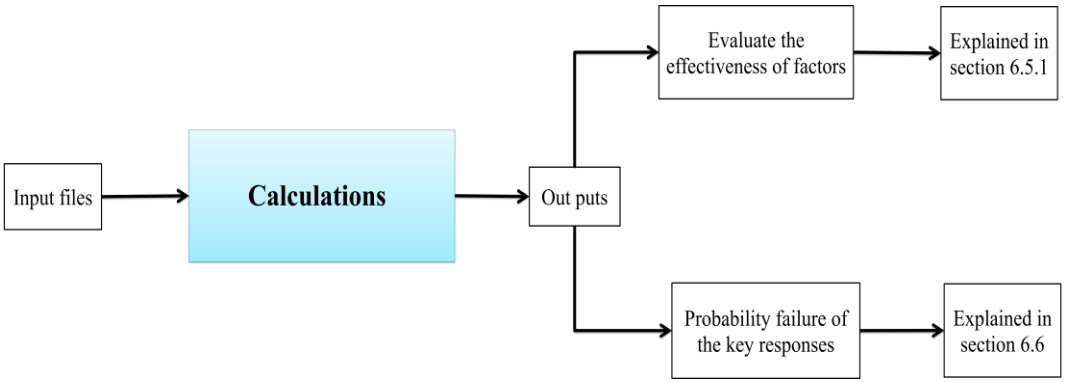

Figure 25: Schematic illustration of the procedure

6.9 Results and Discussion

6.9.1 Evaluate the Effectiveness of the Factors

With regard to Figure 26a, when $\mathrm{PGA/PGV} < 1$, the ratio of isolator displacement to peak ground displacement (PGD) is approximately 0.64, and as it changes to $1 < PGA/PGV < 2$ and further to $\mathrm{PGA/PGV} > 2$, the ratio increases. The graph also shows that the case of $1 < PGA/PGV < 2$ is the mean of the other two cases (i.e., $\mathrm{PGA/PGV} < 1$ and $\mathrm{PGA/PGV} > 2$.).

Moreover, with regard to the number of stories in the base-isolated buildings (Figure 26b), it can be clarified that by increasing the number of stories, marginal changes are observed between 5- and 10-story buildings and the ratio gradually decreases, which is not significant. In addition, the ratio is at the highest level for the 5- and 10-story buildings, which implies that the isolator displacement with respect to the peak ground displacement increases by approximately 0.1. For the case of the 20-story building, the ratio of isolator displacement to peak ground displacement is sharply decreased, which can be the result of the flexibility of the high-rise building and its effect on the base isolation system.

Additionally, the interaction of both the PGA/PGV ratio and the effects of the number of stories show that the trend is quite similar for all types of base-isolated buildings, and the ratio increases. The ratio of isolator displacement to peak ground displacement (ISO DIS TO PGD) for the cases when $\mathrm{PGA/PGV} < 1$ is the lowest and for the case when $\mathrm{PGA/PGV} > 2$ is the highest (Figure 26c). In addition, as the number of stories increases, the ratio decreases, which can also be the result of the flexibility of the high-rise buildings.

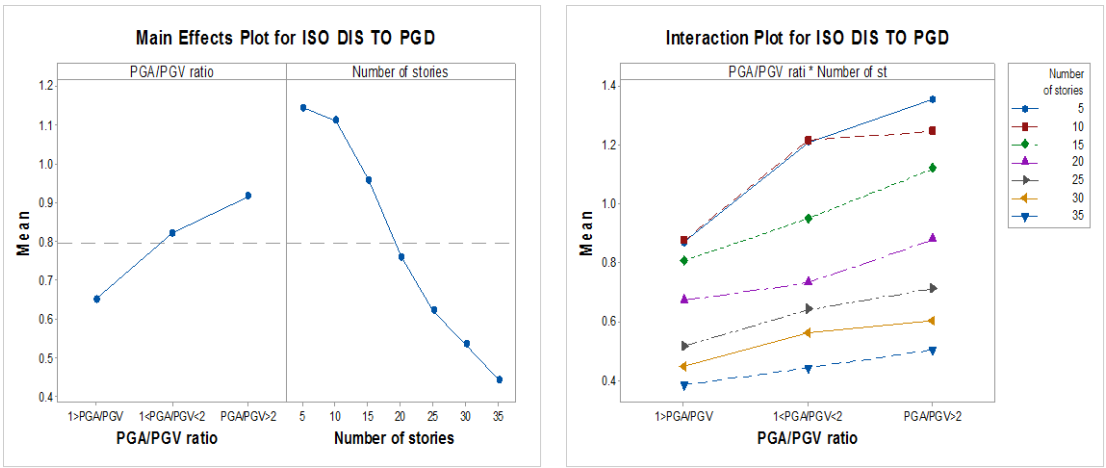

(a) (b) (c)

Figure 26: Main effects and interaction plots for isolator DIS with respect to PGD

Additionally, Figure 27a shows that the ratio of the top floor displacement to the peak ground displacement (ROOF DIS TO PGD) has been significantly increased for the cases between $1 < PGA/PGV < 2$ and $\mathrm{PGA/PGV} < 1$ and remained almost constant between the cases $1 < PGA/PGV < 2$ and $\mathrm{PGA/PGV} > 2$. Moreover, as the ratio of PGA/PGV is more than one, it implies that the displacement for the top floor is highly increased with respect to the peak ground displacement. In addition, in Figure 27b, it can be observed that by increasing the number of stories, the ratio of top floor displacement to peak ground displacement is increased, which is also expected as the height of the building increases. Only the 5 and 10 story buildings have a ratio lower than 1.

Figure 27c, which is the interaction plot, shows that the ratios for 5-, 10-, 15- and 20-story buildings increase with the same trend, which also shows that there is no interaction; however, for 25-, 30- and 35-story isolated buildings, the ratio increased for the case when $1 < PGA/PGV < 2$ and decreased for the case when $\mathrm{PGA/PGV} > 2$. Moreover, the ratio of roof displacement to PGD decreased for 5- and 10-story buildings for the three cases (see Table 4). However, for a 15-story building, roof displacement decreased only in the case when $\mathrm{PGA/PGV} < 1$. In contrast, for the 20-, 25-, 30- and 35-story buildings, roof displacement increased with respect to PGD, which implies that the displacement is higher than the ground displacement.

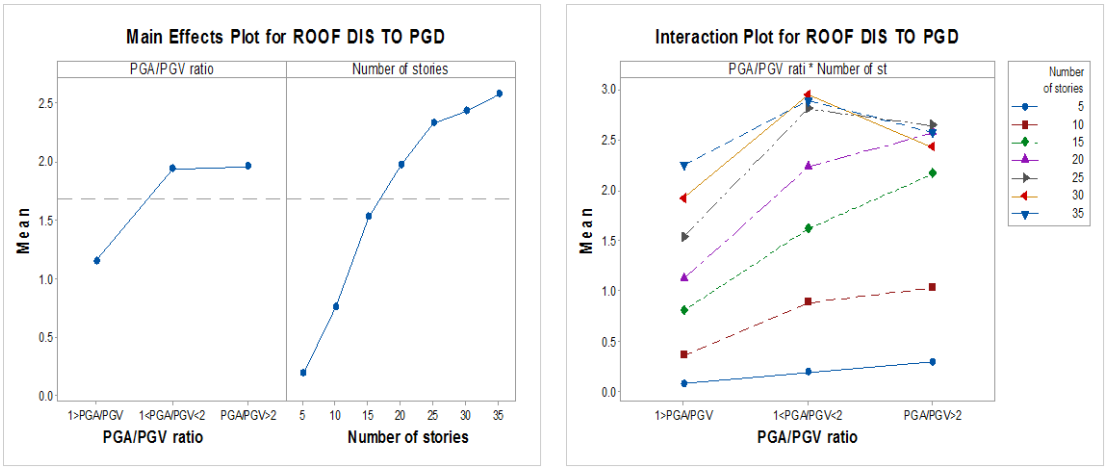

(a) (b) (c)

Figure 27: Main effects and interaction plots for roof DIS with respect to PGD

Figure 28a gives information about the ratio of the isolator acceleration to peak ground acceleration (ISO ACC TO PGA), where this ratio is highly increased for the case of ground motions with $\mathrm{PGA/PGV} < 1$ when compared with the other two cases of $1 < PGA/PGV < 2$ and $\mathrm{PGA/PGV} > 2$. However, overall, the acceleration is not more than the ground acceleration for three different cases.

Moreover, it is seen from Figure 28b that because the number of stories increases, the isolator acceleration with respect to PGA fluctuates. It can be concluded that for different heights and stories, the acceleration of the isolation system in base-isolated buildings will be reduced by approximately 55% with respect to the PGA.

By observing the interaction (Figure 28c) of the ratio of PGA/PGV and the number of stories, it is clear that unlike the displacement ratio mentioned above, the proportion of isolator acceleration to peak ground acceleration (PGA) for all isolated buildings decreases in a similar trend as the ratio of PGA/PGV increases. In all cases, the base isolation acceleration is decreased with respect to the peak ground acceleration. Furthermore, increasing the number of stories has no significant effect for the cases when $1 < PGA/PGV < 2$ and $\mathrm{PGA/PGV} > 2$, and the ratios calculated are closer to each other for all types of buildings in the stated cases (Figure 28c).

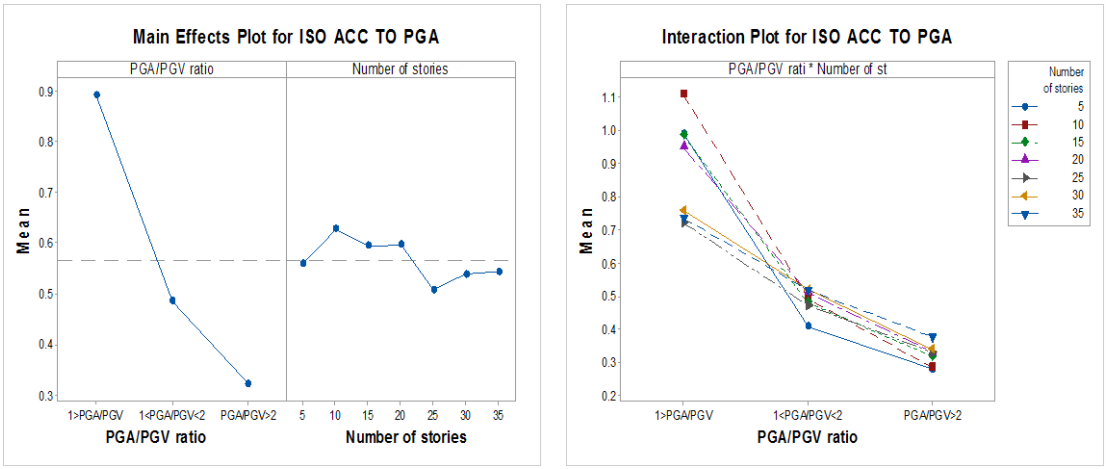

(a) (b) (c)

Figure 28: Main effects and interaction plots for isolator ACC with respect to PGA

Figure 29a shows that when $\mathrm{PGA/PGV} < 1$, roof acceleration is further increased compared to the cases when $1 < PGA/PGV < 2$ and $\mathrm{PGA/PGV} > 2$, which is approximately 1.75 times higher than the PGA. In addition, Figure 29b illustrates that roof acceleration is decreased for 5- and 10-story buildings with reference to the PGA (i.e., roof acceleration is lower than the PGA), but this ratio is higher than one for five other different buildings (i.e., roof acceleration is higher than the PGA), and it also fluctuates because the number of stories increases. In addition, considering the interaction plot (Figure 29c), it can be seen that for all types of isolated buildings, the ratio for the case when $\mathrm{PGA/PGV} < 1$ is more than that of the cases when $1 < PGA/PGV < 2$ and $\mathrm{PGA/PGV} > 2$, and the roof acceleration is more than the PGA. This ratio is decreased for the cases of $1 < PGA/PGV < 2$ and $\mathrm{PGA/PGV} > 2$, which shows that the ratio is less than one and roof acceleration is lower than the peak ground acceleration in these two cases. Additionally, the ratios for the case when $\mathrm{PGA/PGV} > 2$ are closer to each other for all types of buildings (Figure 29c).

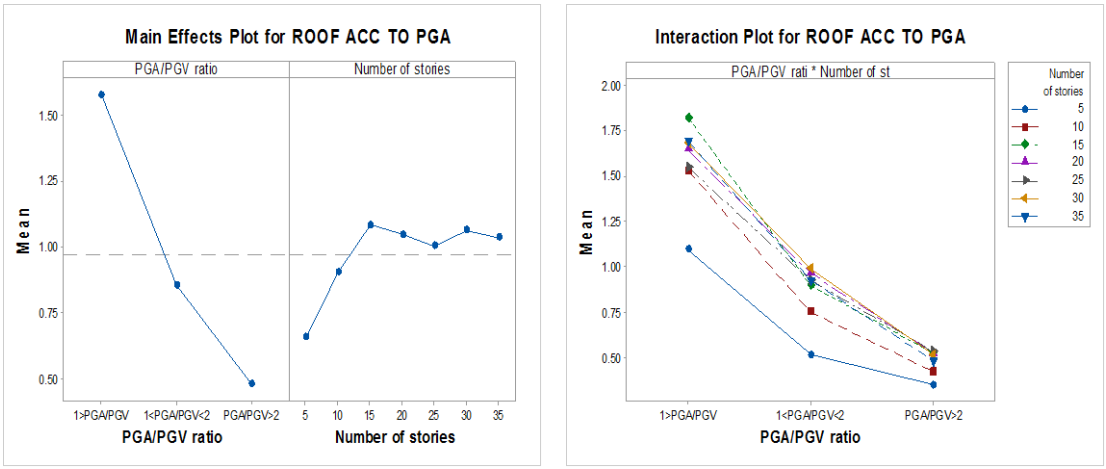

(a) (b) (c)

Figure 29: Main effects and interaction plots for roof ACC with respect to PGA

6.9.2 Probabilistic Performance Evaluation (PPE)

By implementing binary logistic regression method for the key responses criteria following figures (Figure 30 to Figure 33) illustrate the probability of failure of the ratio, which is stated above for the base-isolated buildings.

According to Figure 30, it reveals that the probability of failure of the ratio of peak bearing displacement to peak ground displacement is decreasing as the number of the story is increasing for all cases of the ground motions. Figure 30 also shows that the highest probability of failure occurred for the low-rise base-isolated building, which is about 80% for the group of ground motions whose PGA/PGV is more than 2. However, Figure 31 illustrates that the probability of failure of the bearing acceleration to PGA only happens when PGA/PGV is less than 1 and for other cases of the earthquakes no failure occurred. And the maximum probability of failure occurs for the low-rise (5-story) base-isolated building which is about 43%.

Figure 32 and Figure 33 reveal the results for roof responses. From Figure 32, it can be observed that the probability of failure of peak roof displacement to PGD ratio is increasing as the number of the story is increasing. For when PGA/PGV is less than 1 the probability of failure (PF) is gradually increasing from 5-story to 35-

story base-isolated buildings. For the case when PGA/PGV is between 1 and 2, PF is at the highest level for 30- and 35-story base-isolated buildings. But for the ground motions whose PGA/PGV are more than 2, PF of peak roof displacement to PGD ratio is in the highest level after 20-story base-isolated building.

Moreover, Figure 33 provides information related to PF of the roof acceleration to PGA ratio. As it is clear by this figure, the highest intensity is for the ground motions whose PGA/PGV is less than 1, and the highest probability of failure occurred for high-rise (35-story) base-isolated building that is about 96%. And this PF is reduced for when PGA/PGV is between 1 and 2, and when it is more than 2, respectively. The lowest PF is for the case when PGA/PGV is more than 2 (in this case, approximately, PF=0 for all subjected base-isolated buildings).

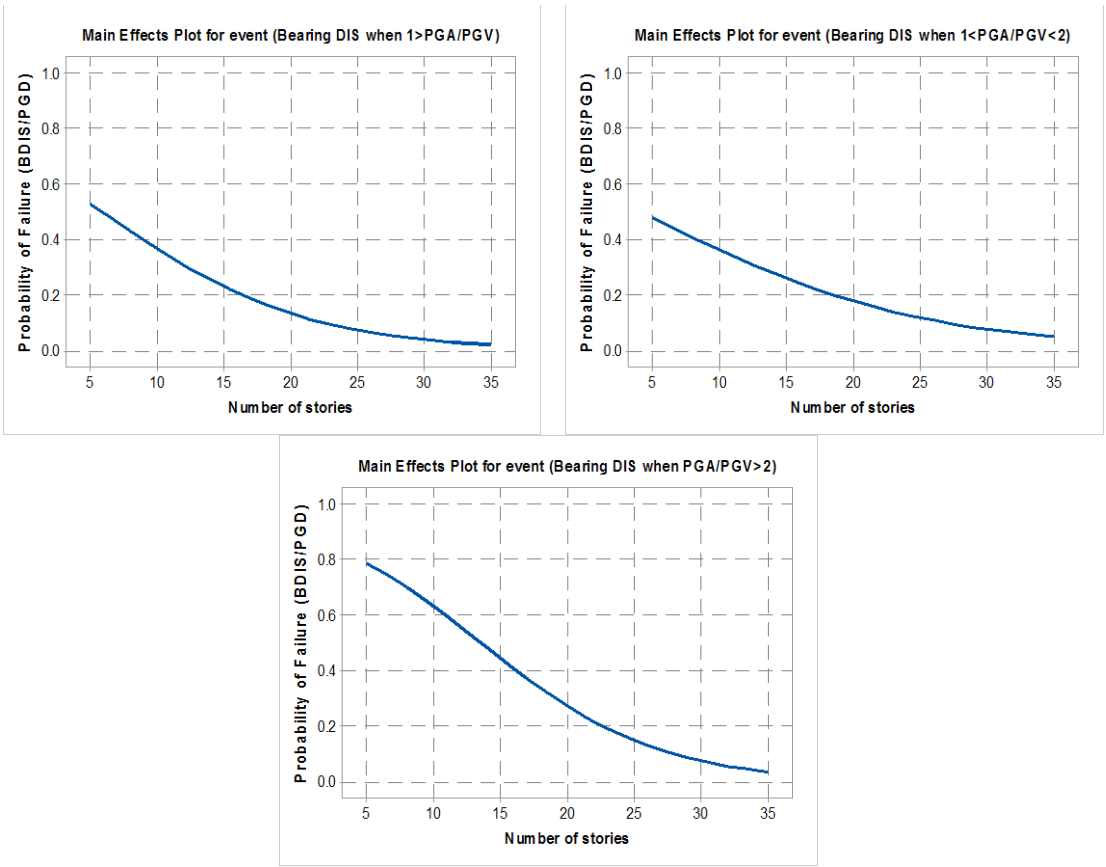

Figure 30: Probability of failure of the peak bearing DIS to PGD ratio

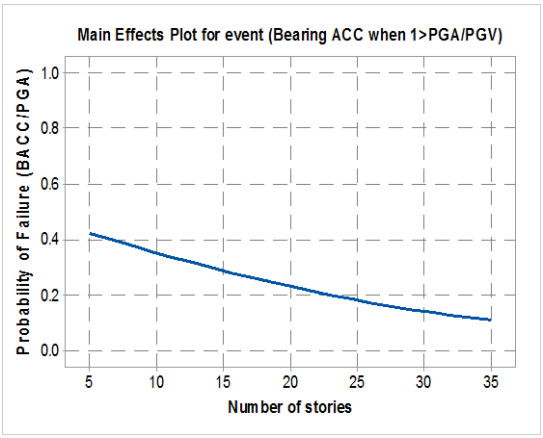

Figure 31: Probability of failure of the peak bearing ACC to PGA ratio

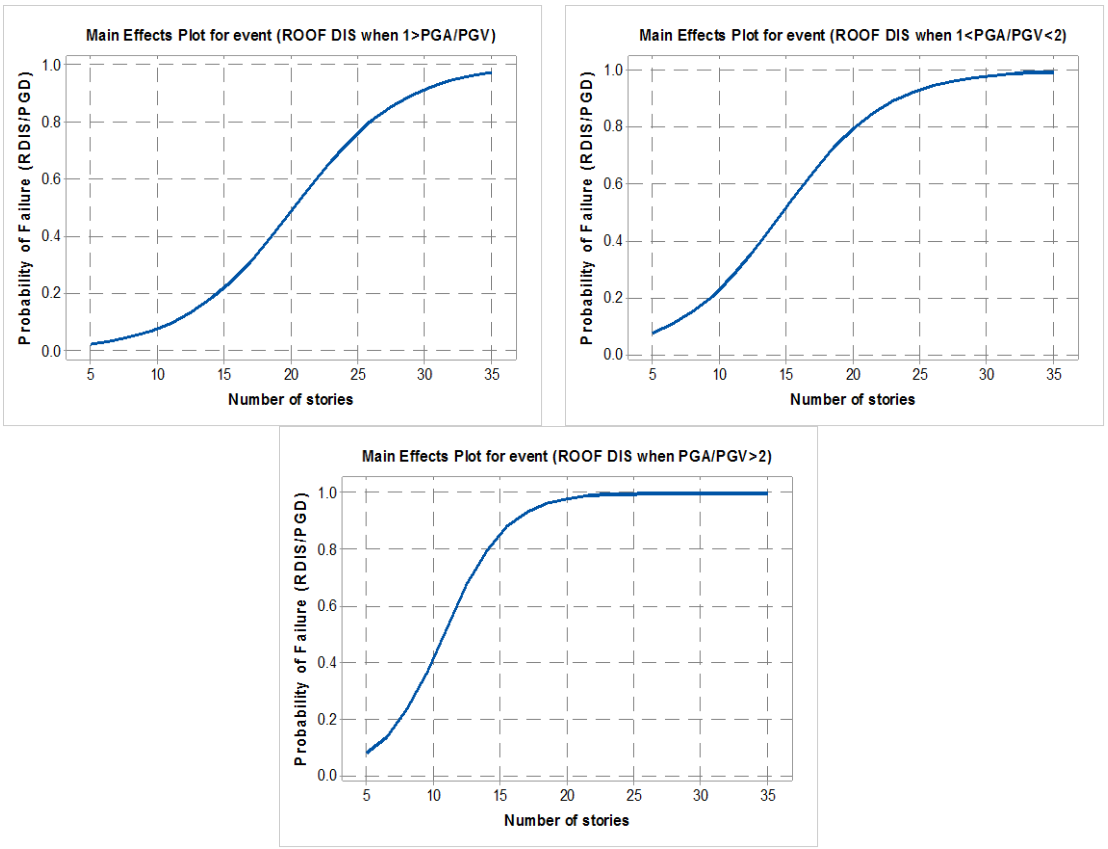

Figure 32: Probability of failure of the peak roof DIS to PGD ratio

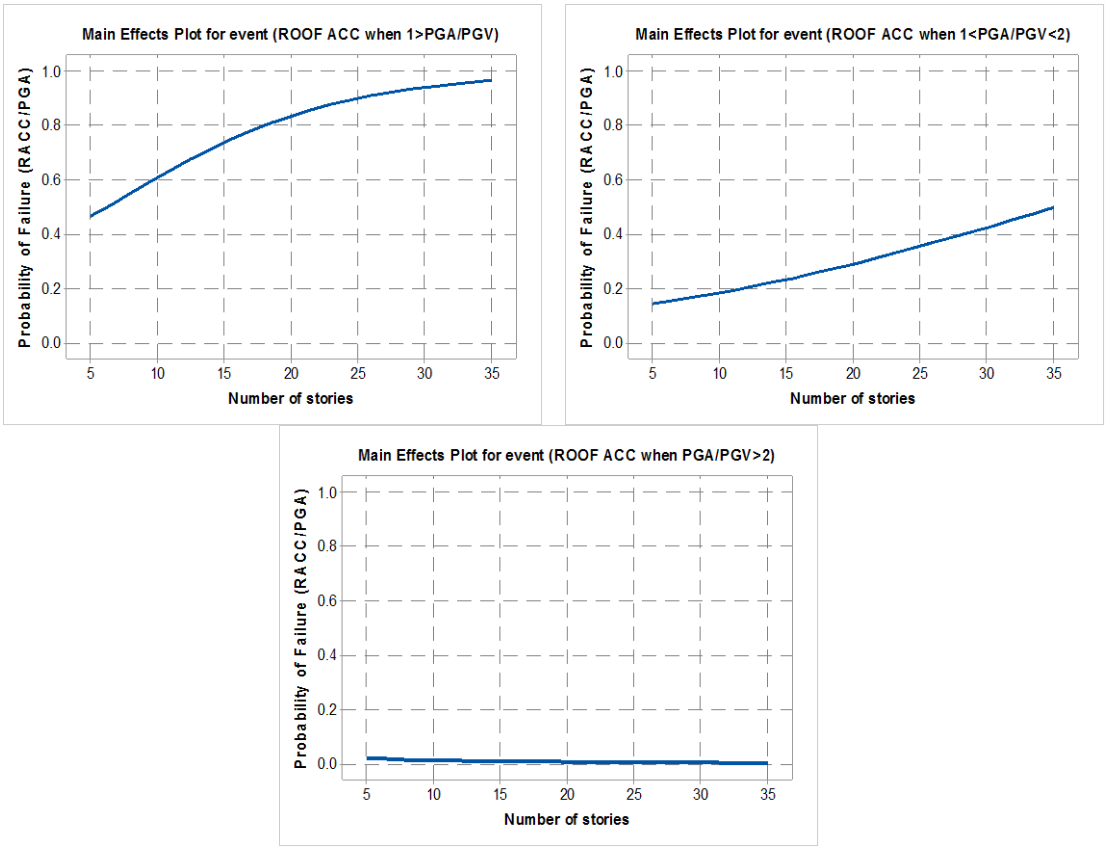

Figure 33: Probability of failure of the peak roof ACC to PGA ratio

6.9.3 Performance of the Base Isolation System and Base-Isolated Buildings

As shown in Figure 34, the fundamental period of the base-isolated building increases as the number of stories increases, which implies that the influence of the base isolation system decreases as the number of stories or the flexibility of the superstructure increases. The Figure also shows that as the number of stories increases, the gap between the fundamental period of the fixed-base building and the base-isolated building decreases. It also seems that as this trend continues, there is no difference between the fixed-base and base-isolated buildings' fundamental periods, and thus, the effect of the base isolation system is reduced.

Furthermore, as the fundamental period of the 5-story fixed base building is exactly 0.5 s, if an isolation system is mounted on this building, the fundamental period increases, which is approximately 5 times higher than that of the fixed base

(Figure 34). However, this shift gradually decreases as the number of stories increases; for example, fundamental period of the 35-story fixed base building decreases by exactly 3.5 s. On the other hand, if an isolation system is mounted on this building, the fundamental period increases by approximately 1.2 times when compared with the 35-story fixed base building.

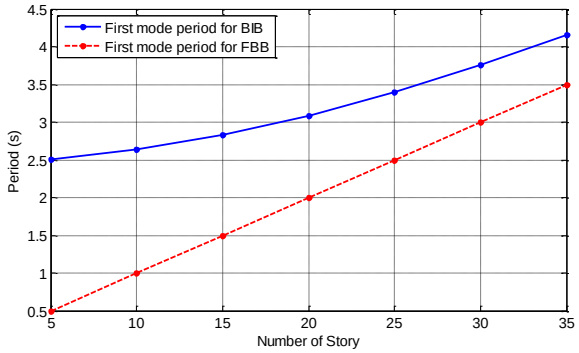

Figure 34: Fundamental period of the superstructure for both fixed-base and base-isolated buildings (when the base isolation system period is T_b = 2.5 s)

For further investigation, from each group of selected earthquakes, one earthquake with the highest PGA was selected to study the amount of dissipated energy as the number of stories increased (Figure 35). Figure 35 illustrates that as the number of stories is increased, the shear force increases; consequently, the amount of dissipated energy by the base isolation system increases simultaneously (i.e., the area under the load-deflection curve increases).

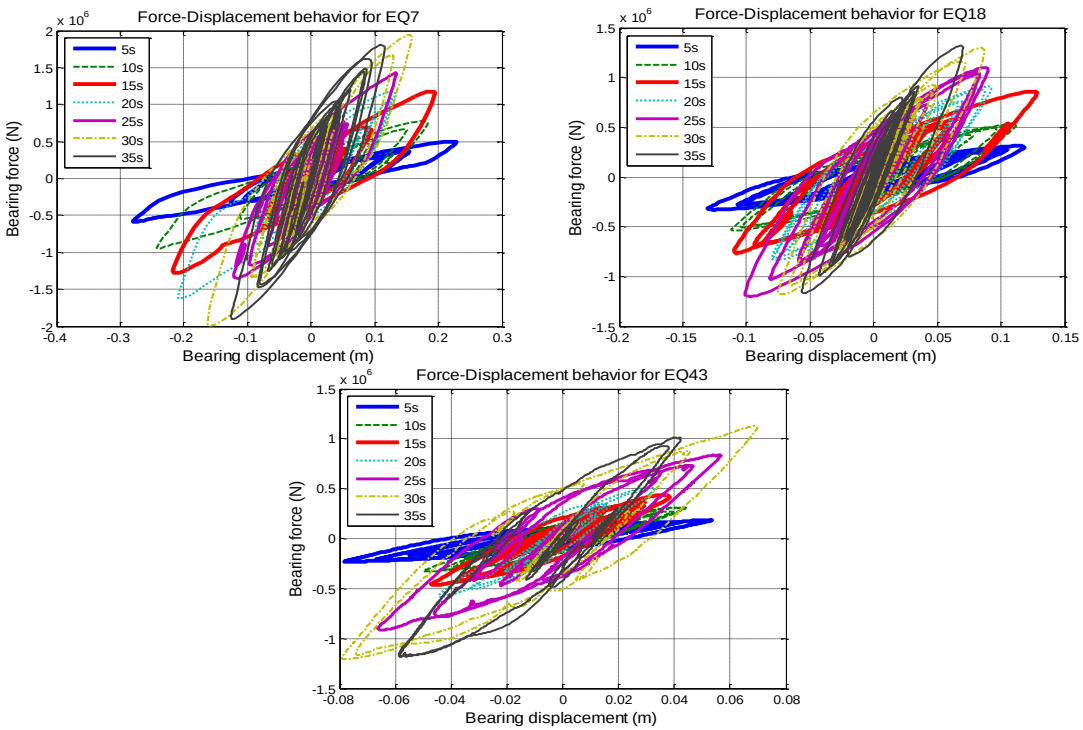

Figure 35: Force-displacement curves for three selected ground motions with the highest PGA

In addition, the force-displacement curves of the base isolation system for three different cases of ground motions with maximum PGAs have been investigated on seven different base-isolated buildings, and the results are illustrated in Figure 36. As seen, less energy has been dissipated for the case when $\mathrm{PGA/PGV} > 2$. Based on Figure 22, according to the characteristics of earthquakes, by shifting the period to 2.5 s, the amount of spectral acceleration for the median is lower for the case of $\mathrm{PGA/PGV} > 2$ when compared with the other two cases. This states that when the base-isolated buildings are subjected to the earthquake of case 3, low earthquake impact loads are applied to the structure, and as a result, less energy is required to be dissipated. Conversely, for the other ground motions, the applied load to the buildings is higher for the cases when $1 < PGA/PGV < 2$ and $\mathrm{PGA/PGV} < 1$. Thus, more energy is required to be dissipated. This result can be clearly seen from the area under the force-displacement curves.

Figure 37 and Figure 38 illustrate the median responses of the subject buildings induced by three different cases of the selected ground motions (see Table 9). Figure 37 shows that the percentage of reduction in acceleration is higher than the displacement at the top of the buildings when compared with fixed-base buildings. This amount of acceleration reduction is higher for low-rise buildings, but this reduction percentage decreases as the number of stories increases, and it can even be seen that there is no difference between the fixed-base and base-isolated buildings for the case when $\mathrm{PGA}/\mathrm{PGV} > 2$ for 30- and 35-story buildings. Moreover, the magnitude of reduced acceleration for 15-, 20-, 25-, 30- and 35-story buildings remains approximately constant for each case of ground motions (see Table 9).

Figure 38 shows that by increasing the number of stories, the magnitude of the top floor displacement varies for the fixed-base for the three different cases. However, for the base-isolated buildings, by increasing the number of stories, the top floor displacement of the buildings gradually increases. It is clear that the displacement has been decreased for the 5-, 10-, 15-, 20- and 25-story buildings but increases for 30- and 35-story buildings when compared with the fixed-base state, the results for which are inverse.

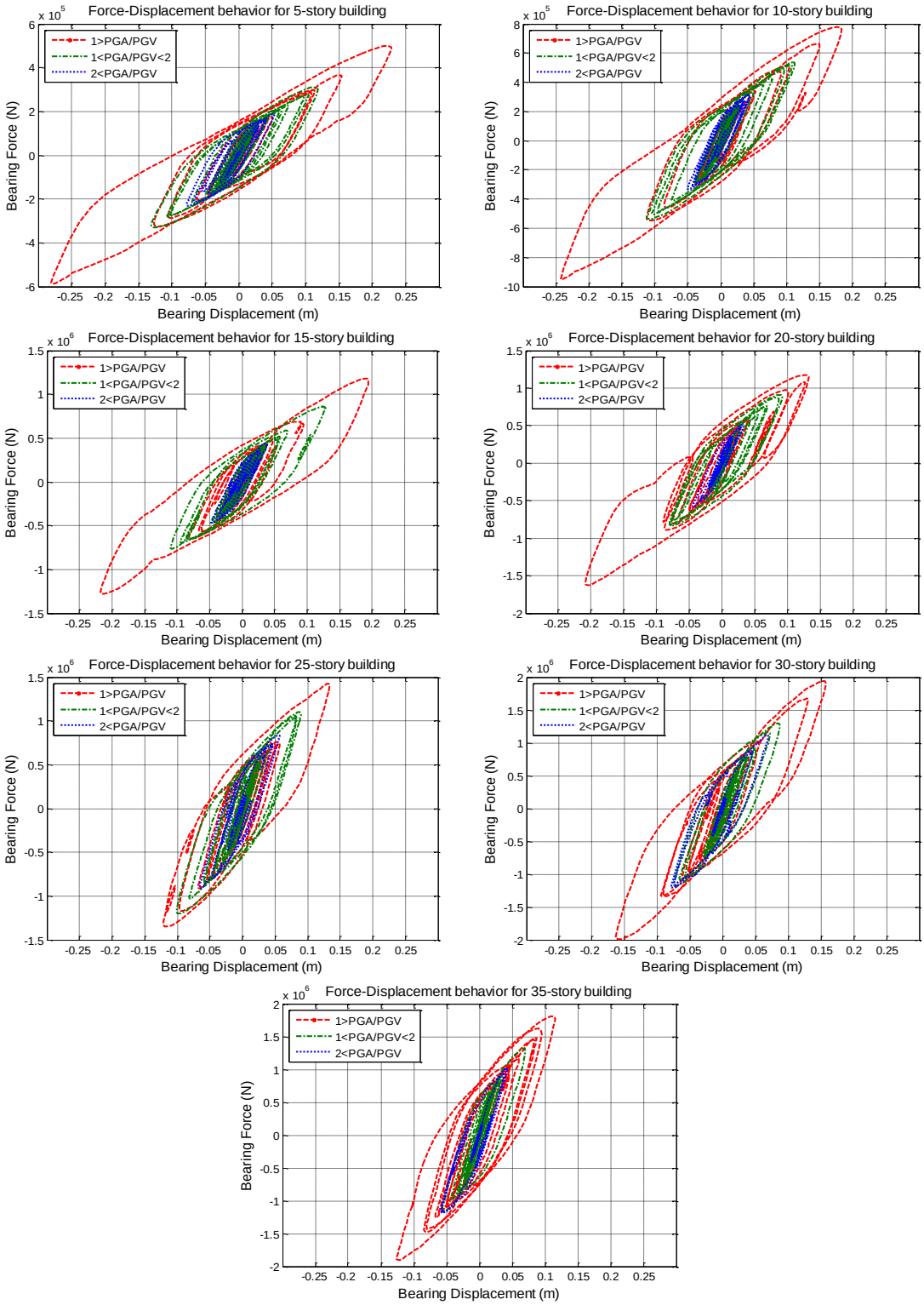

Figure 36: Force-displacement behavior of the isolation system for seven different isolated buildings

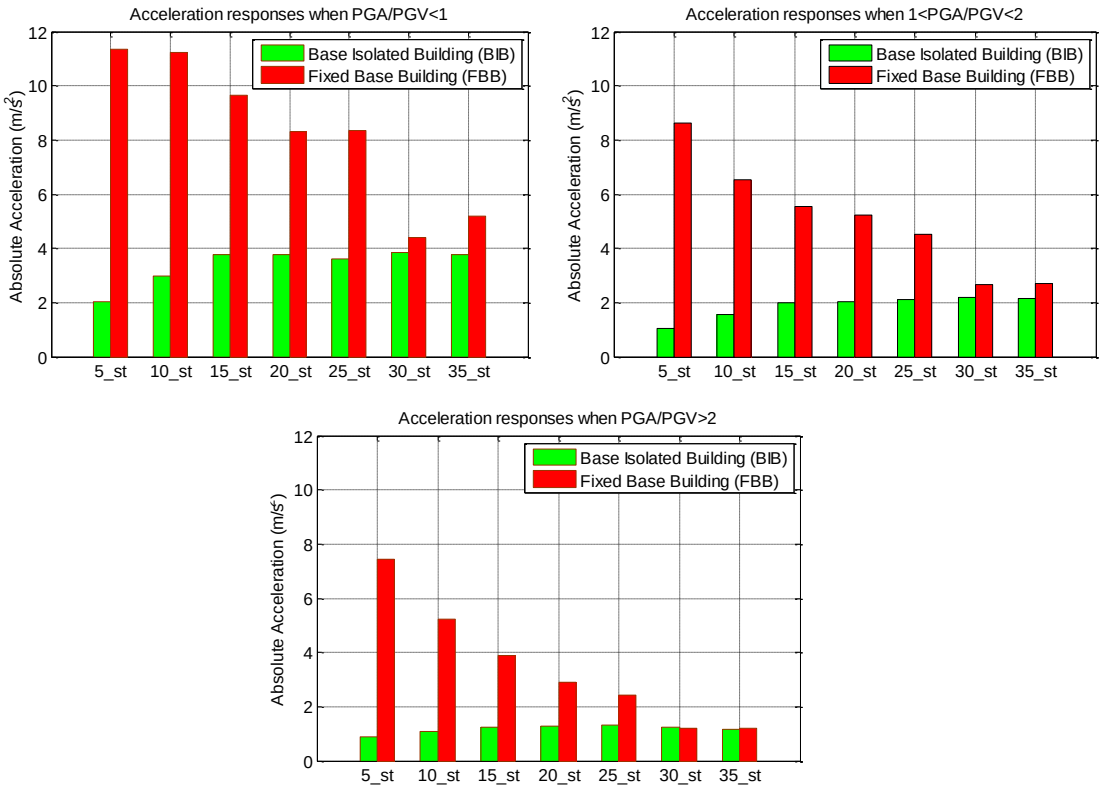

Figure 37: Median of top floor absolute acceleration of the FB and BI buildings

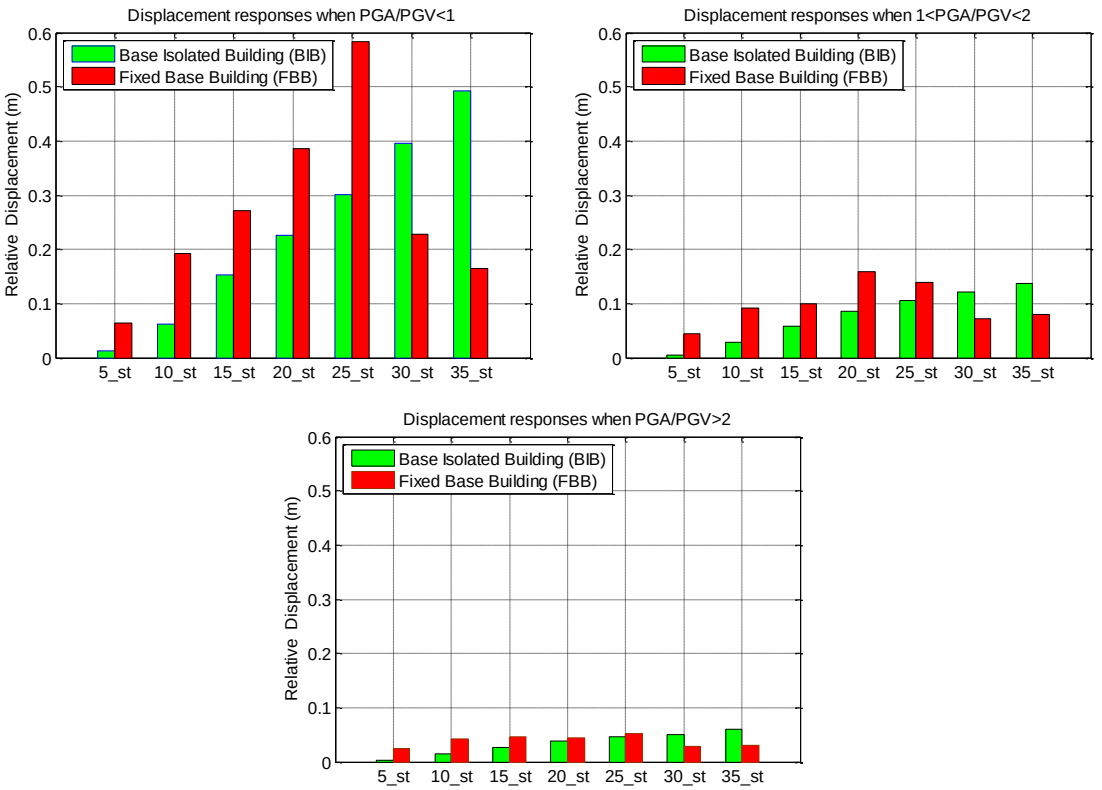

Figure 38: Median of top floor relative displacement of the FB and BI buildings

For further investigation, based on median spectrum ground motions in Figure 22, artificial earthquakes were generated using the SeismoArtif software program (version 2018). In this manner, the Saragoni and Hart envelope curve method was implemented considering the following specifications [73] (Figure 39).

For the above-mentioned method, three parameters are needed to define the envelope shape fully; thus, in this study, these three parameters are kept as follows:

- Duration considered to be 20 s
- t_1 is kept at 4 s. This parameter should be a real number lower than the duration, which is the time instant corresponding to unitary intensity.
- Idur: This parameter should be a real number smaller than unity, which is the value of intensity corresponding to the last instant of time (default value amounts to 0.05).

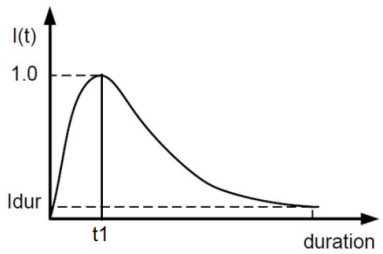

Figure 39: Saragoni & Hart envelope curve [73]

By executing the aforementioned procedure, it can be clearly seen from Figure 40 that the actual spectrum matches the specific target spectrum with 5% damping.

According to the above implementation, artificial earthquakes have been generated based on the median spectrum of the natural ground motions for each case in Table 9 (Figure 41 illustrates accelerograms that are generated with respect to the target spectrum for each case, and Figure 42 shows the velocity time history based on the generated accelerogram). Table 11 depicts the peak ground responses of the

artificial ground motions for three different cases (PGA/PGV). Figure 43 and Table 11 also show that for the case when PGA/PGV <1, the intensity of the ground motion is higher when compared with the two other ratios.

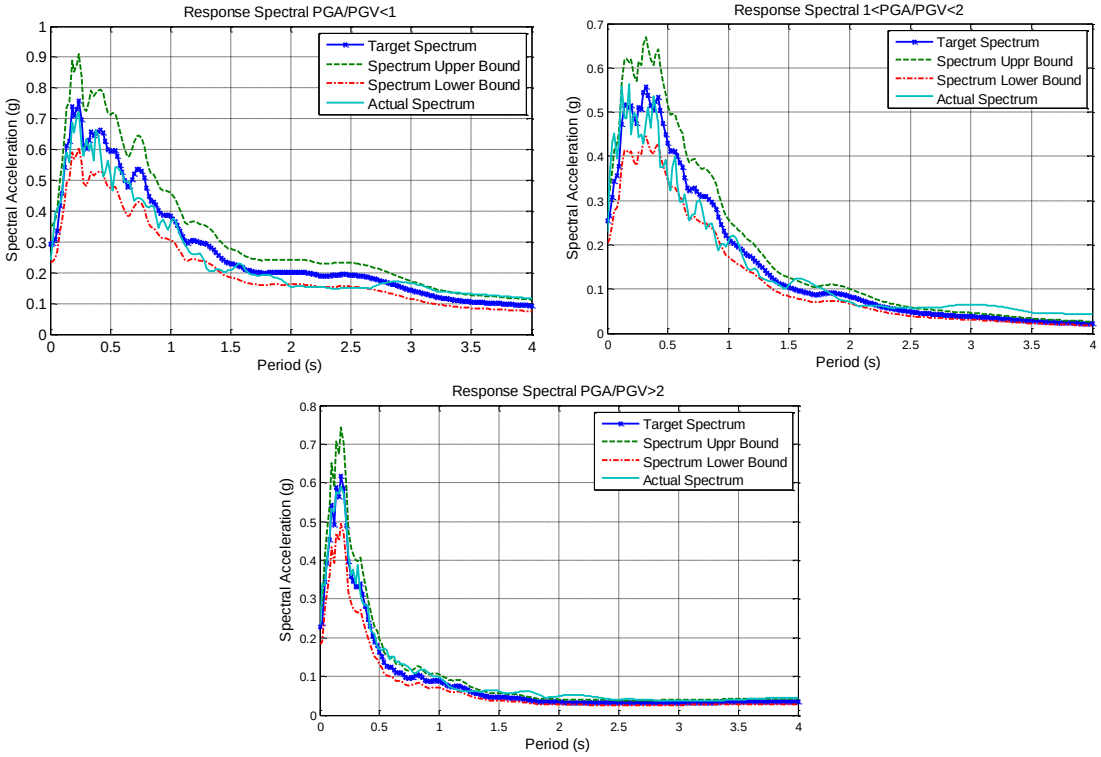

Figure 40: The response spectral matched the target spectrum

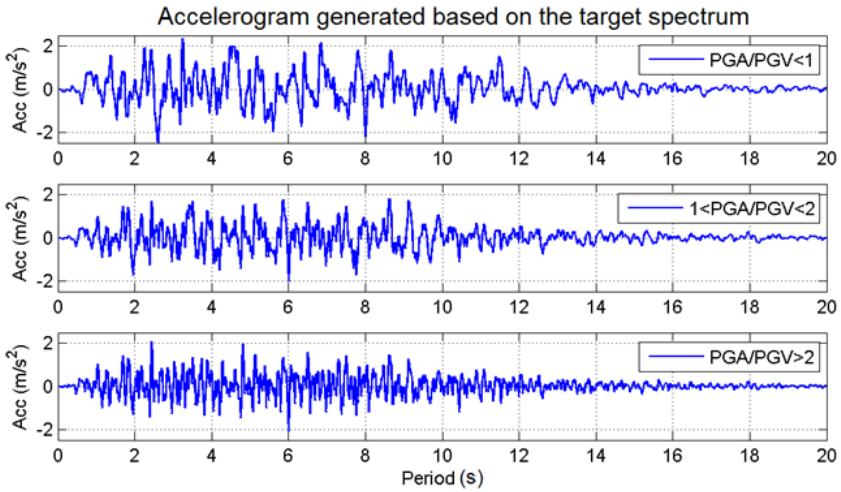

Figure 41: Accelerogram generated based on the target spectrum for each group

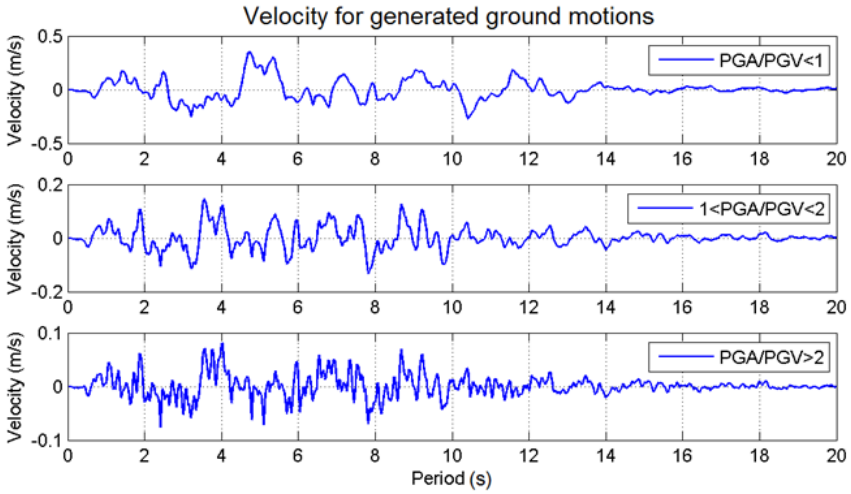

Figure 42: Velocity-time history based on the generated accelerogram

Moreover, to clarify the intensity of the three different groups of ground motions, Power Spectral Density of the above-mentioned earthquakes has been illustrated in Figure 43. It can be observed that the ground motions, whose PGA/PGV<1, have the highest intensity in lower frequency in comparison with other cases (1<PGA/PGV<2 and PGA/PGV>2). It implies that the buildings whose fundamental period is bigger will be more affected under these types of ground motions. Figure 43 illustrates that displacement and velocity responses of the ground motions (when PGA/PGV <1) are more *sharply* increased than the acceleration responses increased.

Table 11: Peak ground responses for artificially generated ground motions based on the median spectrum of the real ground motions

EQ Case	PGA (m/s^2)	PGV (m/s)	PGD (m)	PGA/PGV (g.s/m)	Ratio
1	0.28	0.351	0.152	0.763	PGA/PGV<1
2	0.203	0.145	0.039	1.4	1<PGA/PGV<2
3	0.212	0.081	0.023	2.61	PGA/PGV>2

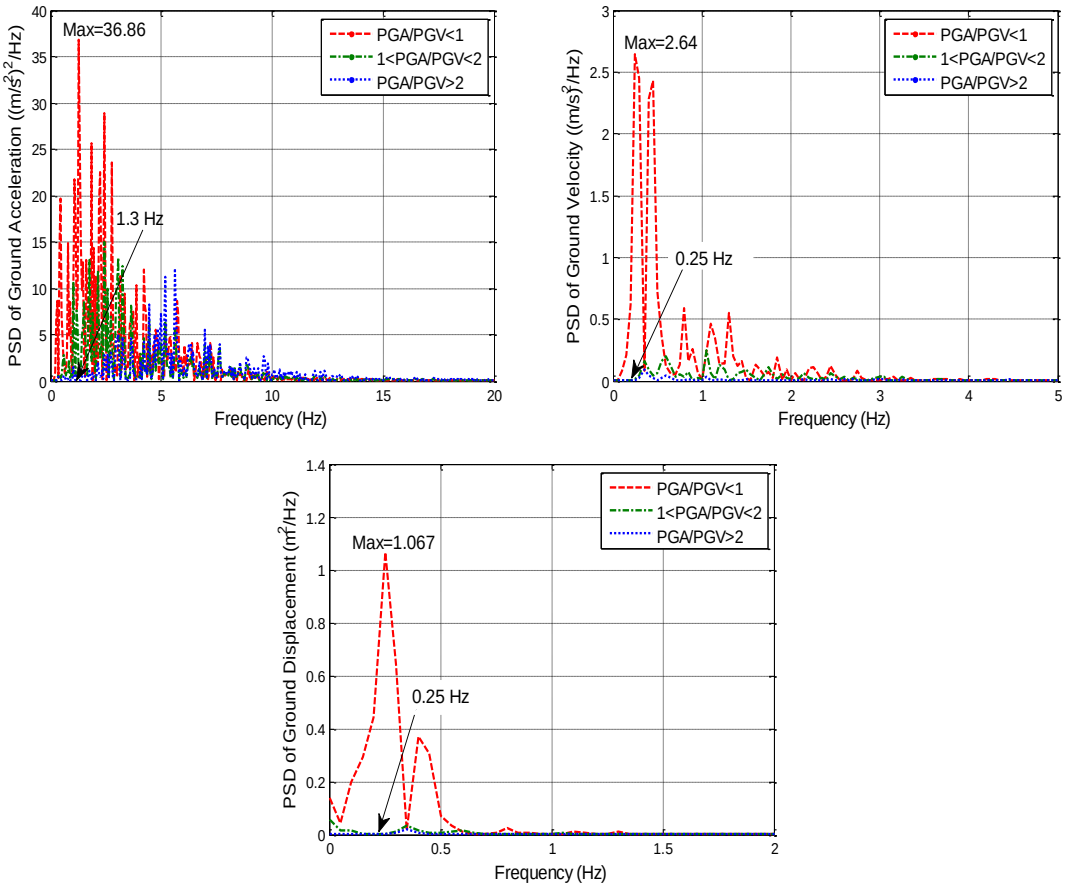

Figure 43: PSD (Power Spectral Density) of generated ground motions based on the target spectrum for each group

Because of space limitations, the plots illustrate the results related to the bearing of the base-isolated buildings (bearing displacement and acceleration) for 5-, 20- and 35-story buildings that are subjected to the generated artificial earthquakes (Figure 44 and Figure 45).

As can be observed from Figure 44 and Figure 45 and Table 12, peak bearing displacement and acceleration are mostly affected by the ground motions whose PGA/PGV <1, where the responses are increased. Moreover, in Table 12, it can be observed that for high-rise base-isolated buildings (20- and 35-story buildings), there are no significant changes between cases 1 (PGA/PGV<1) and 2 (1< PGA/PGV<2) for the peak acceleration of the bearing, while it is in the lowest intensity in case 3 (PGA/PGV>2). Table 12 illustrates the maximum absolute results for both bearing

displacement and acceleration when subjected to the generated ground motions, which are based on the median spectrum of the real ground motions. In Table 12, for the peak bearing displacement, it can be seen that there are considerable changes between the three cases, and as the ratio increases, displacement highly decreases. In addition, according to the accelerogram generated based on the target spectrum for each case of ground motions in Figure 42 (Power Spectral Density of the generated ground motions are also illustrated in Figure 43) and the PSD of bearing displacements achieved for these kinds of earthquakes (Figure 45), it can be concluded that as the ratio of PGA/PGV decreases, the bearing displacement sharply increases for 35-story base-isolated building in the case when PGA/PGV is smaller than 1 (Figure 45). An implication of this is the possibility that base-isolated high-rise buildings (i.e., 20-, 25-, 30- and 35-story) can be vulnerable to the ground motions when the ratio of PGA/PGV is smaller than 1. In addition, this vulnerability of the high-rise base-isolated building subjected to the ground motions whose PGA/PGV<1 is because of the inherent lower frequency in this kind of earthquakes. According to Figure 43, it can be observed that the maximum displacement and max velocity are happening when the frequency of the ground motions is about 0.25 Hz. As the fundamental period of the 35-story base-isolated building is calculated to be 4.16 s (Table 8) it can be seen that natural frequency of the ground motion match the natural frequency of the subjected 35-story base-isolated building ($\frac{1}{4.16s} = 0.24Hz$). Overall, it can be concluded that as the intensity of the ground motions whose PGA/PGV<1 is higher than the other group of the earthquakes and at the same time in these ground motions maximum responses (displacement and velocity) occurred at lower frequency, this condition is enough to be highly affected the very high-rise

base-isolated building (in this study 35-story). As it can be observed, responses (displacements) are sharply increased in 35-story base-isolated building (Figure 45).

Table 13 is also illustrating the maximum magnitude for three buildings subjected to the ground motions with PGA/PGV<1. It can be clearly seen that the magnitude for 35-story base-isolated building is highly increased when compared with 5-story base-isolated building (approximately two times higher).

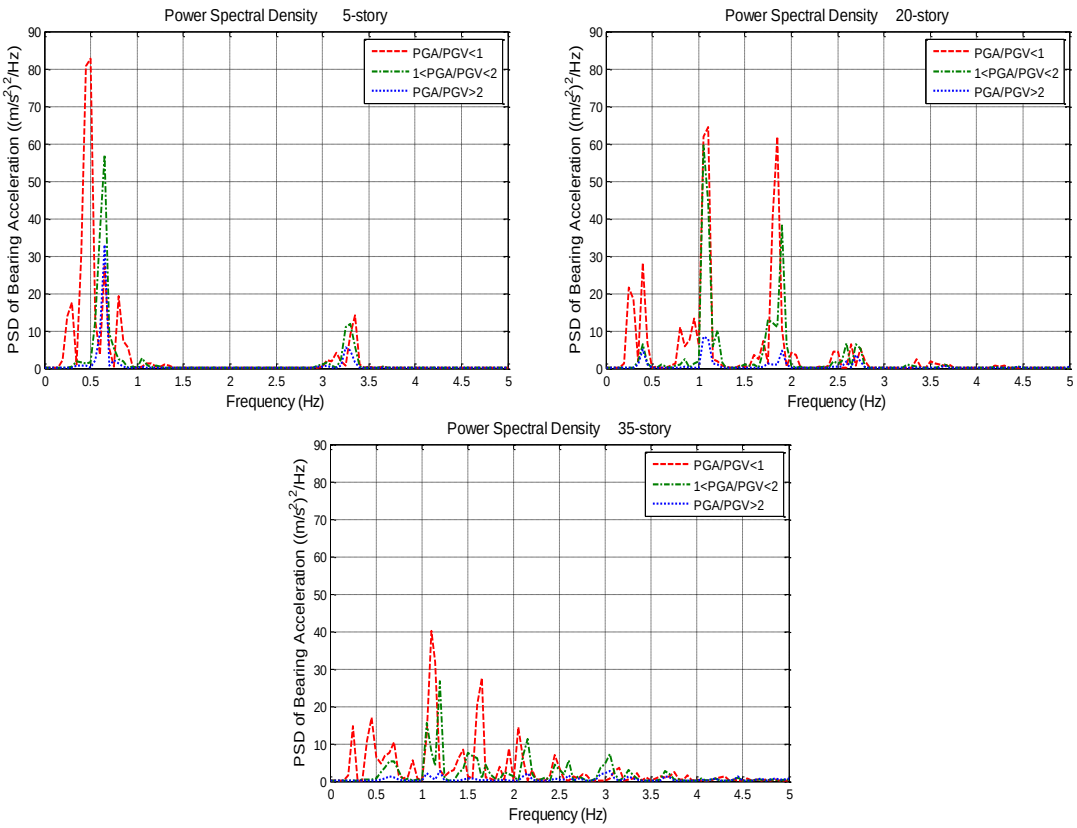

Figure 44: PSD (Power Spectral Density) of bearing acceleration

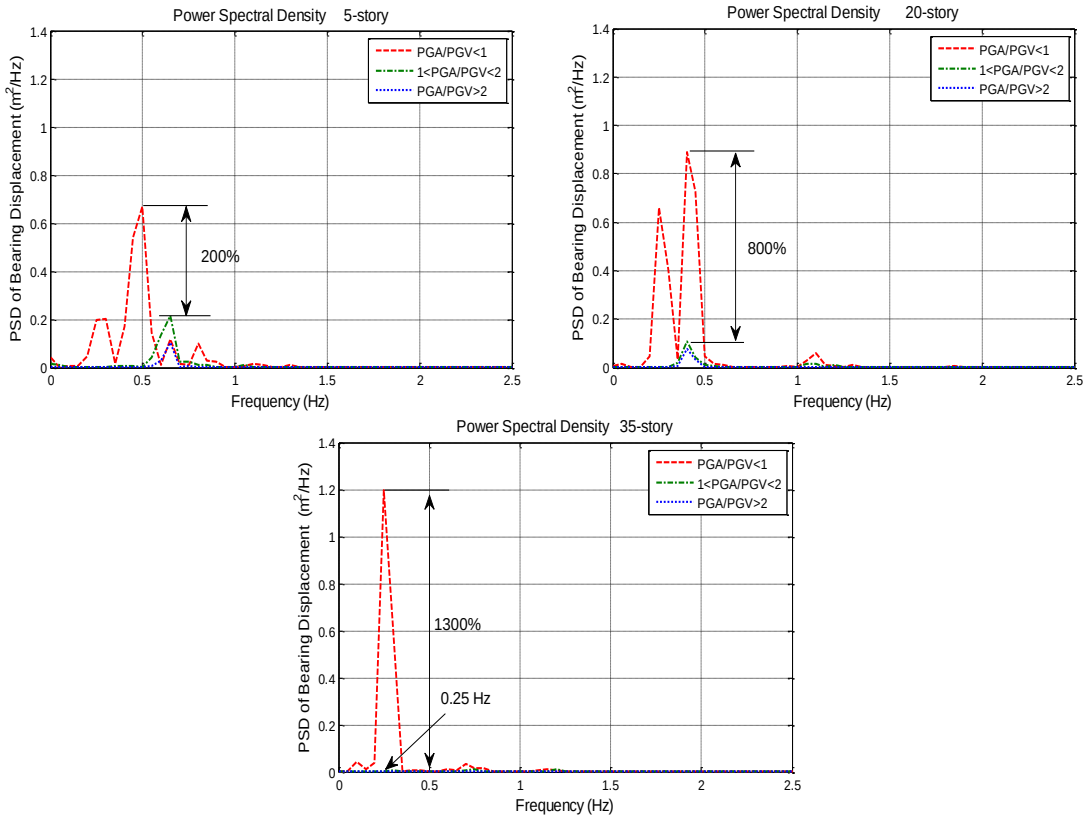

Figure 45: PSD (Power Spectral Density) of bearing Displacement

Table 12: Maximum bearing displacement and absolute acceleration results for generated ground motions based on the median spectrum of the real ground motions (time history results)

EQ Group	5-story		20-story		35-story	
(case)	Dis.	Abs. Acc.	Dis.	Abs. Acc.	Dis.	Abs. Acc.
1	0.112	1.319	0.0881	1.427	0.080	1.512
2	0.047	0.976	0.0385	1.439	0.020	1.315
3	0.024	0.706	0.0189	0.797	0.0078	0.747

Abs. Acc: Absolute Acceleration (m/s^2)
Dis: Displacement (m)

Table 13: Maximum Power Spectral Density of generated ground motions and bearing responses (Magnitude: Dis. (m^2/Hz), Acc. ($(m/s^2)^2/Hz$)) when PGA/PGV<1

	PSD of EQ		PSD of 5-story		PSD of 20-story		PSD of 35-story	
	Dis.	**Acc.**	Dis.	Acc.	Dis.	Acc.	Dis.	Acc.
Frequency (Hz)	**0.25**	**1.3**	0.5	0.5	0.4	1.1	0.25	1.1
Magnitude	**1.067**	**36.86**	0.67	82.72	0.89	64.4	1.2	40

6.9.4 Damage Limitation

6.9.4.1 Ground Motions Selection

According to Eurocode 8 [10], the ground motion at a given point on the surface is represented by the elastic response spectrum. The form of the elastic response spectrum is taken for the no-collapse, and the damage limitation requirement is illustrated schematically in Figure 46.

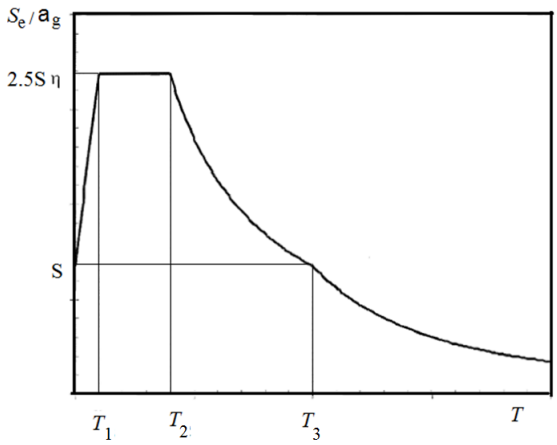

Figure 46: Form of the elastic response spectrum [10]

In Figure 46, "S_e" is the elastic response spectrum; "T" is the vibration period for a single degree of freedom structure; "a_g" is the design acceleration of the ground type A; "S" is the soil factor of the ground type A; "η" is the factor of damping correction (η equals 1 for 5% viscous damping); "T_1" and "T_2" are the lower and upper limits of the spectral acceleration branch, respectively; and "T_3" defines the beginning of the spectral acceleration.

By considering spectrum type 1 for ground type A, the reference peak ground acceleration for the case PGA/PGV<1 results in $a_{gR} = 0.3g$ (Figure 47). The form of the elastic response spectrum described by the value of soil factor (S) and the periods (T_1, T_2, T_3), result in T_1 = 0.15 s, T_2 = 0.4 s, T_3 = 2.0 s and S = 1 [10]. In the present

study, as the buildings are classified as importance class II, the corresponding importance factor is found to be $\gamma_1 = 1$ [72], (part 1, Table 4.3). Therefore, the peak ground acceleration equals the reference PGA, $a_g = \gamma_1 a_{gR}$. Using the equation in the code [10], the elastic response spectrum (ERS) can be shown for 5% damping, as in Figure 47. Figure 47 depicts that the mean response spectrum of the earthquakes for case 1 (PGA/PGV<1) and the elastic response spectrum, which is the damage limitation requirement stated in the code, are compatible.

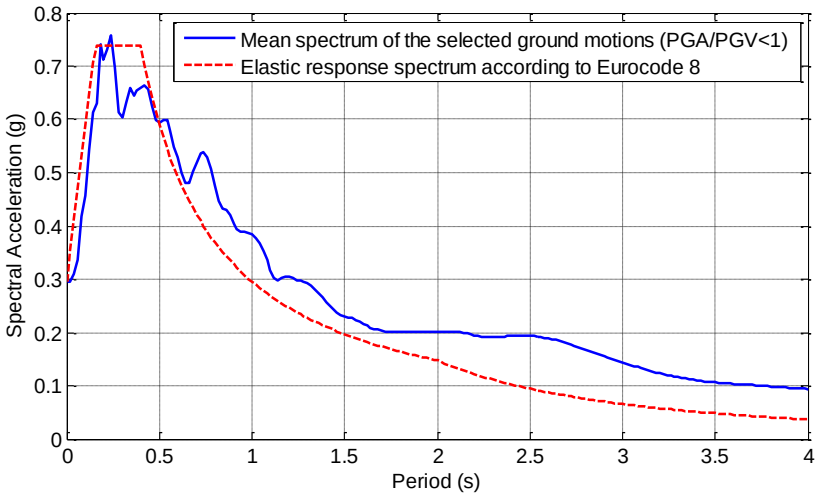

Figure 47: Mean response spectrum of the selected earthquakes (PGA/PGV<1) and elastic response spectrum according to Eurocode 8 for 5% damping

6.9.4.2 Drift Control

Accordingly, In this section, ground motions where ratio of PGA/PGV is smaller than one have been implemented to study the damage limitation of the buildings:

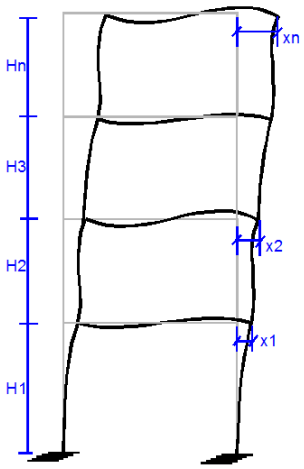

Figure 48: Story drift

As the drift equals the deflection at one level minus the deflection below that level, the requirement of damage limitation should be considered in terms of the inter-story drift (d_r) [10], as follows:

$$d_r \nu \leq \alpha h \rightarrow \frac{d_r}{h} \leq \frac{\alpha}{\nu} \tag{20}$$

The drift of a story (d_r) is assessed as the difference in the average lateral displacements in the center of the mass at the top and bottom of the story. The damage limitation is the requirement of the buildings at the upper limit on the inter-story drift ratio under seismic loading. The limit is set as [10]:

- if there are nonstructural elements in the building and forced to be stable under structural deformation, such as normal partitions ($\frac{d_r}{h} \leq \frac{0.005}{\nu}$)
- if there are nonstructural elements in the building that are ductile ($\frac{d_r}{h} \leq \frac{0.0075}{\nu}$)
- if there are no nonstructural elements in the buildings ($\frac{d_r}{h} \leq \frac{0.010}{\nu}$)

In Eq.(20), ν is the reduction factor (ν depends on the importance class of the buildings). The corresponding reduction factor ν equals 0.5. α is a factor that takes the nonstructural elements into consideration and their adjustment into the subject buildings, which equals 0.5, 0.75, and 1%[10].

Figure 49 illustrates the drifts for both base-isolated and fixed-base states. As it is clear, by increasing the number of stories, the effects of the base isolation system are reduced, but regarding the damage limitation requirement, it can be realized that by the existence of the base isolation system, especially for high-rise buildings, the structure is highly affected, which keeps the damage limitation requirement below 1%. The most severe drift limit ($\frac{\alpha}{\upsilon} = 0.01$, there are nonstructural elements in the building that are forced to be stable under structural deformation) is not exceeded in any story for base-isolated buildings, which causes the structure to remain within the elastic range. Additionally, story drifts are significantly decreased for base-isolated buildings, even for very high buildings.

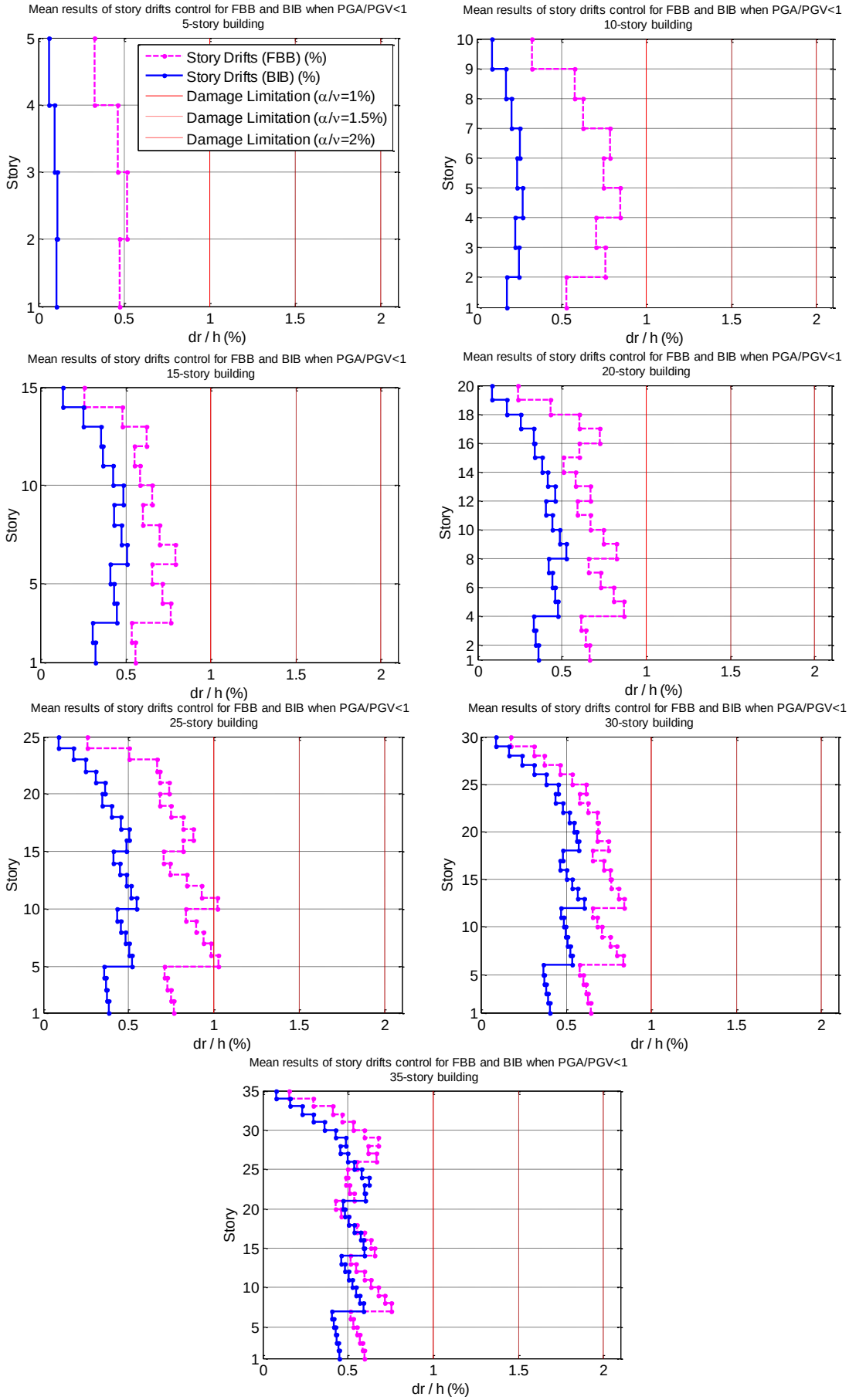

Figure 49: Story drift control for seven different isolated buildings

Chapter 7

EFFECTIVENESS OF FVD-BIS FOR PROTECTING BASE-ISOLATED BUILDINGS AGAINST RESONANCE

7.1 Introduction

After an extensive literature survey, no specific research was found in which the resonance phenomenon can be mitigated using a passive control system which is more economical than an active control system. Further, some may use a different type of passive control system, which is not either economical or easy to build. On the other hand, there are other investigations suggesting that FVD can improve the performance of the base-isolated buildings, but the impact of the supplementary damping system on the base-isolated buildings at the time of resonance phenomenon is not clear yet.

This investigation demonstrates the effectiveness of FVD-BIS for protecting the base-isolated high-rise and low-rise buildings against the resonance phenomenon under the near-field pulse period ground motions. In this regard, first, near-field earthquakes have been created synthetically to do *parametric study* in order to understand the behavior of the buildings. Therefore, an analytical model has been implemented for creating synthetic near-field earthquake records developed by He and Agrawal [15], with a specific pulse period adjusted to be close to the fundamental period of the base-isolated high-rise building. The goal is to represent the resonance phenomenon, and since the fundamental natural period of a structure is not affected by FVD, in this study LCRB system confined by FVD has been

considered which forms a model of Fluid Viscous Damper-Base Isolation System (FVD-BIS). The results revealed that the intensity of the resonance phenomenon is highly mitigated by implementing FVD-BIS in the base-isolated high-rise building.

Finally, in order to confirm the results achieved by artificially generated ground motions, several real pulse-like strong ground motions with different pulse periods have been conducted both for high-rise and low-rise buildings.

7.2 Structural Model

7.2.1 Evaluation of the Seismic Mass According to Eurocode 8

In this investigation, two idealized 20-story and 5-story base-isolated steel structures with six bays in each direction have been considered (Figure 50). The base-isolated buildings are symmetrical square buildings and have been modeled as a shear-type structure mounted on isolation systems with one lateral degree-of-freedom at each floor (Figure 51). The height of each story is 3.4 m; the total height of the 20-story frame is H = 68 m. The self-weight of each story including live load and dead load, where the live load is reduced with a factor of $\psi_{2i} = 0.3$ in a seismic design load case, was calculated to be $8000\ \frac{N}{m^2}$ (total load is defined as "DL+ψ_{2i}LL" in Eurocode 8)[72]. The plan dimensions of the building are 30 m by 30 m. The mass for each story has been calculated to be 720 tons. the details of the mass structure calculation are given in Table 14. The modeling and time history analyses of the benchmark seismically isolated buildings have been carried out using MATLAB considering the elastic shear-beam stick model [41].

Table 14: Details of mass calculation for each story

Total floor area for a single story	$30\ \text{m} \times 30\ \text{m} = 900\ \text{m}^2$
Story Dead load (Floor Dead load)	$650\frac{\text{kg}}{\text{m}^2} \times 900\ \text{m}^2 = 585000\frac{\text{kg}}{\text{story}}$
Other assumed mass	$53100\frac{\text{kg}}{story}$
ψ_{2i}LL where LL=$300\frac{kg}{m^2}$	$0.3 \times 300\frac{kg}{m^2} \times 900\ m^2 = 81000\frac{kg}{story}$
Seismic mass (DL+ψ_{2i}LL)	$719100\frac{\text{kg}}{\text{story}} \cong 720000\frac{\text{kg}}{\text{story}}$

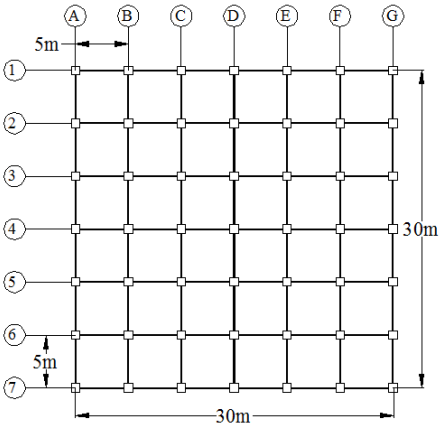

Figure 50: Dimensions of the case study building

7.2.2 Superstructure

Figure 51 demonstrates the case study buildings with one lateral Degree of Freedom (DOF) at each floor where all vibration modes are included in analysis. The Stiffness (k) of each story is taken in the proportions, as illustrated in Table 15. The value of story stiffness k_i can be calculated by providing the required fundamental period of a 20-story fixed base building as $T_s \cong 2$ s. In this study, according to Eurocode 8, the fundamental period of the superstructure has been defined as $T_s = C_t H^{3/4}$, where $C_t = 0.085$ for moment resistant of steel frame and H is the total height of the superstructure in meters [10]. Although there is a height limit on calculating the fundamental-period of a fixed base building, it has been used throughout this study without a limit. The modal damping ratio of the building has been kept unchanged for all modes (ξ_s) and set at 2% (Table 15). Further, the base mass has

been considered as the mass ratio, $\frac{m_b}{m} = 1$ (m_b is a rigid base mass which is connected to the isolators (Figure 51)).

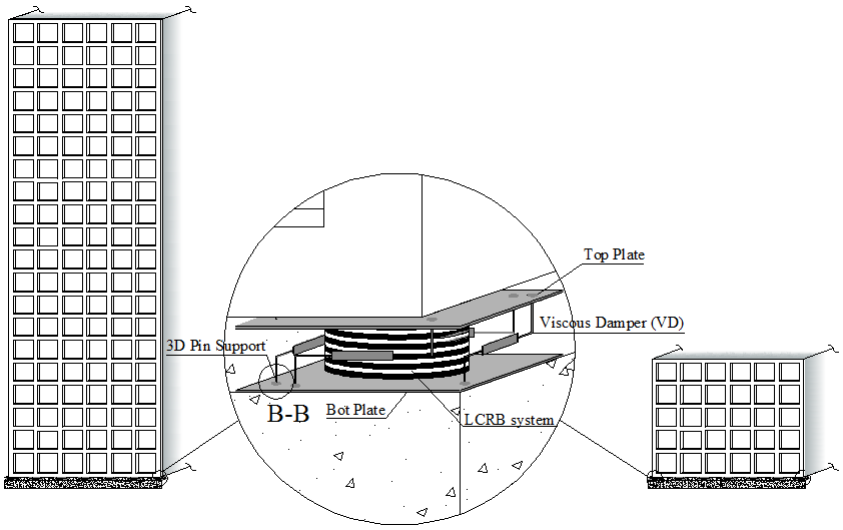

Figure 51: Schematic view of the base-isolated structures by FVD-BIS

Table 15: Stiffness proportion and mass properties of the buildings

Floor level	Mass (ton)	Stiffness proportion	Stiffness (k) (N/cm)	Damping ratio for steel structure (ξ_s)
20-story				
1-4	720	$k_1 = 1k$	1589×10^6	2 %
5-8	720	$k_2 = 0.8k$	1271×10^6	
9-12	720	$k_3 = 0.64k$	1017×10^6	
13-16	720	$k_4 = 0.51k$	814×10^6	
17-19	720	$k_5 = 0.41k$	651×10^6	
20	360	$k_5 = 0.41k$	651×10^6	
Total	14040	-	-	
5-story				
1	720	$k_1 = 1k$	1683×10^6	
2	720	$k_2 = 0.8k$	1346×10^6	
3	720	$k_3 = 0.64k$	1075×10^6	
4	720	$k_4 = 0.51k$	860×10^6	
5	360	$k_5 = 0.41k$	683×10^6	
Total	3240	-	-	

7.2.3 Evaluate the Effectiveness of the Factors "Pulse Periods" and "Multi-Story Base-Isolated Buildings With and Without FVD"

To research the effectiveness of the factors of the base-isolated buildings (the factors are shown in Table 16), a two-factor factorial design was conducted, considering the factors in Table 16 (pulse periods and low/high-rise base-isolated buildings). In Table 16, y_{abn} (i.e., y_{111}, y_{112}, …) is the result of the combination of a (T_P) and b (number of story) levels for nth ground motion. For each group of earthquakes (T_P), two different kinds of buildings (low-rise and high-rise) have been considered, and combinations thereof are generated. Thus, a total of 188 time history analyses were carried out. Then the results illustrated as an interaction plot between the 5-story and 20-story base-isolated buildings.

Table 16: Arrangement for two-factor factorial design

Factor		**Story**	
	Levels	**5 (with or without FVD)**	**20 (with or without FVD)**
Pulse period (T_P)	**0.5<Tp<3.5**	y_{111} y_{112} ⋮ y_{11n}	y_{121} y_{122} ⋮ y_{12n}
	3.5<Tp<6.5	y_{211} y_{212} ⋮ y_{21n}	y_{221} y_{222} ⋮ y_{22n}
	6.5<Tp	y_{311} y_{312} ⋮ y_{31n}	y_{321} y_{322} ⋮ y_{32n}

7.2.4 Fluid Viscous Damper (FVD) and Fluid Viscous Damper-Base Isolation System (FVD-BIS)

In recent years, viscous dampers, both linear and nonlinear, have become popular. The attraction of viscous dampers as energy dissipation devices can be attributed to both the relatively simple design formulas and procedures. Viscous dampers are a

kind of control system with resisting forces, proportional to the velocity [74]. The damping force of the viscous damper in a dynamic system is introduced by the following equation:

$$F_d = c_d v^{\alpha} \tag{21}$$

Where c_d represents the damping coefficient, which can be calculated according to Eq. (22), v shows the relative velocity at both ends of the damping device, and α is usually between 0.3 and 1. In this study, for more simplicity, α has been considered to be 1.

$$c_d = 2m_{td}\xi_d\omega_d \tag{22}$$

In Eq. (22), m_{td} is the total mass above the viscous damper, ξ_d ($\xi_d = 20\%$) represents the damping ratio, and ω_d ($\omega_d = \frac{2\pi}{T_{sBI}}$) denotes the natural frequency of the viscous damper.

Figure 52 illustrates the force-deformation behavior of the combination of Fluid Viscous Damper with Lead Core Rubber Bearing, which forms the Fluid Viscous Damper- Base Isolation System (FVD-BIS).

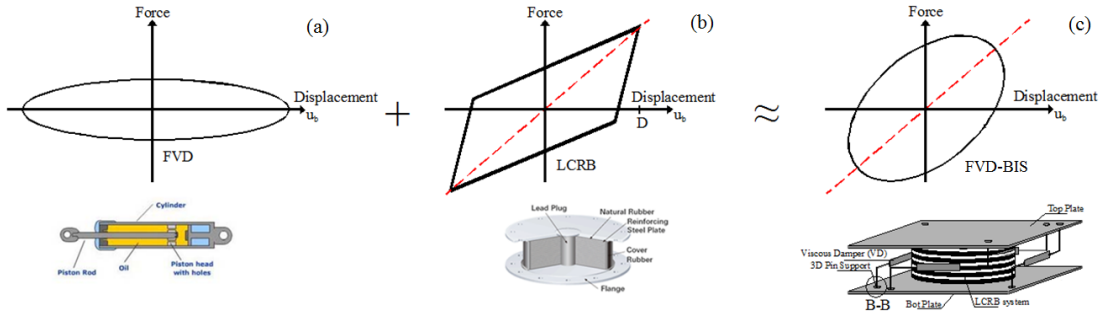

Figure 52: Schematic representations of force-deformation relations in (a) viscous damper, (b) Lead Core Rubber Bearing (Base isolation system), (c) Fluid Viscous Damper-Base isolation System (FVD-BIS)

7.2.5 LCRB Properties

In this part of the study, Equations (12) to (14) have been implemented to calculate the effective stiffness (k_{eff}) and damping coefficient (c_{eff}) of the isolation system. The isolation period of the system is kept to be as $T_b = 2.5\,s$ (the predominant period of the high-rise and low-rise base-isolated buildings are calculated to be 3.13s and 2.65, respectively). As increasing the damping ratio of the isolation system leads to elevated superstructure acceleration [53], the effective damping ratio of the isolator is considered to be $\beta_{eff} = 0.05$.

Moreover, Q, where the hysteresis loop intersects the y axis, is being calculated by the following equation:

$$Q = \frac{\beta_{eff} 2\pi k_{eff} D^2}{4(D - u_y)} \tag{23}$$

k_p is the post-yielding stiffness at base displacement D, which can be calculated as[11]:

$$k_p = k_{eff} - \frac{Q}{D} \tag{24}$$

7.3 Damping Ratio (ξ_i)

According to Table 17 the modal damping ratio (ξ_i) has been calculated by Eq. (25). The modal damping ratio of the fixed base building and that of the base-isolated building for both low-rise and high-rise buildings are given in Table 17 for the first five modes:

$$\xi_i = \frac{\emptyset_i^T C \emptyset_i}{2\omega_i \emptyset_i^T M \emptyset_i} \tag{25}$$

Table 17: Period of vibration and structural damping ratio ξ_i (Eq. (25)) for each mode of isolated buildings and non-isolated buildings

Mode	Period of vibration (s) T			Structural damping ratio (%) ξ_i		
	FB (s)	BI (s)	FVD-BIS (s)	FB (%)	BI (%)	FVD-BIS (%)
			20-story			
1	2.0	3.136	3.136	2	3.5	12.6
2	0.736	1.013	1.013	2	7.7	16
3	0.451	0.544	0.544	2.7	12.5	17.5
4	0.326	0.370	0.370	3.5	17.8	21
5	0.254	0.281	0.281	4.45	23	25.6
			5-story			
1	0.71	2.65	2.65	2	5	23.4
2	0.27	0.37	0.37	2	15	18.6
3	0.17	0.20	0.20	2.6	27	28.4
4	0.14	0.14	0.14	3.1	36	36.8
5	0.11	0.12	0.12	3.8	42	42.7

7.4 Near-Field Ground Motions

In this study, to do *parametrical* investigation on the performance of the seismically retrofitted building under near-field ground motions, an earthquake has been created synthetically in the near-field ground motion area, which typically involves the areas with 10 km distance or less from active faults. Nevertheless, the effects of a near-field earthquake can also be observed at greater distances from the faults.

7.4.1 Generating Near-Field Ground Motions

In artificially generated ground motions, the velocity pulse developed by He and Agrawal [15] is:

$$v(t) = se^{-\zeta_p \omega_p t} \sin\omega_p \sqrt{\left(1-\zeta_p{}^2\right)}t \tag{26}$$

The acceleration can be derived by differentiating velocity pulse in Eq. (26). Thus, it can be written as:

$$a(t) = se^{-\zeta_p \omega_p t}\left[-\zeta_p \omega_p \sin\omega_p \sqrt{\left(1-\zeta_p{}^2\right)}t + \omega_p \sqrt{\left(1-\zeta_p{}^2\right)}\cos\omega_p \sqrt{\left(1-\zeta_p{}^2\right)}t\right] \tag{27}$$

Where, s is the initial amplitude of the pulse (Eq.(28)), ζ_p reflects the pulse damping factor, and ω_p represents the frequency of the sinusoid, where T_p is the pulse period in Eq.(29) [75].

$$s = v_p \Big/ \left(e^{-\zeta_p \omega_p t_p} \sin\omega_p \sqrt{(1-\zeta_p{}^2)}\, t_p \right) \tag{28}$$

$$\omega_p = 2\pi \Big/ \left(T_p \sqrt{(1-\zeta_p{}^2)} \right) \tag{29}$$

t_p can be calculated by equating Eq. (27) to zero and solving it for t:

$$t_p = \tan^{-1}\left(\sqrt{\frac{1}{\zeta_p{}^2} - 1} \right) \Big/ \omega_p \sqrt{(1-\zeta_p{}^2)} \tag{30}$$

For the synthetic near-field earthquakes, the earthquakes presented by Dicleli and Buddaram [76], with various fault-distances (FD) and magnitudes (M_w), have been adopted. In this regard, Eqs. (26)-(28) are used together with Eqs. (31) and (32) [77], which offer the peak ground velocity (v_p) and the pulse period (T_p) for a given r and M_w:

$$\ln(v_p) = -2.31 + 1.15M_w - 0.5\ln(FD) \tag{31}$$

$$\log_{10}(T_p) = -2.5 + 0.425M_w \tag{32}$$

The following results (Figure 53) illustrate the validation of the synthetically generated earthquake with the results in reference [16].

The pulse periods (T_p) of the near-field ground motions are generally long. It can be seen that most of the earthquakes presented in the study of He and Agrawal [15] vary from 1 s to 5.8 s. In this study, an earthquake has been generated synthetically with fault distances of FD = 10 km and pulse damping factor of ξ_p = 3% (Figure 54). The pulse period of the generated earthquake is considered to be $T_p = 3$ s, which is equal to the fundamental period of the base-isolated superstructure. This allows observing the resonance occurring during the motion. Also, the generated earthquake

has been defined at a time step of $\Delta t = 0.02s$ (Figure 54). Figure 55 depicts the velocity spectra for synthetic near-field ground motion with 5% damping.

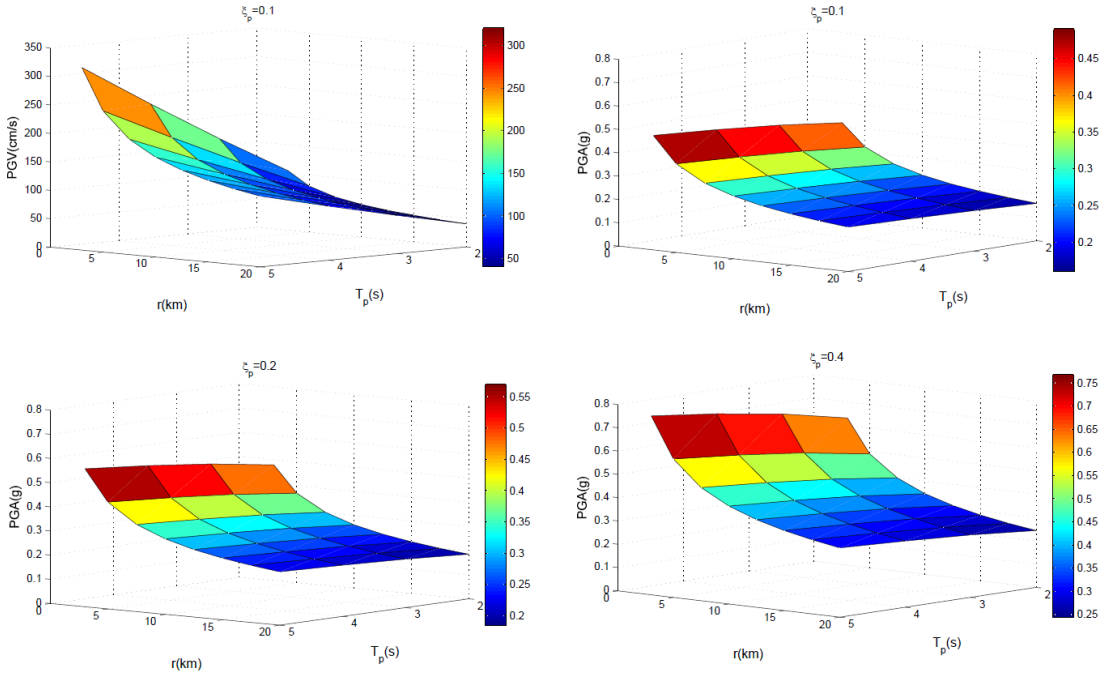

Figure 53: PGV and PGA of synthetic earthquake records generated in this study at different fault distances

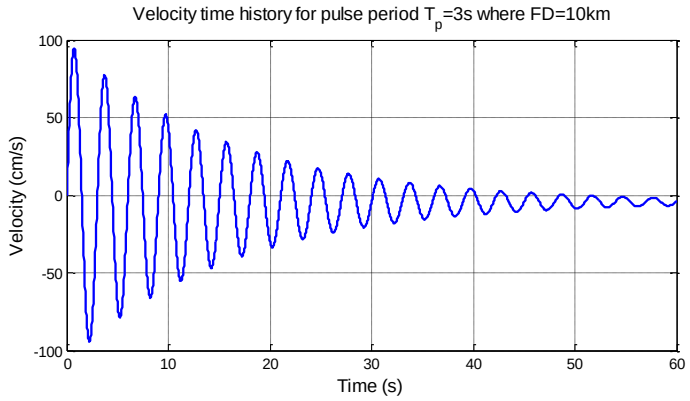

Figure 54: Velocity time history of the generated ground motion ($T_p = 3$ s, $\xi_p = 3\%$, and $\Delta t = 0.02$ s)

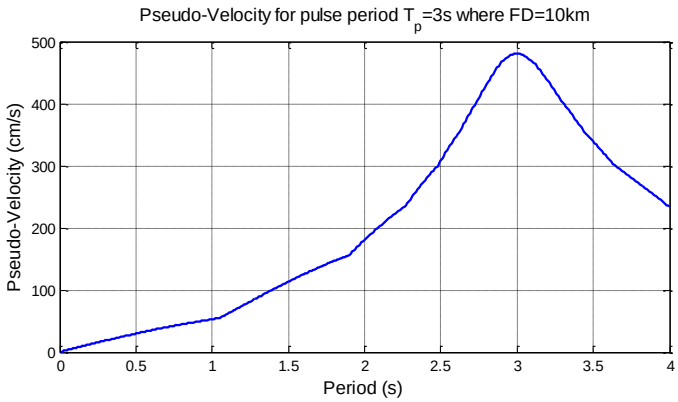

Figure 55: Pseudo-Velocity response spectrum of synthetic near-field ground motion with 5% damping

7.4.2 Pulse-Like Ground Motions Evaluation

For further investigation, the selected pulse-like ground motions have been evaluated for the pulse periods (with ranges lying between 0.5 s and 13.5 s) and the ratios of PGA/PGV and PGV/PGD. Table 18 briefly presents the group of the selected natural ground motions which are illustrated in Table 4 for three different pulse period ranges (0.5 s $< T_p <$ 3.5 s, 3.5 s $< T_p <$ 6.5 s, and 6.5 s $< T_p$). By implementing one-way ANOVA, significant differences between the specified groups have been defined in Figure 56. As can be observed from Figure 56(a), the ratio of PGA/PGV for all selected pulse-like ground motions are lower than 10 in the unit of 1/s or lower than 1 in the unit of g/m/s. Figure 56 also indicates that the ratios of PGA/PGV and PGV/PGD have a descending trend as the pulse period of the ground motions increases.

Table 18: Group of Pulse-like ground motions categorized for three different ranges of pulse periods (According to Table 4 in chapter 5)

	0.5<Tp<3.5	**3.5<Tp<6.5**	**Tp>6.5**
EQ No.	1 to 36	37 to 64	65 to 94

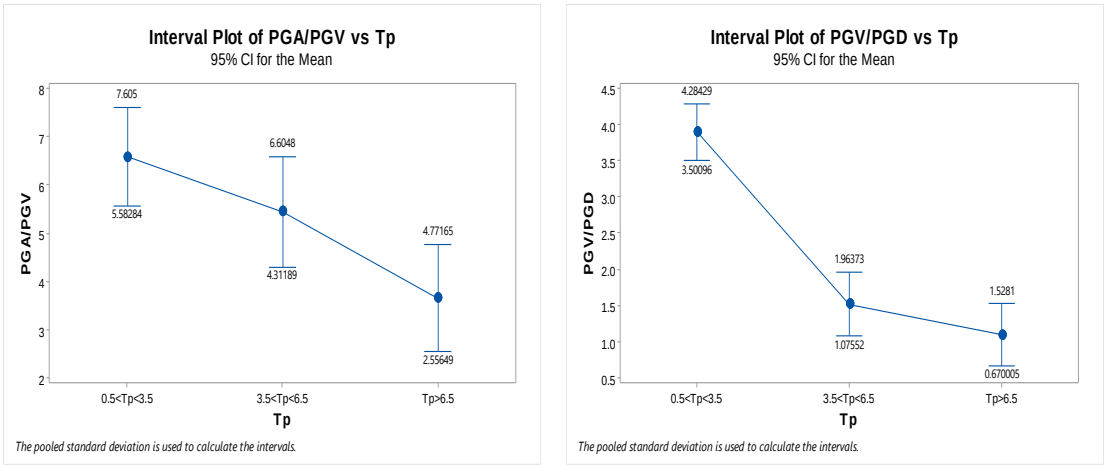

(a) (b)

Figure 56: Interval plot of PGA/PGV and PGV/PGD ratio vs. pulse period of the ground motions (PGA/PGV and PGV/PGD are in the unit of 1/s)

Also, Figure 57 and Figure 58 demonstrate the pseudo-velocity and pseudo-acceleration for each group of ground motions (0.5 s < T_p<3.5 s, 3.5 s < T_p< 6.5 s, and 6.5 s < T_p), respectively. For ease of understanding, the mean of each group has been portrayed and plotted together in Figure 57d and Figure 58d.

Based on Figure 57 and Figure 58, representing the pseudo-velocity and pseudo-acceleration, respectively, the ground motions whose pulse period is between 0.5 and 3.5 have had the greatest response. However, after the peak response, this group of ground motions (0.5 s < T_p< 3.5 s) gradually diminishes by increasing the period, and intersects the mean group of the ground motions 3.5 s < T_p< 6.5 s and 6.5 s < T_p at 2.56 s and 3.28 s, respectively. According to Figure 57, it can be seen that for both groups of ground motions, 3.5 s < T_p<6.5 s and 6.5 s < T_p, pseudo-velocity gradually grows as the period increases. However, for the ground motions with pulse period between 0.5 s and 3.5s, it can be observed that pseudo-velocity drops approximately after the period of 2 s and intersects the ground motions whose pulse period is between 3.5 s and 6.5 s at the period of 2.56 s. This trend continues until intersecting the ground motions whose pulse period is greater than 6.5 s at the period of 3.28 s.

Further, Figure 58 also indicates the same behavior for pseudo-acceleration of the ground motions. Indeed, it shows that, for both groups of ground motions, 3.5 s $< T_p <$ 6.5 s and 6.5 s $< T_p$, pseudo-acceleration gradually falls as the period grows and approximately remains constant after the period of 2.56 s. However, for the ground motions whose pulse period is between 0.5 s and 3.5s, the intensity of the ground motion is continually diminishing and intersects the ground motions whose pulse period is between 3.5 s and 6.5 s at the period of 2.56 s. It also intersects the ground motions whose pulse period is beyond 6.5 s at the period of 3.28 s. Accordingly, as the fundamental period of base-isolated high-rise building increases by implementing the base isolation system (in this study, the fundamental period of the base-isolated high-rise building has been calculated as 3.13 s), it can be seen that the studied base-isolated high-rise building will be affected by the ground motions whose pulse periods are between 3.5 s and 6.5 s. It can be concluded that the base-isolated high-rise buildings whose fundamental period is usually between 2.5 s and 5 s will be highly affected when subjected to the ground motions with a period (T_p) between 3.5 s and 6.5 s.

The above point stands out clearly in Figure 62. In this figure, the bearing and the roof displacement for the base-isolated high-rise building grows dramatically when subjected to the group of the ground motions whose pulse period is between 3.5 s and 6.5 s compared to the two other ground motions. As a result, in this study for the tested base-isolated high-rise building (the fundamental period is 3.13 s), resonance phenomena are mostly observed for the ground motions whose pulse periods are lying between 3.5 s and 6.5 s.

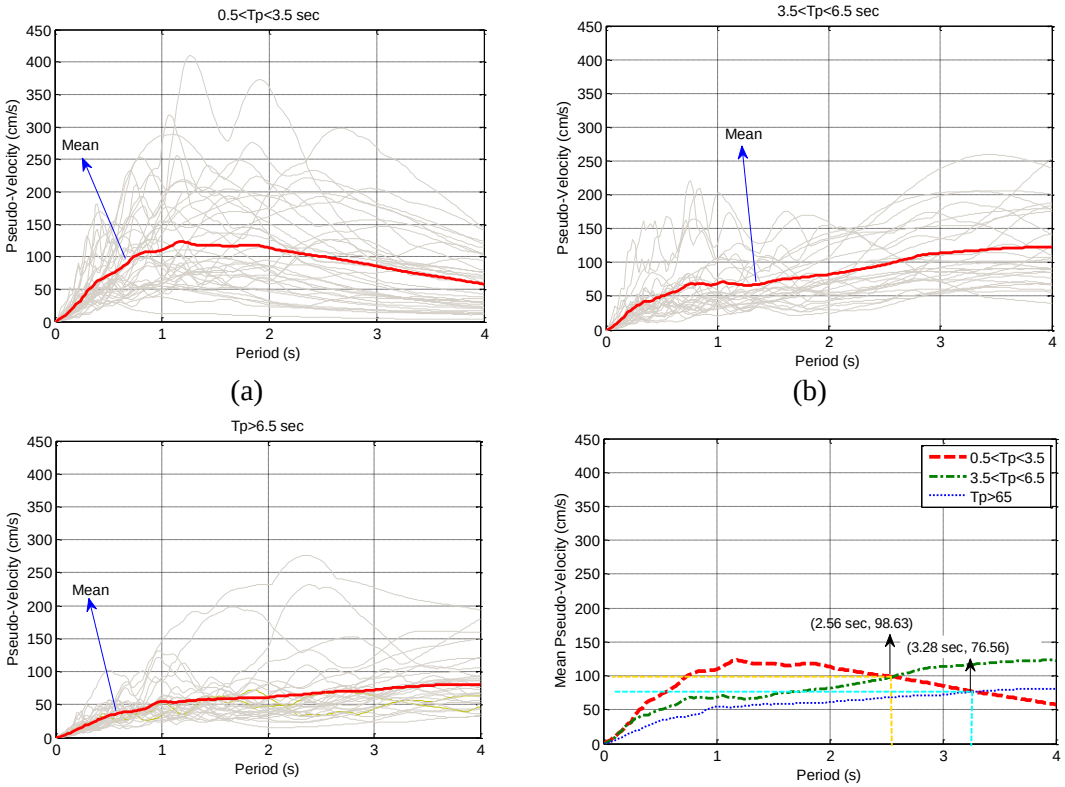

Figure 57: Pseudo-velocity for the selected strong ground motions, d) Mean of each group

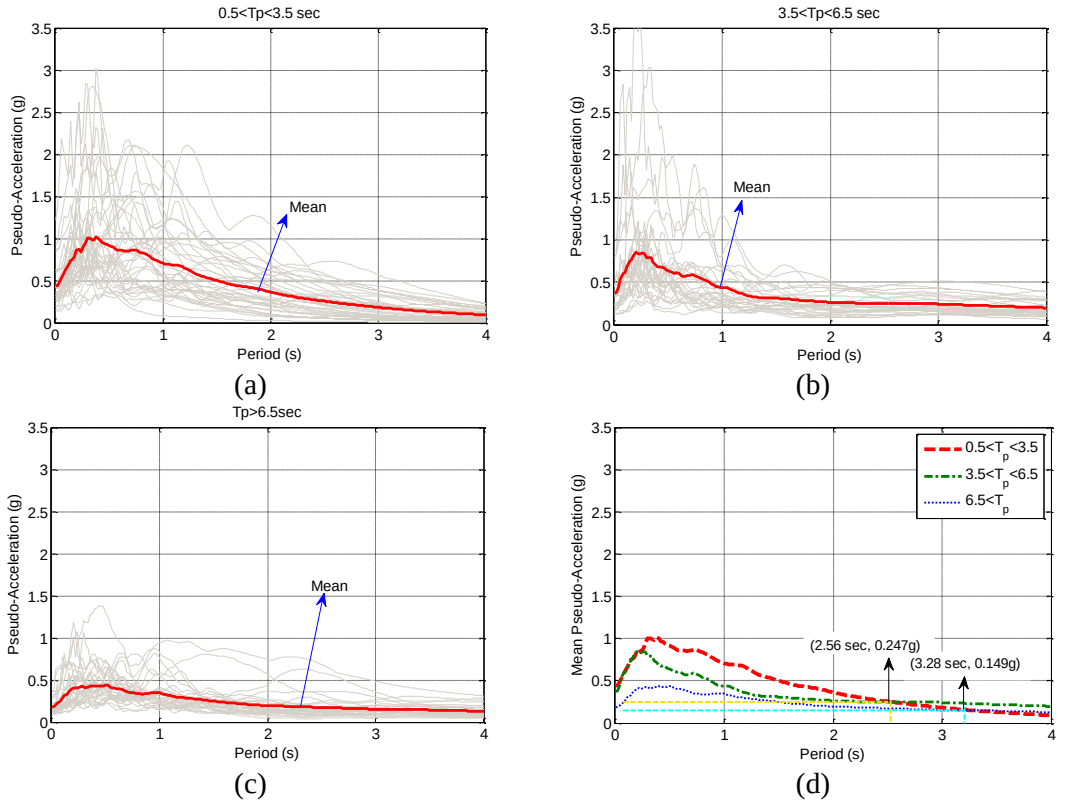

Figure 58: Pseudo-Acceleration for the selected strong ground motions, d) Mean of each group

7.5 Results and Discussion

To investigate the response of multistory base-isolated buildings subjected to different pulse period ground motions with different components, a computer program was developed. The analysis results are discussed in the following sections.

7.5.1 Results with Synthetic Ground Motion

In this section, because of the high vulnerability of the base-isolated high-rise building, 20-story base-isolated building has been chosen to examine the behavior of the building at resonance. For this reason, synthetically generated earthquakes were applied to the 20-story base-isolated building. The isolator period has been calculated as to be $T_b = 2.5$ s, for a 20-story LCRB base-isolated building, and its fundamental period has been calculated as $T_{sBI} = 3.13$ s. For observation of the effects of resonance, the pulse period of the artificially generated earthquake has been adjusted to be equal to the fundamental period of the base-isolated high-rise building ($T_p = T_{sBI} = 3.13$ s). With the above condition in mind, it can be observed from Figure 59 that the intensity of the ground motions was increased by about 95%.

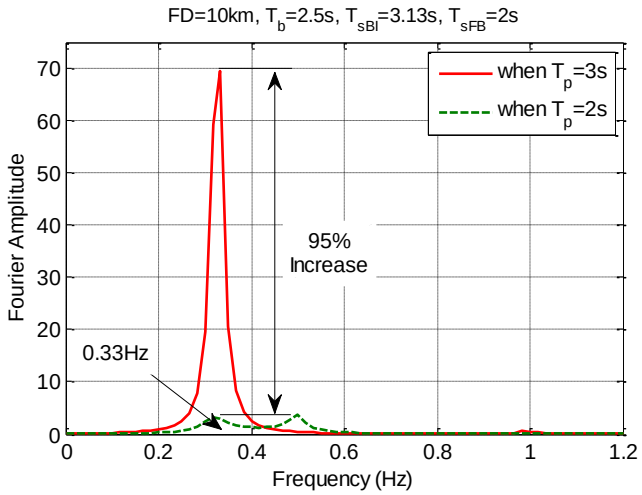

Figure 59: Fourier Amplitude of the bearing for the base-isolated high-rise building

To represents the effectiveness of the FVD-BIS at the time of resonance, the following figures (Figure 60 and Figure 61) illustrate the amplitude of bearing and roof time history displacement of the high-rise base-isolated building for the case when the fault distance is considered to be 10km. As can be observed from Figure 60, by implementing FVD-BIS, the bearing amplitude is significantly reduced by about 57%, suggesting the effectiveness of the FVD-BIS at the time of resonance. Note that, because of space limitation, only time history displacement of the roof has been illustrated for the conventional building, base-isolated building with LCRB, and the building retrofitted by FVD-BIS for the case when the fault distance is FD=10km (Figure 61). It can be seen from Figure 61 that when the pulse period of the ground motion matches the fundamental period of the conventional base-isolated building (resonance phenomenon), roof displacement grows considerably, while it has been significantly reduced by implementing FVD-BIS.

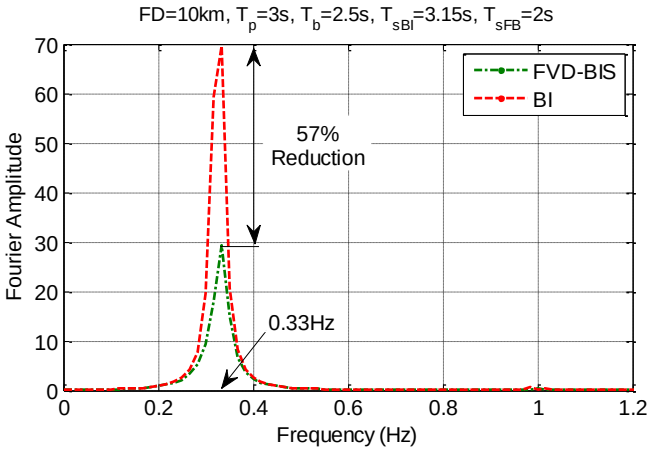

Figure 60: Reduction of the amplitude of the bearing at the time of resonance when FVD-BIS is used

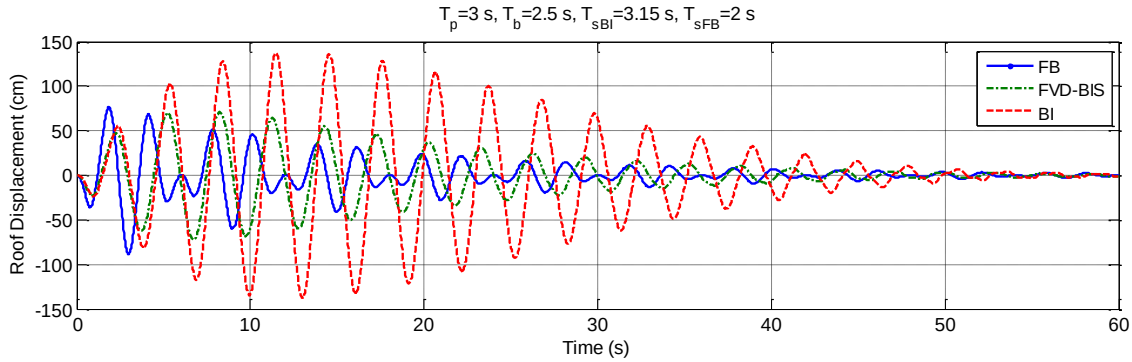

Figure 61: Time history response for roof

7.5.2 Results with Natural Ground Motions

According to the previous section, it has been demonstrated that when the pulse period of the natural ground motion is close to the fundamental period of the base-isolated building, resonance could occur and amplify the responses.

Figure 62 reveals the statistical analysis results for 94 selected pulse-like ground motions for three different groups (0.5 s < T_p< 3.5 s, 3.5 s < T_p< 6.5 s, and 6.5 s < T_p). Based on Figure 62, the maximum response occurred for the 20-story base-isolated building when the pulse period ground motions lied within the range of 3.5 s and 6.5 s (Figure 62a). In this interval, it is even higher than the median responses. And this amount has been significantly decreased when FVD-BIS has been implemented (Figure 62b). Moreover, Figure 63 depicts the responses for 5-story base-isolated building, it shows that maximum responses (responses of bearing and roof) occurred when 0.5 s < T_p < 3.5 s and 3.5 s < T_p < 6.5 s for the building which is merely isolated by LCRB system (Figure 63a), but these responses are also highly reduced when FVD-BIS has been used.

20-story

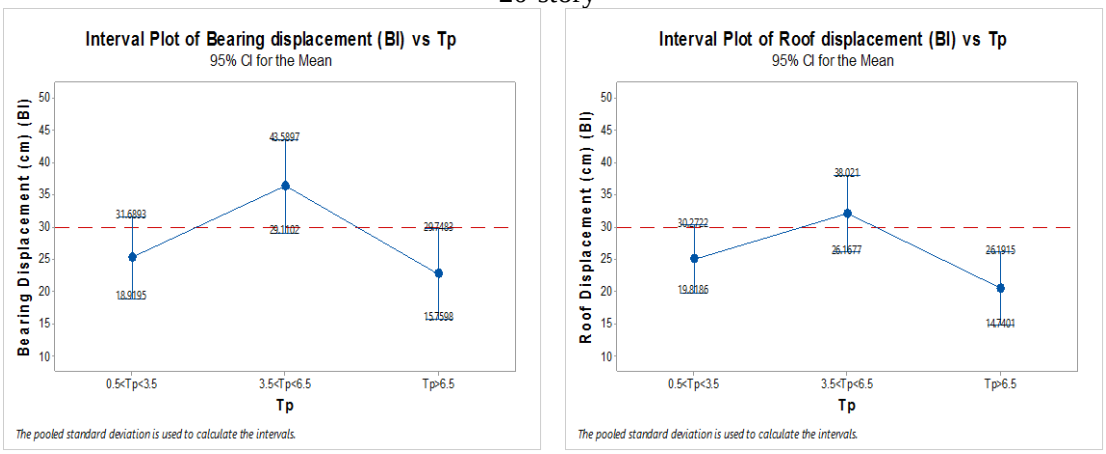

(a)

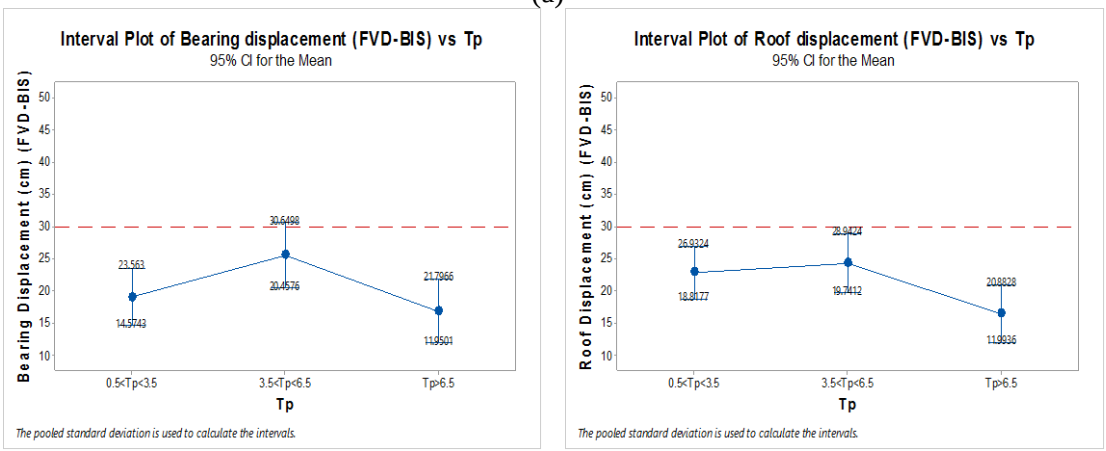

(b)

Figure 62: Interval plot of bearing and roof displacement of the base-isolated high-rise building both for LCRB and FVD-BIS (*20-story*)

5-story

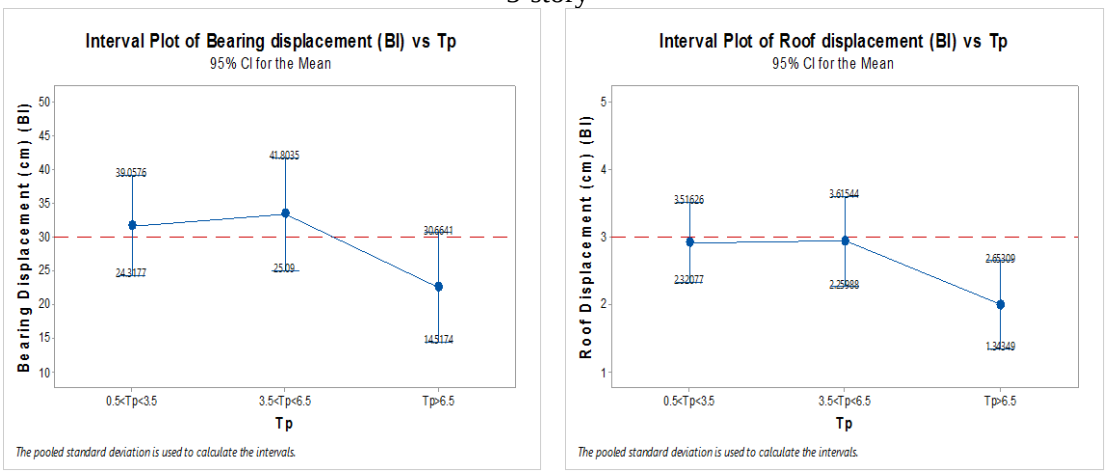

(a)

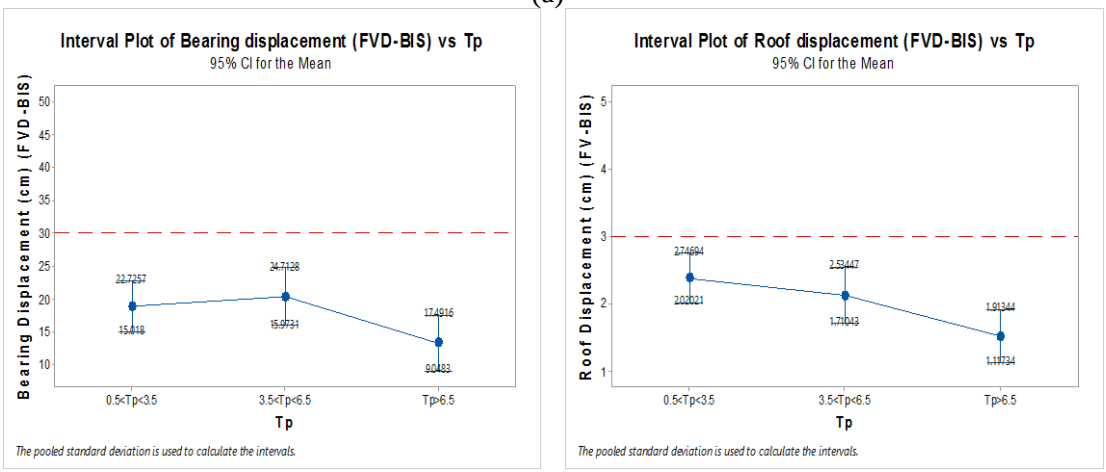

(b)

Figure 63: Interval plot of bearing and roof displacement of the base-isolated high-rise building both for LCRB and FVD-BIS (*5-story*)

For the sake of brevity, limited number of figures (Figure 64 - Figure 66) has been illustrated for the responses induced by strong pulse-like ground motions with a pulse period close to the fundamental period of the tested isolated building ($T_{sBI} \cong T_p$). The figures mentioned above clearly show that by providing the required condition ($T_{sBI} \cong T_p$), the roof and bearing displacement of the conventionally base-isolated building grows dramatically (Figure 64 to Figure 66 in frames a, b, c, and d). Figure 64d, Figure 65d, and Figure 66d reveal that at the time of resonance phenomenon by implementing FVD-BIS, the resonance phenomenon is considerably mitigated and the amplitude of bearing diminishes by more than 60%.

According to the Eurocode 8 [10], Figure 64e, Figure 65e, and Figure 66e illustrate that the damage limitation is increased for the conventional base-isolated high-rise building up to 1.5%. On the other hand, this value is lower in the building isolated by FVD-BIS; it keeps the damage limitation to approximately 1% or lower. This suggests that nonstructural elements are stable under structural deformation such as partitions [10] in the base-isolated high-rise building at the time of resonance. In addition, Figure 64f, Figure 65f, and Figure 66f compare the results obtained from the lateral displacement of the base-isolated high-rise building (either with LCRB and FVD-BIS) and the conventional fixed base building. Yet, it can be seen that lateral displacement increased significantly for conventionally base-isolated high-rise buildings (base isolated by LCRB) which is even greater than the fixed base building responses (Figure 64, Figure 65). Overall, it can be concluded that although the buildings have been retrofitted by LCRB systems to withstand the strong ground motions, the aforementioned figures clearly indicate that the results can be unexpectedly higher. Further, due to the resonance phenomenon, the responses of the base-isolated high-rise building with LCRB can be considerably amplified and may cause the studied building to collapse under such pulse-like ground motions.

T_p=3.773s, T_b=2.5s, T_{sBI}=3.14s, T_{sFB}=2s (RSN181)

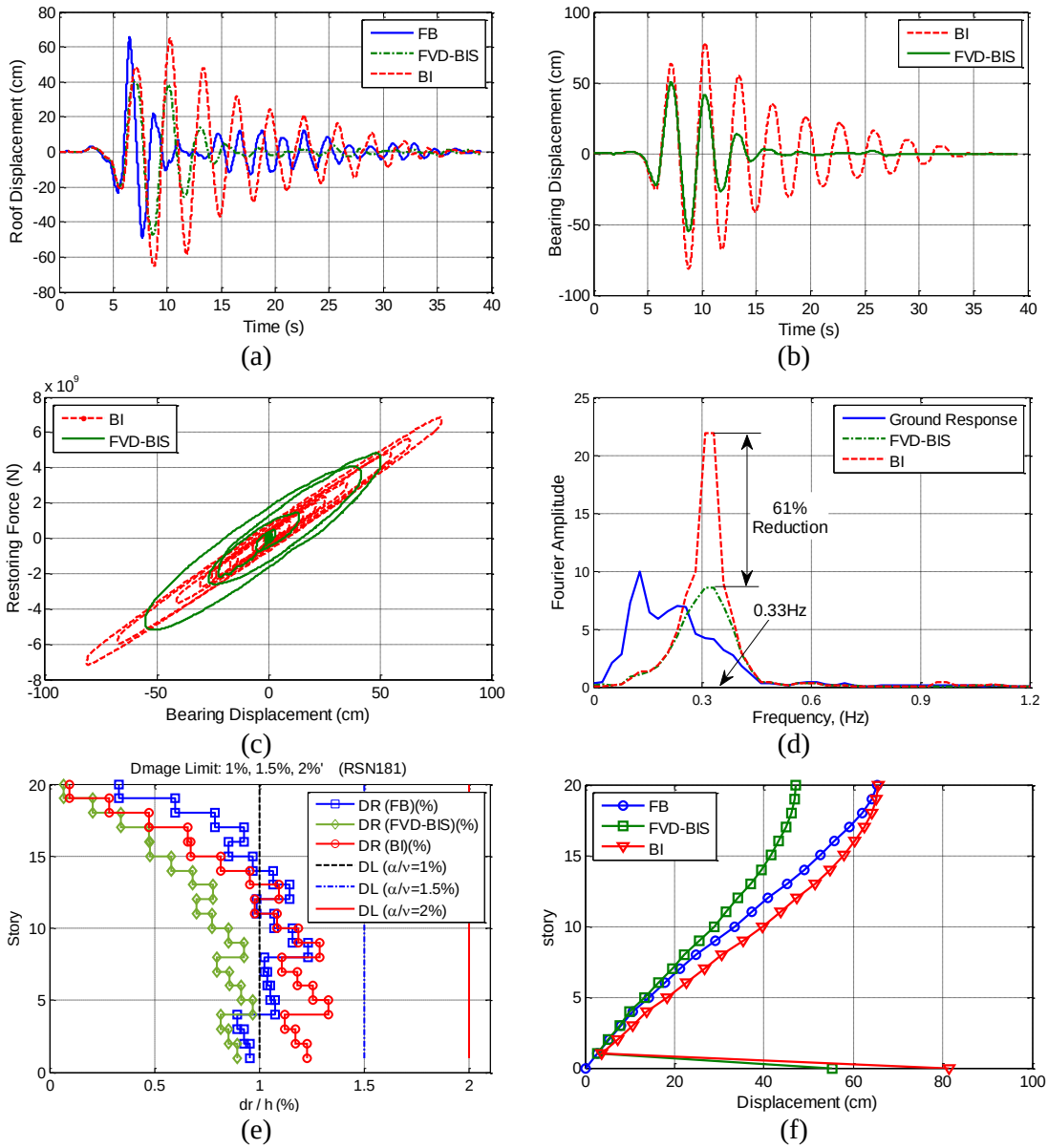

Figure 64: Responses for the tested building when $T_p = 3.773$ s and $T_{sBI} = 3.13$ s for real earthquake (RSN181): a) Time history displacement for the roof, b) Time history displacement for bearing, c) Force-deformation behavior of bearing, d) Frequency domain vs. amplitude of bearing, e) Damage ration control, f) Absolute maximum lateral relative displacement for each story

T_p=5.341s, T_b=2.5s, T_{sBI}=3.14s, T_{sFB}=2.0008s (RSN1244)

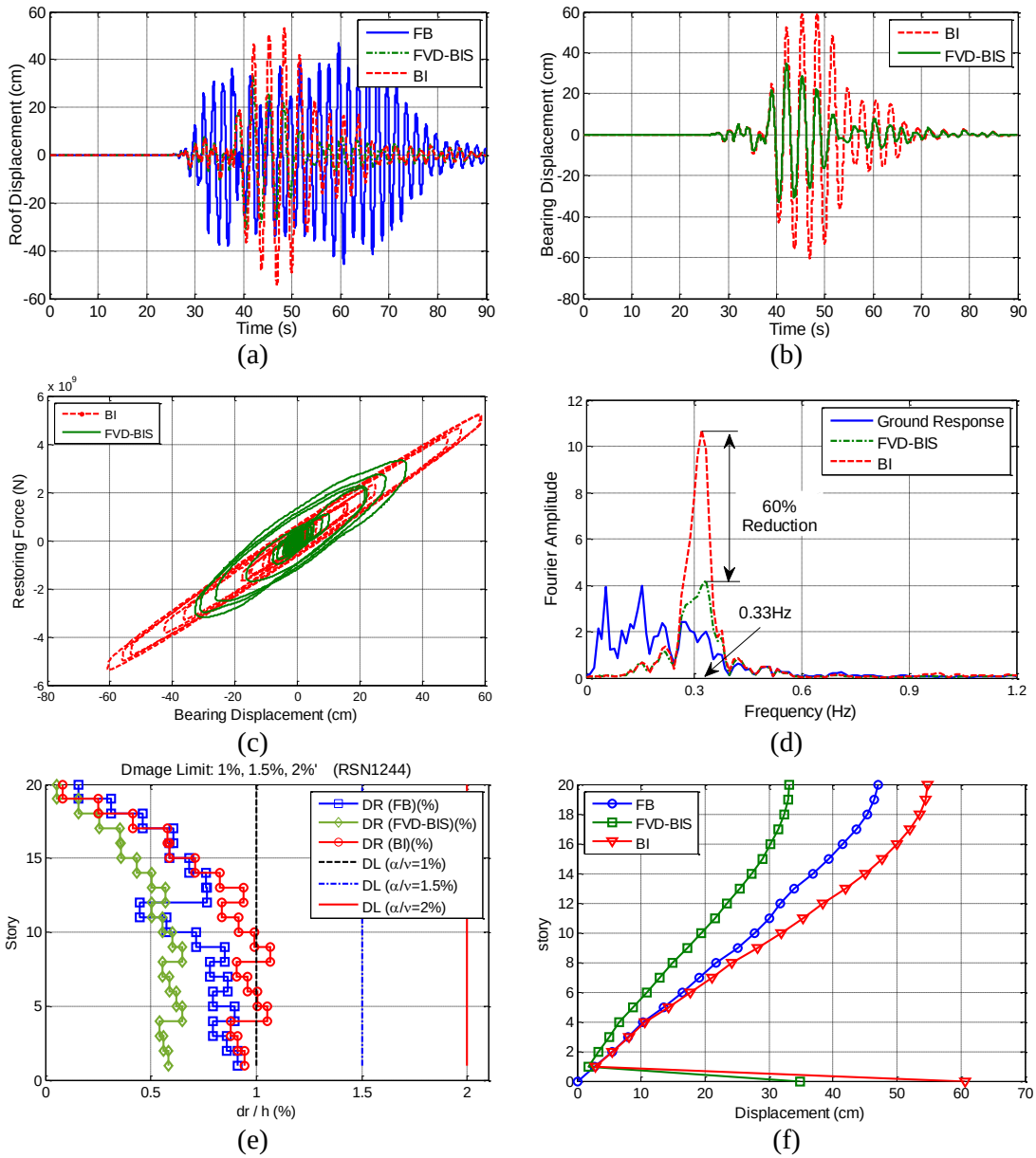

Figure 65: Responses for the tested building when $T_p = 5.341$ s and $T_{sBI} = 3.13$ s for recorded earthquake (RSN1244): a) Time history displacement for the roof, b) Time history displacement for bearing, c) Force-deformation behavior of bearing, d) Frequency domain vs. amplitude of bearing, e) Damage ration control, f) Absolute maximum lateral relative displacement for each story

T_p=2.982s, T_b=2.5s, T_{sBI}=3.14s, T_{sFB}=2s (RSN1084)

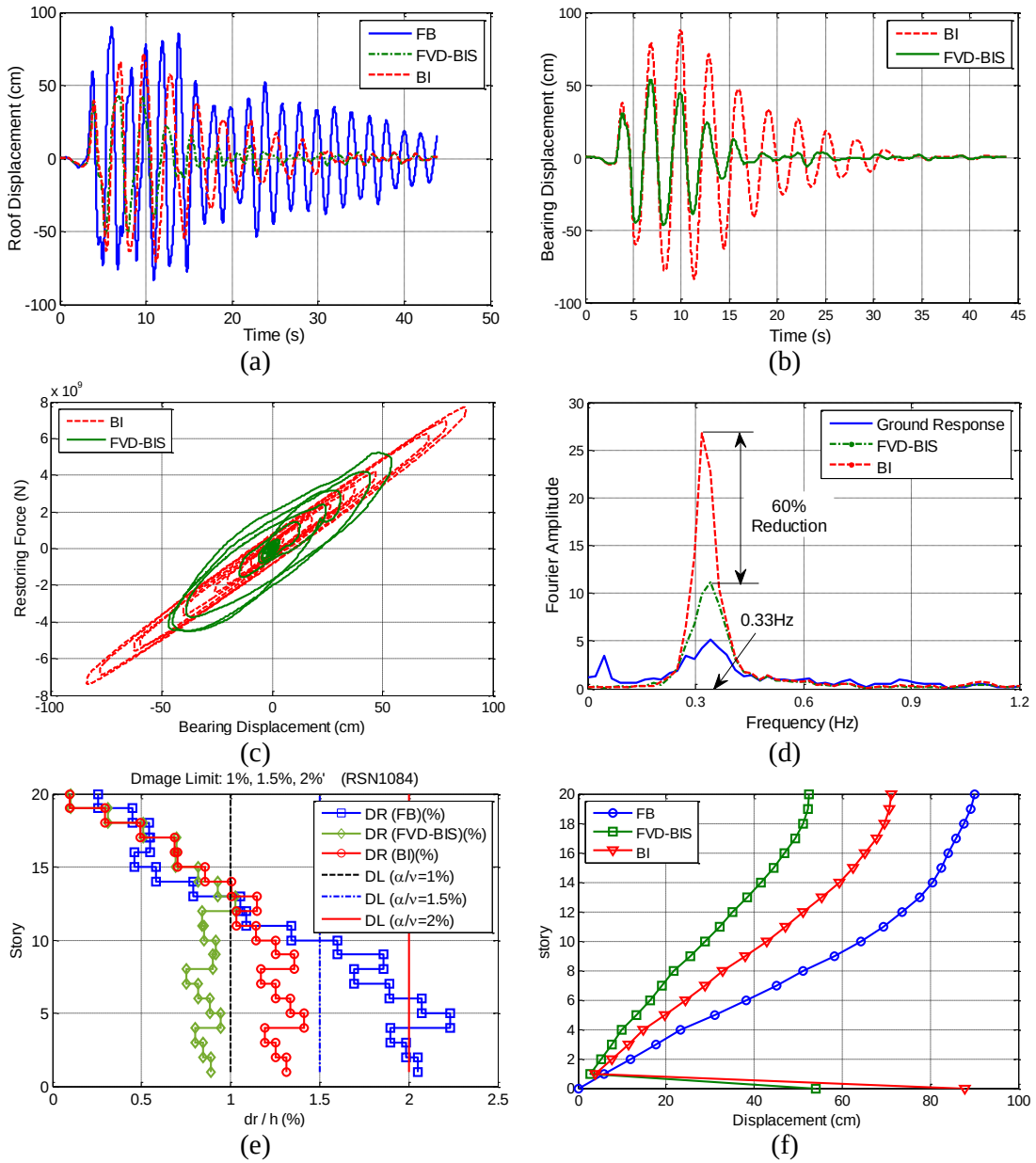

Figure 66: Responses for the building when $T_p = 2.98$ s and $T_{sBI} = 3.13$ s for recorded earthquake (RSN1084): a) Time history displacement for the roof, b) Time history displacement for bearing, c) Force-deformation behavior of bearing, d) Frequency domain vs. amplitude of bearing, e) Damage ration control, f) Absolute maximum lateral relative displacement for each story

Using Minitab software (version 2017), ANOVA (Analysis of Variance) method has been implemented for the responses of 94 selected ground motions and interaction plot illustrated in Figure 67. Based on Figure 67, it can be observed that for 20-story base-isolated building the resonance phenomenon is highly induced

(response is highly increased) for the ground motions whose pulse period (T_p) is between 3.5s and 6.5s, and for 5-story base-isolated building when the pulse period is within 0.5 s < T_p < 3.5 s and 3.5 s < T_p < 6.5 s. Then, the amplitude of bearing is considerably reduced by implementing FVD-BIS by more than 50%.

In addition, regarding the bearing amplitude for the selected ground motions, Figure 68 depicts the amplitude of the bearing both for low and high-rise buildings as bar graphs for all 94 pulse-like ground motions. Based on Figure 68, it can be clearly seen that by implementing FVD-BIS the amplitude of bearing is decreased by about 50% for all cases of ground motions.

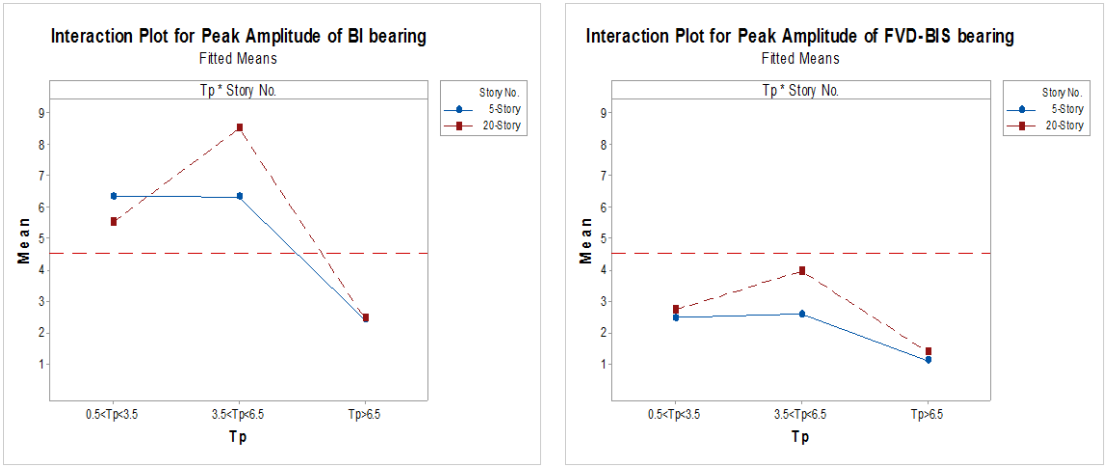

(a) (b)

Figure 67: Interaction plot of peak amplitude of bearing for 5 and 20-story base-isolated building vs. pulse period (T_p): a) BI; b) FVD-BIS

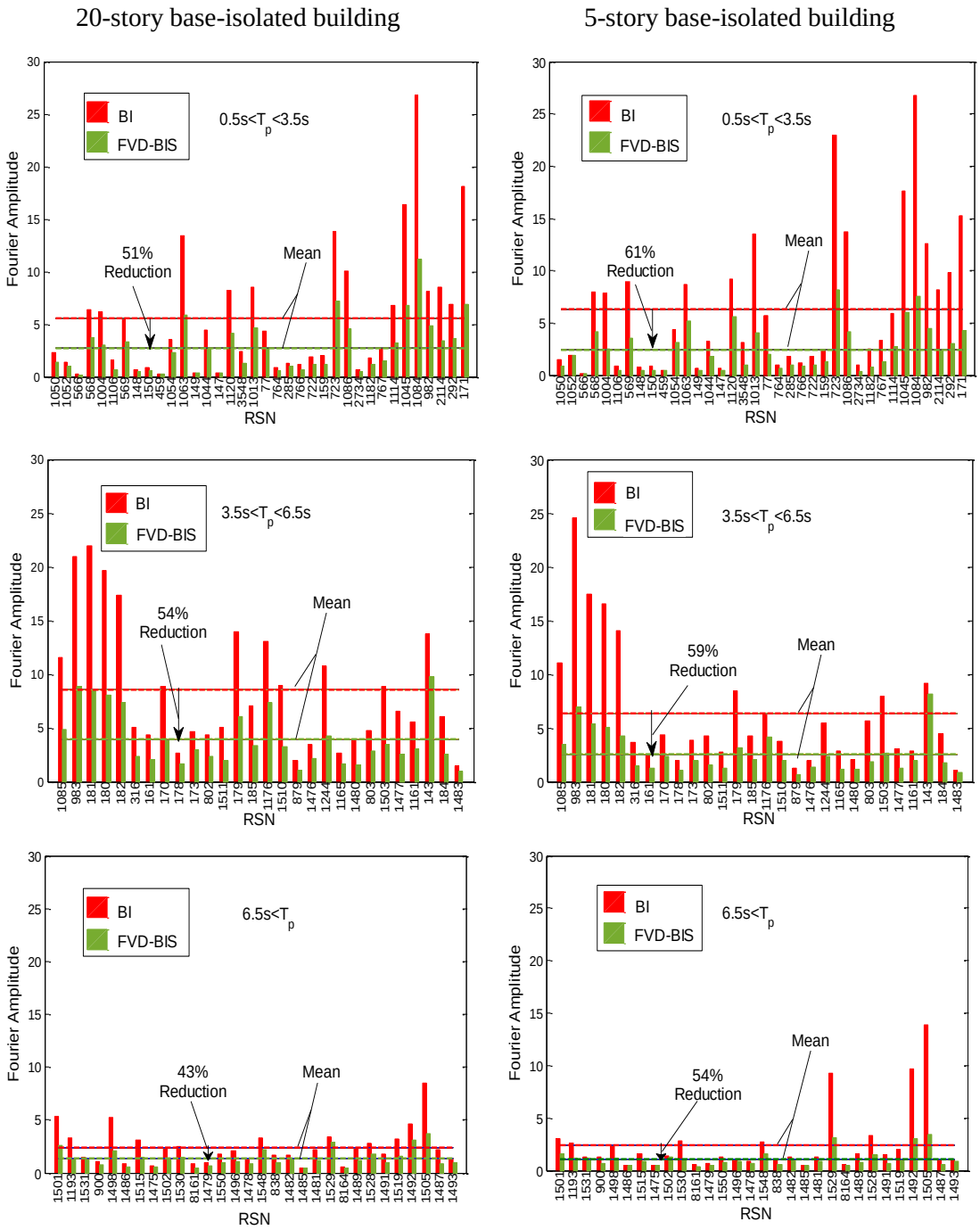

Figure 68: Amplitude of bearing for 94 pulse-like strong ground motions for 20-story and 5-story base-isolated building

Eight pulse-like ground motions with the highest intensity have been selected to study the behavior of the subject building (20-story base-isolated building). According to Table 19, the damage limitation (column "a"), story acceleration (column "b"), and displacement (column "c") for the base-isolated building have

been illustrated both with LCRB and FVD-BIS. Accordingly, it is observed that the story drift of the base-isolated building considering FVD-BIS is considerably lower than that of the base-isolated building with LCRB. Also, according to Eurocode 8 [10], damage limitations have been kept below 1% in the base-isolated building using FVD-BIS which is the requirement for buildings at the upper limit on the inter-story drift ratio under seismic loading. In addition, by implementing FVD-BIS, the acceleration for all stories has diminished, which is crucial for the convenience of residents (column "b" in Table 19 illustrates the absolute maximum acceleration for each story). Table 19c indicates that displacements of each story for the base-isolated building with LCRB have grown considerably (responses are reversed), which are even greater than those of the fixed base building (e.g., RSN180C and RSN179C). However, by retrofitting the tested building using FVD-BIS, the story displacements have been highly mitigated. Similarly, the interaction plot (Figure 69) indicates that roof acceleration for the buildings (LCRB and FVD-BIS seismically isolated buildings) is significantly reduced when compared to the fixed base building. Also, it can be seen when FVD-BIS is used for high-rise building (20-story building) roof acceleration is considerably reduced for the following range of pulse period, 3.5 s $< T_p <$ 6.5 s, and this amount remains constant for low-rise building (5-story) when compared with the responses of the conventionally base-isolated buildings (LCRB).

Table 19: Damage limitation, acceleration, and story displacement for eight pulse-like ground motions for 20-story base-isolated building

	(a) Damage Limitation (%)	(b) Acceleration (cm/s^2)	(c) Displacement (cm)
RSN1045	T_p=2.982 s, T_b=2.5 s, T_{sBI}=3.14 s, T_{sFB}=2 s		
	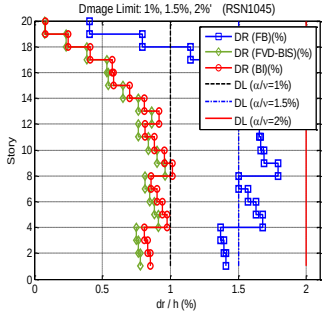	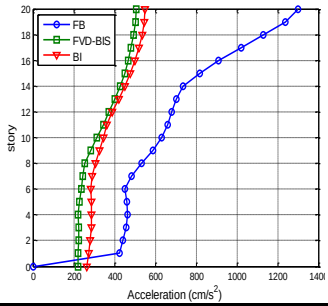	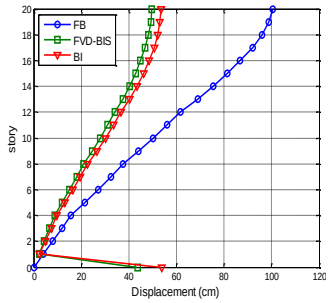
RSN1492	T_p=12 s, T_b=2.5 s, T_{sBI}=3.14 s, T_{sFB}=2 s		
	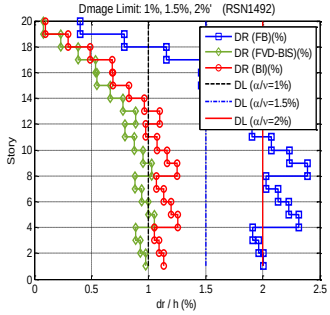	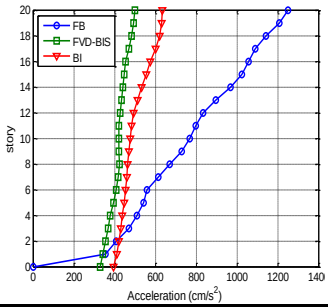	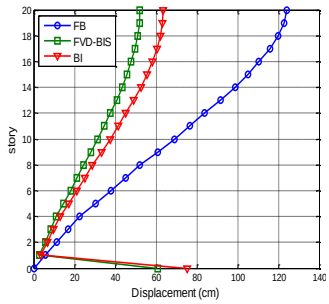
RSN180	T_p=4.13 s, T_b=2.5 s, T_{sBI}=3.14 s, T_{sFB}=2 s		
	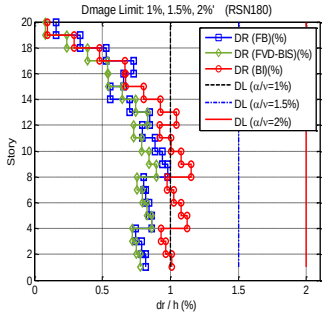	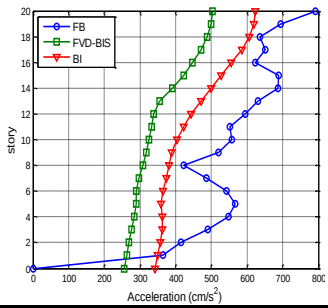	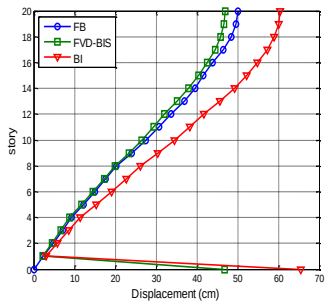
RSN171	T_p=3.423 s, T_b=2.5 s, T_{sBI}=3.14 s, T_{sFB}=2 s		
	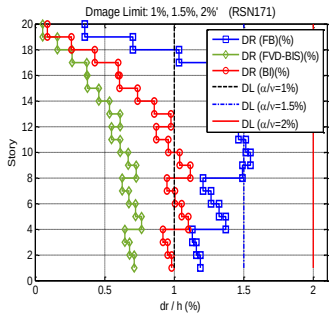	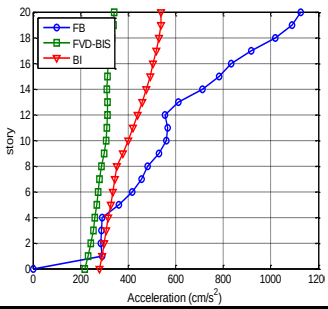	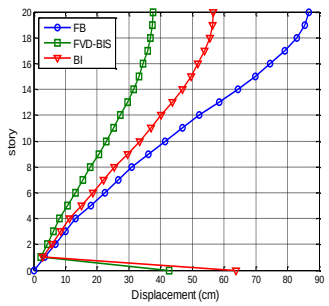

Table 19 (Cont.)

RSN983

T_p=3.535 s, T_b=2.5 s, T_{sBI}=3.14 s, T_{sFB}=2 s

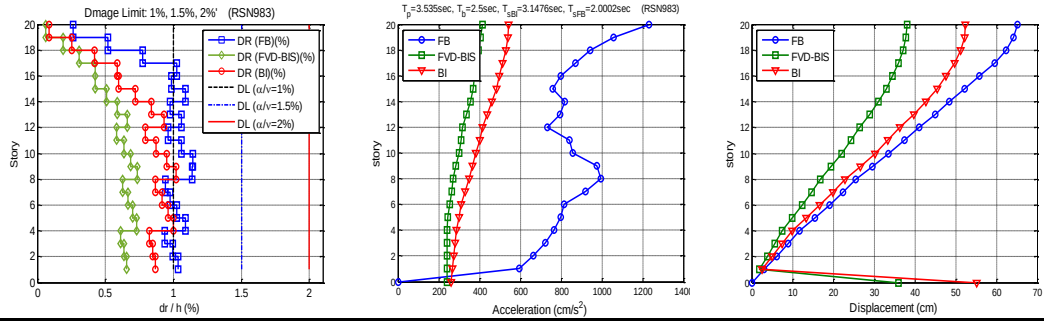

RSN1505

T_p=12.285 s, T_b=2.5 s, T_{sBI}=3.14 s, T_{sFB}=2 s

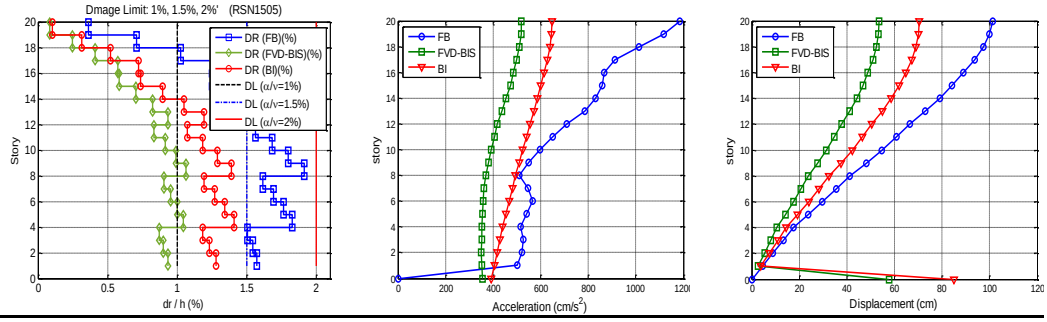

RSN182

T_p=4.375 s, T_b=2.5 s, T_{sBI}=3.14 s, T_{sFB}=2 s

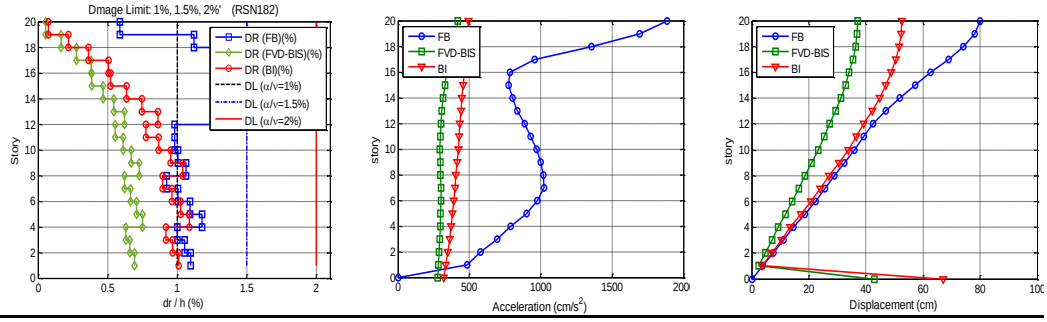

RSN179

T_p=4.788 s, T_b=2.5 s, T_{sBI}=3.14 s, T_{sFB}=2 s

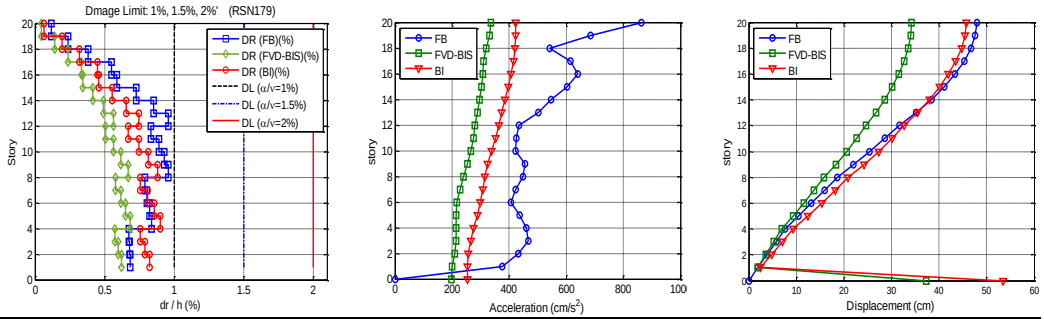

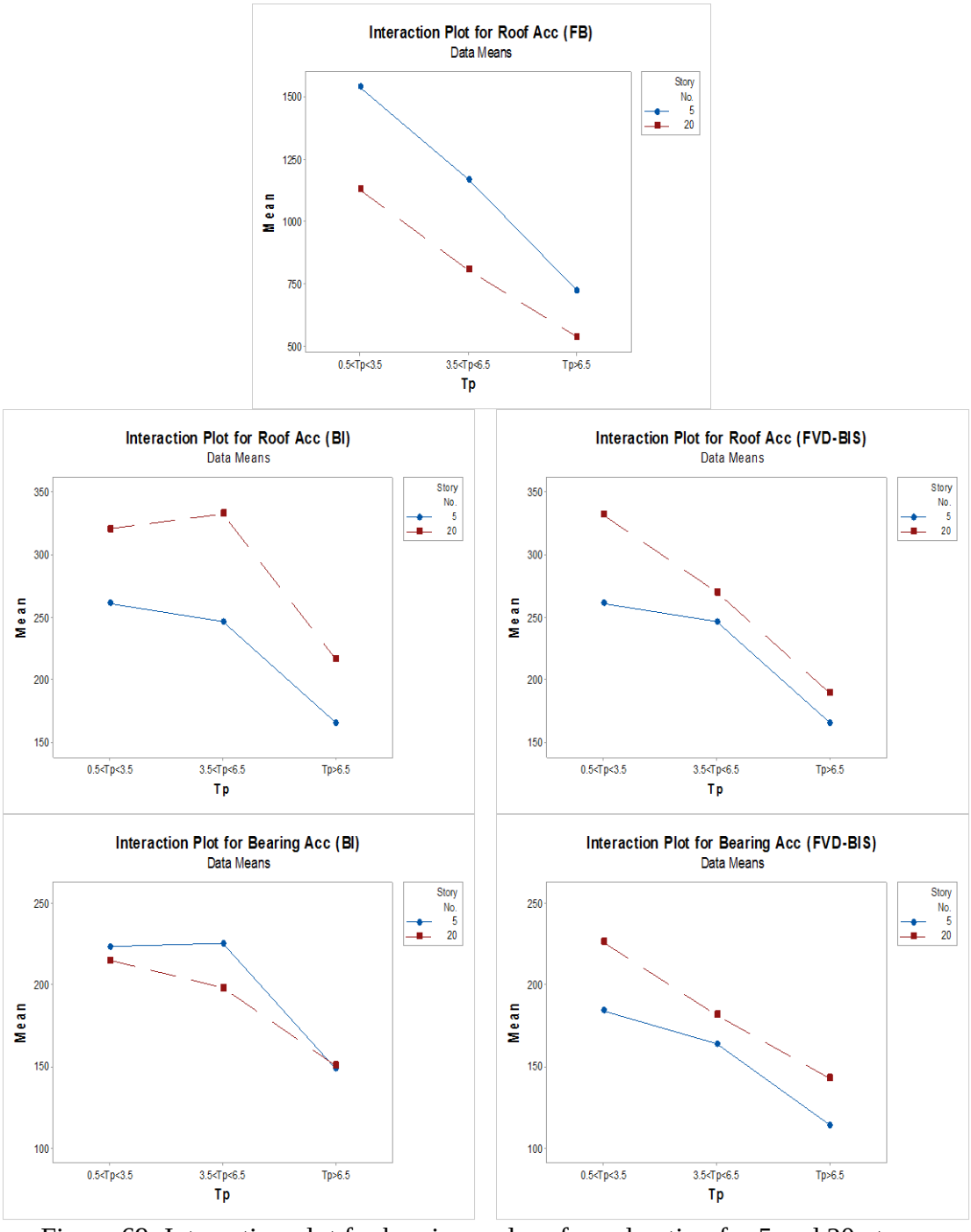

Figure 69: Interaction plot for bearing and roof acceleration for 5 and 20-story building (unit: cm/s^2)

7.6 Comparison of the Isolator Responses Based on Peak Ground Responses

In order to enable the comparison of several approaches for 5 and 20-story buildings, response changes of isolation system regards to the ground responses were

calculated as in Eq. (33) and illustrated in interaction graphs (Figure 70 and Figure 71). In interaction graphs, dashed line emphasizes the median of the responses.

$$\text{Response Changes} = \frac{\text{peak response of isolator} - \text{peak ground response}}{\text{peak ground response}} \quad (33)$$

Figure 70 illustrates the interaction of both the number of stories and the pulse periods (T_P) of the ground motions. With regard to Figure 70, for 5-story seismically isolated building when the pulse period ground motions are between 0.5 s and 3.5 s, isolator displacement is increased by about 37% compared to the peak ground displacement (PGD) of the earthquakes. But, for the ground motions whose pulse periods are between 3.5 s and 6.5 s, and also more than 6.5 s, isolator displacement is decreased by about 25% and 65% compared to the PGD of earthquakes, respectively. Accordingly, it can be concluded that for the low-rise base-isolated building (in this study 5-story building), which is subjected to the ground motions with the pulse period between 0.5 s and 3.5 s, bearing displacement will be highly increased. For high-rise building (20-story building), it can be seen from the interaction plot (Figure 70a) that the bearing displacement is increased by about 10% and for the ground motions whose 3.5 s $< T_P <$ 6.5 s and 6.5 s $< T_P$ the bearing displacements are decreased by about 20% and 65%, respectively.

Moreover, interaction plot in Figure 70b shows that 5-story base-isolated building, which is seismically isolated by FVD-BIS, bearing displacement is reduced by about 12% regards to the PGD for the case when 0.5 s $< T_P <$ 3.5 s, but for 20-story building with the same pulse periods it is about 20%. For the two other cases of the ground motions, it can be clearly seen that the reduction percentage for 5-story is higher than the percentage reduction for 20-story building where the differences are negligible for both low-rise and high-rise buildings.

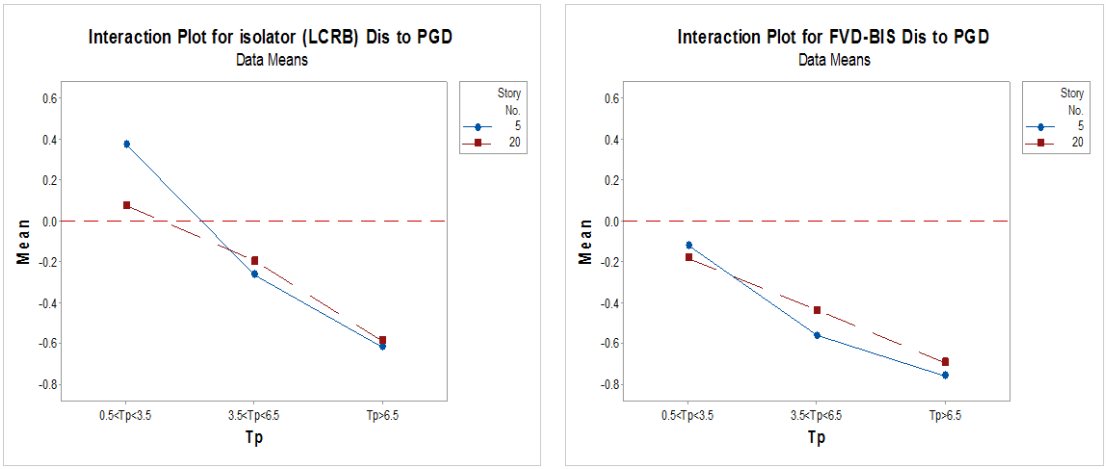

(a) (b)

Figure 70: Bearing *response (displacement)* changes related to the peak ground displacement (PGD) of the ground motions: a) LCRB, b) FVD-BIS

Figure 71a gives information about isolator acceleration (LCRB) related to the peak ground acceleration, where this acceleration is reduced by about 18%, 27% and 45% for 5-story building and 18%, 35% and 47% for 20-story building for the ground motions with pulse period of 6.5 s < T_P, 3.5 s < T_P < 6.5 s and 0.5 s < T_P < 3.5 s, respectively. For the ground motions whose pulse period is bigger than 6.5s and between 0.5 s and 3.5 s, response reduction (acceleration reduction) of the isolator for 5 and 20-story is approximately the same. But this reduction of isolator's responses for 20-story building is slightly higher than the isolator's responses for 5-story building for when the pulse period is within 3.5 s < T_P < 6.5 s. It is clear that the isolator acceleration both for 5-story and 20-story is significantly reduced by about 47% with respect to the responses of the ground motions whose pulse period is between 0.5 s and 3.5 s. And this amount of reduction is reduced as the pulse period increases, where the lowest percentage of reduction occurred by about 15% for the ground motions whose pulse period is more than 6.5 s.

Figure 71b shows that the FVD-BIS acceleration for 5-story building is highly reduced for all three different groups of ground motions when compared to the FVD-

BIS responses of the 20-story building. FVD-BIS acceleration for 5-story building is reduced by about 37%, 47% and 55% and for 20-story building is about 25%, 45% and 47% for the ground motions with pulse period of 6.5 s < T_P, 3.5 s < T_P < 6.5 s and 0.5 s < T_P < 3.5 s, respectively. Accordingly, it can be concluded that when the FVD-BIS is used, the reduction percentages are increased regards to the ground responses.

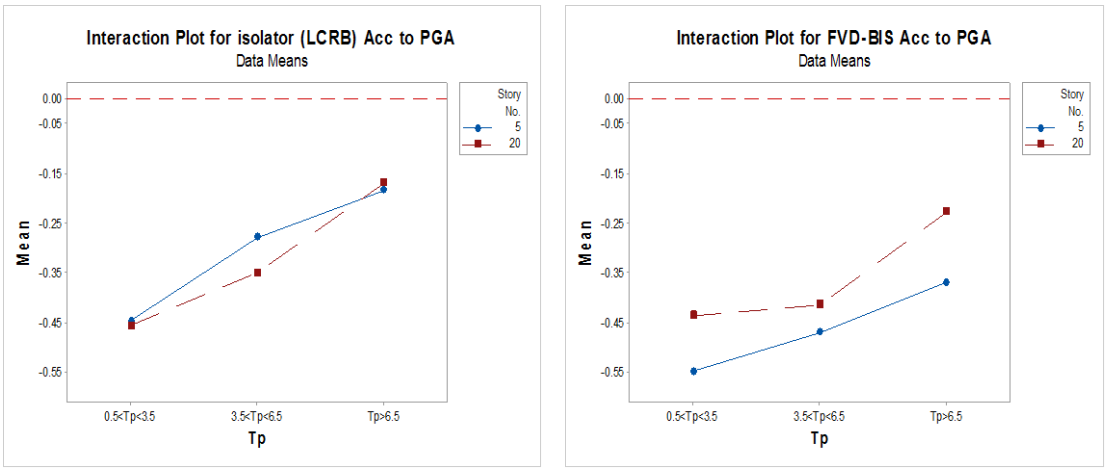

(a) (b)

Figure 71: Bearing *response (acceleration)* changes related to the peak ground acceleration (PGA) of the ground motions: a) LCRB, b) FVD-BIS

Finally, it can be concluded that by implementing FVD-BIS, bearing displacement and acceleration based on PGD and PGA are highly decreased for all cases of the ground motions. However, for the conventionally base-isolated building (LCRB), the isolator displacement with regards to the peak ground displacement is increased for both 5 and 20-story base-isolated buildings.

Chapter 8

CONCLUSION

Seismic isolation systems have been used as alternative lateral force resisting methods that have the potential to protect nonstructural and structural components. While many control systems have been proposed not only for response reduction in base-isolated buildings under different strong ground motions but also to maintain a safety function of base isolation systems to reduce the effects of large accelerations induced by the ground motions, these systems still seem to be quite complicated to use.

Moreover, its success is still questioned in near-field strong ground motions that have pulse-like components, where a situation resembling resonance can arise and cause a large-amplitude response. In this section, the results indicated that the isolation system used and the base-isolated buildings are period dependent, making them vulnerable against near-field pulse period ground motions as a result of resonance.

Consequently, the research findings enhance our understanding of the behaviors of base-isolated buildings and base isolation system under various ground motions with different components and effectiveness of the FVD-BIS for protecting base-isolated high-rise building against resonance.

Accordingly, following are the main outcomes of this investigation for **chapter 6** and **chapter 7**, respectively.

The most obvious findings to emerge from **Chapter 6** are as follows**:**

- There is a significant decrease in the top floor displacement for the three cases of PGA/PGV compared to fixed-base buildings (i.e., 5-, 10-, 15-, 20- and 25-story buildings), but the results are inverse for 30- and 35-story buildings and the displacements in the base-isolated buildings are higher than those in the fixed-base buildings. Moreover, acceleration of the top floor of the base-isolated building is also decreased for the three cases (PGA/PGV<1, 1<PGA/PGV<2, PGA/PGV>2) when compared to the acceleration of the top floor of the fixed-base building, but it remains unchanged for the 30- and 35-story buildings. In another words, in low-rise structures, there is a considerable decrease in the acceleration at the top floor of the base-isolated buildings for all three different cases. In addition, it can be concluded that the influence of the isolator system is decreased as the number of stories increase.

- By increasing the number of stories (from 5 to 35-story), the ratio of the base isolation displacement to PGD and the ratio of the top floor displacement to the PGD behave inversely. Alternatively stated, the ratio of the base isolation displacement to PGD is higher for low-rise buildings, but when compared with the ratio of the top floor displacement to PGD, this ratio for low-rise buildings becomes smaller.

- For different high-rise base-isolated buildings, the acceleration of the isolation system is reduced by approximately 55% with reference to the PGA for three cases of PGA/PGV.

- For the three cases of PGA/PGV, as the ratio increases, the amount of energy dissipation is decreased by the base isolation system.

- The acceleration of the isolation system compared to the PGA is decreased for the three cases of PGA/PGV (as the ratio increases). In contrast, the displacement of

the isolation system with reference to the PGD increased for the mentioned cases in order.

- It was observed that the probability of failure of the ratio of peak bearing displacement to peak ground displacement (regardless of the magnitude) happened for all cases of the ground motions. But, probability of failure of the bearing acceleration to PGA only happened when PGA/PGV is less than 1 and for other cases of the earthquakes, no failure occurred, which can be concluded that the ground motions whose PGA/PGV are less than one are highly effective to the base-isolated buildings.

- It was observed that the probability of failure of the ratio of peak bearing responses to peak ground responses reduced as the number of the story increased for all cases of the ground motions.

- According to the results achieved, the probability of failure of peak roof displacement to PGD ratio increased as the number of the story increased. And when PGA/PGV was less than 1 the probability of failure (PF) gradually increased from 5-story to 35-story base-isolated buildings. For the case when PGA/PGV was between 1 and 2, PF was observed that it is at the highest level for 30- and 35-story base-isolated buildings. But for the ground motions that PGA/PGV was more than 2, PF of peak roof displacement to PGD ratio was at the highest level after 20-story base-isolated building.

- However the PF of the key responses of the roof displacement to the PGD ratio was in the highest level for 20, 25, 30 and 35-story base-isolated buildings for when the PGA/PGV was more than 2, It was observed that PF of the roof acceleration to the PGA ratio was in the highest level for when PGA/PGV was less than 1, and the

lowest PF was when PGA/PGV was more than 2 (approximately zero) for the acceleration responses of the roof.

- According to the accelerogram generated based on the target spectrum for each case of the ground motions (see Figure 42) and the bearing displacements observed for these kinds of earthquakes, it can be concluded that as the ratio of PGA/PGV decreases, the bearing displacement is sharply increased for 35-story base-isolated building in the case when PGA/PGV<1 (see Figure 19). In another words, as the intensity of the ground motions, whose PGA/PGV<1, is more than the other group of the ground motions, the responses of the base-isolated buildings subjected to these types of ground motions were increased. Especially, high-rise base-isolated buildings are more affected when subjected to the above-mentioned ground motions. Therefore, the base-isolated high-rise buildings (i.e., 20-, 25-, 30- and 35-story) can be vulnerable to the ground motions when PGA/PGV ratio is smaller than 1(g.s/m). (Maximum response for the group of the ground motions whose PGA/PGV<1 occurs when the frequency is about 0.25 Hz, which is close to the natural frequency of the 35-story base-isolated building ($\frac{1}{4.16s} = 0.24Hz$, 4.16 s is the 1st mode period of the 35-story base-isolated building (Table 8)).

- As was observed, by increasing the number of the stories, the effects of the base isolation system are reduced. However, considering the damage limitation criteria, it can be observed that the effects of the base isolation system, especially for high-rise buildings, are highly observable and keep the damage limitation requirement below 1%. Furthermore, story drifts are significantly decreased for base-isolated buildings even for truly high-rise ones (i.e., 25-, 30-, 35-story).

The second major findings in **Chapter 7** are as follows**:**

- The results reveal that when the pulse-like ground motions attack base-isolated buildings with a long fundamental period, they amplify the responses and cause resonance. This, in turn, can result in major damages in the base-isolated buildings intended to withstand these ground motions. Our results show that the resonance phenomenon occurs mostly when the pulse period of the ground motions lay within the range 3.5 s and 6.5 s for a 20-story base-isolated building and within the range 0.5 s and 6.5 s for 5-story base-isolated building.

- It is concluded that as both base-isolated low-rise and high-rise buildings whose fundamental periods are usually between 2.5 s and 5 s would be affected when subjected to the near-field pulse-like ground motions. For this reason, base-isolated high-rise buildings are better to be designed for the ground motions whose pulse periods are approximately between 3 s and 7 s and low-rise buildings for the pulse periods between 0.5 s and 6.5 s.

- To mitigate the resonance phenomenon, FVD was selected as a supplementary energy dissipation system and implemented in the base-isolated buildings. The single most striking observation to emerge from the data comparison clearly illustrated that the use of FVD-BIS in the base-isolated buildings would reduce the intensity of the resonance phenomenon for a different type of pulse-like ground motions by more than 50%.

- The results reveal that the use of FVD-BIS first caused a considerable reduction in the intensity of the resonance induced by strong ground motions. Also, the maximum displacement and acceleration of the stories significantly diminished compared to the conventionally base-isolated buildings controlled by LCRB system.

- Considering the damage limitation criteria according to Eurocode 8[10], for the tested buildings, the effects of FVD-BIS were keeping the damage limitation

requirement below 1% for most of the selected pulse-like ground motions for the tested buildings.

- It was observed that the isolator displacement is significantly increased for the pulse period 0.5 s < T_p < 3.5 s based on peak ground displacement (PGD) for 5-story and 20-story base-isolated buildings. In contrast, it was seen that the above responses are decreased by about 20% and 60% for the group of the ground motions whose pulse periods are 3.5 s < T_p < 6.5 s and 6.5 s < T_p, respectively, and reduction of isolator displacement respected to the PGD for both 5-story and 20-story buildings are approximately the same, and the differences are negligible. By implementing FVD-BIS, it was observed that FVD-BIS displacement is decreased for all three cases of the ground motions based on the PGD and this amount of reduction increased as the pulse period of the earthquakes increased.

- It can be concluded that the acceleration of the isolator (LCRB) is decreased for all types of pulse-like ground motions based on the PGA by using FVD. And highly reduction of acceleration was observed when the pulse period is between 0.5 s and 3.5 s for the buildings. This amount of reduction of acceleration is decreased as the pulse period increased. In addition, with the help of FVD-BIS, the reduction of responses (acceleration) of the 5-story building is higher than the 20-story building for all three different groups of ground motions.

8.1 Future Studies

- This study mainly investigates the LCRB base isolator, and different isolation systems could have different results. Multiple base isolation systems (LCRB, LRB, FPS etc.) with different mechanical properties can be subjected to different ground motions with different components for different type of buildings at height to evaluate the behavior of the subjected buildings.

- Probabilistic behavior assessment of base isolation systems and base isolated buildings considering soil-structure interaction for base-isolated buildings.
- As the base-isolated buildings and base isolation systems are period dependent, investigating their seismic behavior under velocity pulse period ground motions can be a part of future study (risk of resonance happening in base isolation systems and base isolated buildings).

REFERENCES

[1] Higashino, M., & Okamoto, S. (2006). *Response Control and Seismic Isolation of Buildings.* London: SPON Press.

[2] *RB (Multilayer Natural Rubber Bearing)*. (n.d.). Retrieved from OILES Bearing: https://www.oiles.co.jp/en/

[3] Robinson, W. H., & Tucker, A. G. (1977). A lead-rubber shear damper. *bulletin of the new zealand national society for earthquake engineering , 10* (3), 151-153.

[4] Robinson, W. H., & Tuker, A. G. (1983). Test results for lead-rubber bearings for the William M. Clayton Building, Toe Toe bridge, and Waiotukupuna bridge. *bulletin of the new zealand national society for earthquake engineering , 14* (1), 21-33.

[5] *The Leading Supplier of Quality Bridge Bearings*. (n.d.). Retrieved from Lead rubber bearing for earthquake resistance: https://www.bridgebearings.org/product/lead-rubber-bearing.html

[6] *FIP Industriale*. (1992). Retrieved from Lead rubber bearings: https://www.fipindustriale.it/index.php?area=106&menu=68&lingua=1

[7] *FPS Sliding Pendulum Type Seismic Isolation Device*. (n.d.). Retrieved from OILES Bearing: https://www.oiles.co.jp/en/menshin/building/menshin/products/fps/

[8] Skinner, R. I., Kelly, T. E., & Robinson, B. (1993). *Seismic Isolation for Designers and Structural Engineers.* Wiley and Sons.

[9] Symans, M. D. (2003). *Seismic Protective Systems: Seismic Isolation.* NEHRP Recommended Provisions: Instructional and Training Materials, FEMA 451B, Topic 15-7: Seismic Isolation.

[10] *Eurocode 8, Design of structures for earthquake resistance- Part 1 : General rules, seismic actions and rules for buildings, EN.* (1998-1.).

[11] Naeim, F., & Kelly, M. J. (1999). *Design of seismic isolated structures: from theory to practice.* United States of America: John Wiley & Sons.

[12] Matsagar, V. A., & Jangid, R. S. (2004). Influence of isolator characteristics on the response of base-isolated structures. *Engineering Structures , 26*, 1735–1749.

[13] Xu, C., Chase, J. G., & Rodgers, G. W. (2014). Physical parameter identification of nonlinear base-isolated buildings using seismic response data. *Computers & Structures , 145*, 47-57.

[14] Kulkarni, J. A., & Jangid, R. S. (2002). Rigid body response of base-isolated structures. *Journal of structural control , 9* (3), 171-188.

[15] Agrawal, A. K., & He, W. L. (2008). Analytical model of ground motion pulses for the design and assessment of seismic protective systems. *Journal of Structural Engineering , 134* (7), 1177-1188.

[16] Alhan, C., & Öncü-Davas, S. (2016). Performance limits of seismically isolated buildings under near-field earthquakes. *Engineering Structures , 116*, 83-94.

[17] Touaillon, J. (1870). *Patent No. 99,973.* U.S. Patent.

[18] Constantinou, M. C., Whittaker, A. S., Kalpakidis, Y., Fenz, D. M., & Warn, G. P. (2008). *Performance of Seismic Isolation Hardware under Service and Seismic Loading.* Buffalo:: Multidisciplinary Center for Earthquake Engineering Research, State University of New York: Buffalo, NY, USA.

[19] Fenz, D., & Constantinou, M. C. (2006). Behaviour of the double concave Friction Pendulum bearing. *Earthquake Engineering Structural Dynamics , 35*, 1403–1424.

[20] Clarke, C. S., Buchanan, R., & Efthymiou, M. (2005). Structural platform solution for seismic arctic environments-Sakhalin II offshore facilities. *In Proceedings of the Offshore Technology Conference.* Houston.

[21] Boardman, P. R., Wood, B. J., & Carr, A. J. (1983). Union house—a cross-braced structure with energy dissipators. *Bulletin of the New Zealand National Society for Earthquake Engineering , 16* (2).

[22] Charleson, A. W., Wright, P. D., & Skinner, R. I. (1987). Wellington Central Police Station Base Isolation of an Essential Facility. *Proceeding Pacific Conference on Earthquake engineering*, *12*, pp. 377-388.

[23] Kelly, J. M. (1986). Aseismic base isolation: review and bibliography. *Soil Dynamics and Earthquake Engineering , 5* (4), 202-216.

[24] Buckle, I. B., & Mayes, R. M. (1990). Seismic isolation: History, application, and performance—A world view. *Earthquake Spectra , 6*, 161–201.

[25] Taylor, A. E., Lin, A. N., & Martin, J. W. (1992). Performance of elastomers in isolation bearings:A literature review. *Earthquake Spectra , 8*, 279–303.

[26] Soong, T. T., & Constantinou, M. C. (1994). *Passive and Active Structural Vibration Control in Civil Engineering.* New York,: Springer-Verlag.

[27] Kunde, M. C., & Jangid, R. S. (2003). Seismic behavior of isolated bridges: A-state-of-the-art review. *Electronic Journal of Structural Engineering , 3*, 140–170.

[28] Symans, M. D., Cofer, W. F., & Fridley, K. J. (2003). Base isolation and supplemental damping systems for seismic protection of wood structures: Literature review. *Earthquake Spectra , 18*, 549–572.

[29] Taylor, A. W., & Igusa, T. (2004). *Primer on seismic isolation.* Reston: ASCE publications.

[30] Castaldo, P., Palazzo, B., & Della, V. (2015). Seismic reliability of base-isolated structures with friction pendulum bearings. *Engineering Structures , 95*, 80–93.

[31] Tavakoli, H. R., Naghavi, F., & Goltabar, A. R. (2014). Dynamic Responses of the Base-Fixed and Isolated Building Frames Under Far- and Near-Fault Earthquakes. *Arabian Journal for Science and Engineering , 39* (4), 2573–2585.

[32] Choun, Y. S., Park, J., & Cho, I. K. (2014). Effects of mechanical property variability in lead rubber bearings on the response of seismic isolation system for different ground motions. *Nuclear Engineering and Technology , 46* (5), 605–618.

[33] Alhan, C., & Şahin, F. (2011). Protecting vibration-sensitive contents: an investigation of floor accelerations in seismically isolated buildings. *Bulletin of Earthquake Engineering* , 9: 1203.

[34] Sayani, P. J., & Ryan, K. L. (2009). Comparative evaluation of base-isolated and fixed-base buildings using a comprehensive response index. *ournal of Structural Engineering , 35*, 698–707.

[35] Mazza, F., & Vulcano, A. (2009). Nonlinear response of RC framed buildings with isolation and supplemental damping at the base subjected to near-fault earthquakes. *Journal of Earthquake Engineering , 13* (5), 690-715.

[36] Harvey, P. S., & Gavin, H. P. (2015). Assessment of a rolling isolation system using reduced order structural models. *Engineering Structures , 99*, 708–25.

[37] Jangid, R. S. (2007). Optimum lead–rubber isolation bearings for near-fault motions. Engineering structures. *Engineering structures , 29* (10), 2503-2513.

[38] Deringöl, A. H., & Bilgin, H. (2018). Effects of the isolation parameters on the seismic response of steel frames. *Earthquakes and Structures , 15* (3).

[39] Samali, B., Wu, Y. M., & Li, J. (2003). Shake table tests on a mass eccentric model with base isolation. *Earthquake Engineering & Structural Dynamics , 32*, 1353–1372.

[40] Mavronicola, E., Polycarpou, P., Papaloizou, L., & Komodromos, P. (2015). Computer-aided Investigation Of Special Issues Of The Response Of Seismically Isolated Buildings. *International Journal of Computational Methods and Experimental Measurements , 3* (1), 21-32.

[41] Chimamphant, S., & Kasai, K. (2016). Comparative response and performance of base-isolated and fixed-base structures. *Earthquake engineering & structural dynamics* (45), 5-27.

[42] Takewaki, I. (2008). Robustness Of Base-Isolated Hıgh-Rıse Buıldıngs Under Code-Specıfıed Ground Motıons. *Tall and Special Buildings , 17*, 257–271.

[43] Jalali, A., & Narjabadifam, P. (2006). Optimum modal characteristics for multi-story buildings isolated with lrbs. *4th International Conference on Earthquake Engineering, 187*. Taipei.

[44] Lu, L. Y., Shih, M. H., Tzeng, S. W., & Chien, C. C. (2003). Experiment of a sliding isolated structure subjected to near-fault ground motion. *In Proceedings of the 7th pacific conference on earthquake engineering*, (pp. 13-15).

[45] Alhan, C., & Göktaş, Y. (2009). Effects of near-field earthquakes on seismically isolated buildings. *InProceedings, WCCE-ECCE-TCCE joint conference: earthquake and tsunami*, (pp. 22-24).

[46] Hall, J. F., & Ryan, K. L. (2000). Isolated buildings and the 1997 UBC near-source factors. *Earthquake Spectra , 16* (2), 393-411.

[47] Cancellara, D., & De Angelis, F. (2016). A base isolation system for structures subject to extreme seismic events characterized by anomalous values of intensity and frequency content. *Composite Structures journal , 157*, 285-302.

[48] Alhan, C., Hatice, G., & Hakan, K. (2016). Significance of stiffening of high damping rubber bearings on the response of base-isolated buildings under near-fault earthquakes. *Mechanical Systems and Signal Processing , 79*, 297-313.

[49] Yang, J., Shuaishuai, S., Tongfei, T., Weihua, L., Haiping, D., Gursel, A., et al. (2016). Development of a novel multi-layer MRE isolator for suppression of building vibrations under seismic events. *Mechanical Systems and Signal Processing , 70* (71), 811-820.

[50] Politopoulos, I., & Sollogoub, P. (2005). Vulnerability of elastomeric bearing isolated buildings and their equipment. Journal of earthquake engineering. *Journal of Earthquake Engineering , 9* (04), 525-546.

[51] *NEHRP recommended provisions for seismic regulations for new buildings and other structure, Part 1: Provisions (FEMA 368).* (2001). Washington, D.C.

[52] Hall, J. F., Heaton, T. H., Halling, M. W., & Wald, D. J. (1995). Near-source ground motion and its effects on flexible buildings. Earthquake spectra. *Earthquake spectra , 11* (4), 569-605.

[53] Jangid, R. S., & Kelly, J. M. (2001). Base isolation for near-fault motions. *Earthquake Engineering Structure* (30), 691{707.

[54] Lu, L.-Y., & Lin, G.-L. (2009). Improvement of near-fault seismic isolation using a resettable variable stiffness damper. *Engineering Structures journal , 31* (9), 2097-2114.

[55] Zhang, Y., & Iwan, W. D. (2002). Protecting Base-Isolated Structures from Near-Field Ground Motion by Tuned Interaction Damper. *Journal of Engineering Mechanics , 128* (3), 287-295.

[56] Kandemir-Mazanoglu, E. (2017). Effects of isolator properties on viscous damper capacity of base isolated adjacent buildings. *Journal of Vibroengineering* , 2739-2748.

[57] Alhamaydeh, M. H., Barakat, S. A., & Abed, F. H. (2013). Multiple regression modeling of natural rubber seismic-isolation systems with supplemental viscous damping for near-field ground motion. *Civil Engineering and Management , 5*, 665–682.

[58] Providakis, C. (2008). Effect of LRB isolators and supplemental viscous dampers on seismic isolated buildings under near-fault excitations. *Engineering Structures* , 1187–1198.

[59] Wolff, E., Ipek, C., Constantinou, M., & Tapan, M. (2015). Effect of viscous damping devices on the response of seismically isolated structures. *EARTHQUAKE ENGINEERING & STRUCTURAL DYNAMICS , 44*, 185–198.

[60] Pan, P., Zamfirescu, D., Nakashima, M., Nakayasu, N., & Kashiwa, H. (2005). Base-isolation design practice in Japan: introduction to the post-Kobe approach. *Journal of Earthquake Engineering , 09* (01), 147-171.

[61] Ikhouane, F., & Rodellar, J. (2007). *Systems with hysteresis: analysis, identification and control using the Bouc-Wen model.* England: John Wiley & Sons Ltd.

[62] Chopra, A. (1995). *Dynamics of structures: theory and applications to earthquake engineering.* New Jersey: Prentice Hall.

[63] Ryan, K. L., & Polanco, J. (2008). Problems with Rayleigh damping in base-isolated buildings. *Journal of Structural Engineering , 134* (11), 1780–4.

[64] Pant, D., Wijeyewickrema, A., & ElGawady, M. (2013). Appropriate viscous damping for nonlinear time-history analysis of base-isolated reinforced concrete buildings. *Earthquake Engineering Structural Dynamics* , 2322-2339.

[65] Robinson, W. H. (1982). lead-rubber hysteretic bearings suitable for protecting structures during earthquakes. *Earthquake Engineering and Structural Dynamics , 10*, 593-604.

[66] Skinner, R. I., Kelly, J. M., & Heine, A. J. (1974). Hysteretic dampers for earthquake-resistant structures. *Earthquake Engineering and Structural Dynamics , 3* (3), 287-296.

[67] Lindblad, E., Valiev, D. M., Muller, B., Rantakokko, J., Lotstedt, P., & Liberman, M. A. (2006). Implicit-explicit runge-kutta method for combustion simulation. *European Conference on Computational Fluid Dynamics* (pp. 1-20). Netherlands: TU Delft.

[68] Dormand, J. R., & Prince, P. J. (1980). A family of embedded Runge–Kutta formulae. *Computational and Applied Mathematics , 6*, 19-26.

[69] Franke, K. (2017, Jan 25). Ground Motion Parameters and Signal Processing. *CEEN 545* .

[70] Minitab 17. (2016).

[71] *Eurocode 1, Actions on structures – part 1-1: general actions – densities, self-weight, imposed loads for buildings, EN.* (1991-1-1.).

[72] *Eurocode, basis of structural design,EN.* (1990).

[73] Saragoni, G., & Hart, G. (1974). Simulation of artificial earthquakes. *Earthquake Engineering-and Structural Dynamics , 2*, 219-267.

[74] Makris, N. (1997). Rigidity–plasticity–viscosity: can electrorheological dampers protect base-isolated structures from near-source ground motions? *Earthquake engineering & structural dynamics , 26* (5), 571-591.

[75] Agrawal, A. K., & He, W. L. (2002). A closed form approximation of near-field ground motion pulses for flexible structures. *In: 15th ASCE proceeding of engineering mechanics conference.* New York.

[76] Dicleli, M., & Buddaram, S. (2007). Equivalent linear analysis of seismic-isolated bridges subjected to near-fault ground motions with forward rupture directivity effect. *Engineering Structures , 29* (1), 21-32.

[77] Somerville, P. G. (1998). Development of an improved representation of near fault ground motions. *In SMIP98 Seminar on Utilization of Strong-Motion Data.*